TRANSPORT OF MICELLE-SOLUBILIZED COMPOUNDS THROUGH MICROPOROUS MEMBRANES

By

KEITH A. JOHNSON

A DISSERTATION PRESENTED TO THE GRADUATE SCHOOL
OF THE UNIVERSITY OF FLORIDA IN
PARTIAL FULFILLMENT OF THE REQUIREMENTS
FOR THE DEGREE OF DOCTOR OF PHILOSOPHY

UNIVERSITY OF FLORIDA

1987

ACKNOWLEDGMENTS

I am grateful to my advisor, Dinesh Shah, for introducing me to colloid and interface science and for his guidance during my research. I am also grateful to Drs. Brij Moudgil and Jerry Westermann-Clark for serving on my supervisory committee. I would like to thank Drs. Ranga Narayanan and Ken Sloan who participated in my examinations and provided me with many helpful suggestions. The late Professor Federico Vilallonga made a significant contribution to this work by inspiring and encouraging me during the early stages of the research.

I am grateful to Conny Bogentoft for giving me the opportunity to work at ACO Lakemedel AB in Solna, Sweden, and to Peter Sponbergs for his friendship and support during my stay. I am also grateful to Dr. Nickolas Bodor for giving me the opportunity to work on a transdermal drug delivery project in his lab for one semester. Alcon Laboratories in Fort Worth, Texas, generously supported the research presented in this dissertation for the last three years.

I would like to thank Ronnie Baxley and Tracy Lambert for constructing and maintaining some of the equipment used during this work. Donna Williams assisted me with some of the electron microscopy work and Nancy Gildersleeve assisted me with the HPLC equipment in Dr. Bodor's lab.

Finally, I am grateful to my parents, brother, family and friends for their support and encouragement during the course of this work.

TABLE OF CONTENTS

	Page
ACKNOWLEDGMENTS	ii
LIST OF TABLES	v
LIST OF FIGURES	vii
LIST OF SYMBOLS	xiii
ABSTRACT	xvi
CHAPTERS	
I INTRODUCTION	1
Surface Active Agents and Solubilization	1
Surfactants and Synthetic Membranes	4
Particle Diffusion in Microporous Membranes	8
Previous Studies in Transport of Micelle-Solubilized Compounds Through Synthetic Membranes	11
Scope and Significance	13
II THEORY	16
Diffusion of Nonionic Micelles	16
Diffusion of Ionic Micelles	19
Diffusion of a Micelle-Solubilized Compound	22
III EXPERIMENTS	28
Materials	28
Diffusion Measurements	30
Membrane Characterization	36
Boundary Layer Resistance	44
Solubilization of Compounds by Micelles	45
Micelle Characterization	48
Solute Diffusion Coefficients	52
Membrane Surface Charge	54

IV DIFFUSION OF MICELLES IN MICROPOROUS MEMBRANES. 61

Calculations for Hindered Diffusion of Micelles in Microporous Membranes. 61
Micelle Diffusion in Free Solution. 72
Nonionic Micelle Diffusion in Microporous Membranes 80
Diffusion of Charged Micelles in Microporous Membranes. 85
Conclusions 97

V TRANSPORT OF MICELLE-SOLUBILIZED COMPOUNDS THROUGH MICROPOROUS MEMBRANES. 100

Solubilization of Steroids by Micelles. 100
Effect of Steroid Solubilization on Transport Through Microporous Membranes. 106
Transport of Micelle-Solubilized Pyrene Across Microporous Membranes. 117
K Values Below Saturation 129
Conclusions 132

VI FORMULATION AND PROPERTIES OF AN ALCOHOL-FREE PHARMACEUTICAL MICROEMULSION 134

Screening Experiment. 136
Weight Ratio Effect 139
Salt Effect 142
Oil Chain Length Effect 146
Light Scattering Experiments. 152
Conclusions 152

VII SUMMARY AND RECOMMENDATIONS 157

Summary of Results. 157
Major Contributions of this Work. 158
Potential Applications. 160
Recommendations for Future Work 160

APPENDIX. 164

REFERENCES. 169

BIOGRAPHICAL SKETCH 176

LIST OF TABLES

Table		Page
3-1	Chemical Composition of ICI Surfactants Used in this Study	29
3-2	Membrane Pore Diameters and Pore Densities from Electron Microscopy	37
3-3	Comparison of the Ratios of Membrane Pore Area-to-Thickness (A/L) from Hydrocortisone Diffusion and Electron Microscopy	40
3-4	Pore Size, Pore Density and Pore Length for Membranes with Nominal Pore Diameters of 300 Å	43
3-5	Membrane Parameters and Mass Transfer Coefficients	46
4-1	Parameters for Equation 4-13	71
4-2	Diffusion Coefficients and Hydrodynamic Radii for Micelles Determined from QELS	76
4-3	Ratio of Membrane Pore Area-to-Thickness (A/L) After Exposure to Triton-X 100 and Brij 35	82
4-4	Comparison of Micelle Diameters Determined from QELS and Thickness of Adsorbed Surfactant Layer on Membrane Pore Wall	88
4-5	Parameters used for Calculations in Figures 4-14 and 4-15.	95
5-1	Distribution Coefficients (K, mM^{-1}) for Steroids in Triton-X 100, Brij 35 and SDS.	101
5-2	Distribution Coefficients (K, mM^{-1}) for Pyrene in Micellar Solutions.	121
5-3	Ratio of Peak III to Peak I (III/I) from the Fluorescence Spectrum of Pyrene in Micellar Solutions.	125
6-1	Effect of Cosurfactant on Water Solubilization in Microemulsions with Hexadecane as the Oil and AOT as the Surfactant. Initial Concentrations of Surfactant and Cosurfactant in Hexadecane Were Each 20% (w/v)	137

6-2 Effect of AOT/Arlacel 20 Weight Ratio on the Slope and Intercept of Plots of Solubilization of Water Versus Initial Concentration of Surfactants in Hexadecane 141

6-3 Effect of Salt Concentration on the Slope and Intercept of Plots of Solubilization of Water Versus Initial Concentration of Surfactants (AOT/Arlacel 20 1:1) in Hexadecane. 147

6-4 Effect of Oil Chain Length on the Slope and Intercept of Plots of Solubilization of Water Versus Initial Concentration of Surfactants (AOT/Arlacel 20 1:1). 151

LIST OF FIGURES

Figure		Page
1-1	Schematic of a surfactant micelle in an aqueous solution. . .	2
1-2	Schematic of a surfactant solution above the CMC in contact with a nonporous membrane.	5
1-3	Schematic of a surfactant solution above the CMC in contact with a porous membrane. The pores of this membrane are large enough to allow the micelles to enter.	6
1-4	Schematic of a spherical particle translating in a solvent-filled pore.	9
1-5	Schematic of a spherical particle partitioning into a solvent-filled pore. The shaded region is excluded to the particle since the center can approach the pore wall no closer than one particle radius.	10
2-1	Schematic representation of micelle diffusion through a solvent-filled membrane pore. The membrane separated two compartments that are both above the CMC.	17
2-2	Schematic representation of two sides of a diffusion cell separated by a microporous membrane. Initially, side 1 contains micelles plus a solute while side 2 contains only micelles at a lower concentration than side 1.	23
3-1	Schematic of the glass and Teflon diffusion cell used in experiments. Stirrers were rotated by an external magnet. . .	31
3-2	Total mass of pyrene in the diffusion cell at time t ($M_T(t)$) relative to the initial mass of pyrene in the cell (M_{T0}) versus time when Neoprene or Teflon gaskets were used to seal the cell. Pyrene was absorbed by the Neoprene gaskets but not by the Teflon gaskets.	32
3-3	The natural logarithm of the initial surfactant concentration difference across the membrane (ΔC_{s0}) relative to the concentration difference at time t ($\Delta C_s(t)$) versus time for CPC micelles diffusing across a Nuclepore membrane with nominal pore diameters of 300 Å. The slope of this plot is βD_M.	34

3-4 Carbon and platinum replica of a Nuclepore membrane with nominal pore diameters of 500 Å viewed by a transmission electron microscope. The bar represents 2600 Å. 38

3-5 Flow rate of water through a Nuclepore membrane with nominal pore diameters of 300 Å (V_f) versus pressure drop across the membrane. 42

3-6 Total concentration of testosterone (C_{ST}) versus Triton-X 100 micelle concentration (C_M'). The slope (KC_{SA}) and intercept (C_{SA}) of the line were obtained by fitting the data to Equation (2-35) where $K^*C_M = KC_M'$. 47

3-7 The natural logarithm of the fluorescence intensity of 5.2×10^{-5} M RBP in 45 mM SDS solution in the absence of MA(I^o) relative to the fluorescence intensity with MA(I) versus concentration of MA. 51

3-8 Conductance of TBAC solutions versus C_S where the break point of the plot is the CMC. 53

3-9 Streaming potential (ΔV) across a Nuclepore membrane with nominal pore diameters of 300 Å versus pressure drop across the membrane (ΔP). The electrolyte solution was 2.5 mM KCl. . 56

4-1 The partition coefficient (K_M) of a neutral hard sphere into a cylindrical pore versus the ratio of particle to pore radii (ξ) calculated from Equation (4-2). 62

4-2 The partition coefficient (K_M) of a charged hard sphere into a cylindrical pore with the same charge versus the ratio of particle pore radii (ξ) at various concentrations of a 1:1 supporting electrolyte: (i) 5 mM; (ii) 10 mM and (iii) 100 mM. The sphere radius was 25 Å and the charge densities on the sphere and pore were both 0.2 $\mu C/cm^2$. 67

4-3 The partition coefficient (K_M) of a charged hard sphere into a cylindrical pore with the same charge versus the ratio of particle to pore radii (ξ) where curves (i) and (ii) are for spheres with surface charge densities of 1.0 and 8.0 $\mu C/cm^2$, respectively. The sphere radius was 25 Å, the charge density on the pore was 0.2 $\mu C/cm^2$ and the concentration of the 1:1 electrolyte was 0.1 M. 68

4-4 Ratio of particle diffusion coefficients in a pore and in free solution (D_{M_p}/D_{M_∞}) versus the ratio of particle to pore radii (ξ) calculated using three different corrections for the Stokes law friction factor. 73

4-5 Free solution diffusion coefficient of Brij 35 micelles (D_{M_∞}) measured by QELS versus the micelle concentration (C_M'). . . . 75

4-6 Free solution diffusion coefficient of CPC micelles ($D_{M\infty}$) measured by QELS versus the micelle concentration (C_M') at various concentrations of a supporting electrolyte. 77

4-7 Free solution diffusion coefficient of TBAC micelles ($D_{M\infty}$) measured by QELS versus the micelle concentration (C_M') at various concentrations of a supporting electrolyte. 78

4-8 Free solution diffusion coefficient of SDBS micelles ($D_{M\infty}$) measured by QELS versus the micelle concentration (C_M') at various concentrations of a supporting electrolyte. 79

4-9 Hydrodynamic radius (r_M) and aggregation number (n) of SDBS micelles versus the concentration of a supporting electrolyte (NaCl). 81

4-10 The ratio of the intrapore micelle diffusion coefficient to the micelle diffusion coefficient in free solution ($D_M/D_{M\infty}$) for Triton-X 100 micelles versus the ratio of micelle to pore radii (ξ). The curve is Equation (4-15) where K_M was calculated for a neutral hard sphere by Equation (4-2). 84

4-11 Schematic representation of cationic surfactant adsorption on the surface of a negatively charged Nuclepore membrane. . . 86

4-12 Streaming potential (ΔV) across a Nuclepore membrane with a nominal pore diameter of 300 Å versus pressure drop across the membrane (ΔP) before (▲) and after (●) the membrane was exposed to a cationic surfactant (CPC). The electrolyte solution was 1.0 mM KCl. 89

4-13 Surface charge density (σ_M) of a Nuclepore membrane with a nominal pore diameter of 300 Å as a function of KCl concentration with no surfactant present (■), with CPC present (●) and with TBAC present (▲). 91

4-14 The ratio of the intrapore micelle diffusion coefficient to the micelle diffusion coefficient in free solution for CPC micelles in a Nuclepore membrane with a nominal pore diameter of 300 Å (#1) versus the concentration of a supporting electrolyte (NaCl). The solid curve is Equation (4-15) where K_M was calculated for a charged hard sphere by Equation (4-3) using the program in the appendix. 93

4-15 The ratio of the intrapore micelle diffusion coefficient to the micelle diffusion coefficient in free solution for TBAC micelles in a Nuclepore membrane with a nominal pore diameter of 300 Å (#2) versus the concentration of a supporting electrolyte (NaCl). The solid curve is Equation (4-15) where K_M was calculated for a charged hard sphere by Equation (4-3) using the program in the appendix. 94

4-16 The ratio of the intrapore micelle diffusion coefficient to the micelle diffusion coefficient in free solution for SDBS micelles in a Nuclepore membrane with a nominal pore diameter of 300 Å (#3) versus the concentration of a supporting electrolyte (NaCl). The curve is Equation (4-15) where K_M was calculated for a neutral hard sphere by Equation (4-2). . 98

5-1 K for hydrocortisone in SDS versus concentration of NaCl. . . 103

5-2 K for testosterone in SDS versus concentration of NaCl. . . . 104

5-3 K for progesterone in SDS versus concentration of NaCl. . . . 105

5-4 Total concentration of hydrocortisone in the receptor phase (C_{ST2}) versus time (t) where the surfactant is Brij 35 (0.15 M NaCl); the nominal membrane pore diameter is 2000 Å, $C_{M10'}$ = 1.88 mM, $C_{M20'}$ = 0.13 mM and C_{ST10} = 9.12 x 10^{-4} M. (A) K = 0, (B) K = ∞, (C) C_{ST10} from aqueous solubility in Table 5-1, and (D) model calculations from Equation (2-42). 107

5-5 Total concentration of testosterone in the receptor phase (C_{ST2}) versus time (t) where the surfactant is Brij 35 (0.15 M NaCl); the nominal membrane pore diameter is 2000 Å, $C_{M10'}$ = 1.87 mM, $C_{M20'}$ = 0.14 mM and C_{ST10} = 1.57 x 10^{-4} M. (A) K = 0, (B) K = ∞, (C) C_{ST10} from aqueous solubility in Table 5-1, and (D) model calculations from Equation (2-42). 108

5-6 Total concentration of progesterone in the receptor phase (C_{ST2}) versus time (t) where the surfactant is Brij 35 (0.15 M NaCl); the nominal membrane pore diameter is 2000 Å, $C_{M10'}$ = 1.80 mM, $C_{M20'}$ = 0.14 mM and C_{ST10} = 1.02 x 10^{-4} M. (A) K = 0, (B) K = ∞, (C) C_{ST10} from aqueous solubility in Table 5-1, and (D) model calculations from Equation (2-42). 109

5-7 Total concentration of testosterone in the receptor phase (C_{ST2}) versus time (t) where the surfactant is Triton-X 100 (0.15 M NaCl); $C_{M10'}$ = 2.7 mM, $C_{M20'}$ = 0.27 mM and C_{ST10} = 1.31 x 10^{-4} M, and the nominal membrane pore diameters are: ●, 4000 Å; ▲, 2000 Å; and ■, 500 Å. 111

5-8 Total concentration of hydrocortisone in the receptor phase (C_{ST2}) versus time (t) where the surfactant is SDS (0.15 M NaCl); the nominal membrane pore diameter is 300 Å, (#4) $C_{M10'}$ = 4.0 mM, $C_{M20'}$ = 1.0 mM and C_{ST10} = 1.53 x 10^{-4} M. (A) K = 0, (B) K = ∞, (C) C_{ST10} from aqueous solubility in Table 5-1, and (D) model calculations from Equation (2-42). 113

5-9 Total concentration of testosterone in the receptor phase (C_{ST2}) versus time (t) where the surfactant is SDS (0.15 M NaCl); the nominal membrane pore diameter is 300 Å, (#4) $C_{M10'}$ = 4.0 mM, $C_{M20'}$ = 1.0 mM and C_{ST10} = 5.0 x 10^{-4} M. (A) K = 0, (B) K = ∞, (C) C_{ST10} from aqueous solubility in Table 5-1, and (D) model calculations from Equation (2-42). 114

5-10 Total concentration of progesterone in the receptor phase (C_{ST2}) versus time (t) where the surfactant is SDS (0.15 M NaCl); the nominal membrane pore diameter is 300 Å, (#4) $C_{M10'}$ = 4.0 mM, $C_{M20'}$ = 1.0 mM and C_{ST10} = 5.1 x 10^{-4} M. (A) K = 0, (B) K = ∞, (C) C_{ST10} from aqueous solubility in Table 5-1, and (D) model calculations from Equation (2-42). 115

5-11 Total concentration of pyrene in the receptor phase (C_{ST2}) versus time (t) where the surfactant SDS; the nominal membrane pore diameter is 300 Å, (#5), $C_{M10'}$ = 4.0 mM, $C_{M20'}$ = 1.0 mM and C_{ST10} = 4.05 x 10^{-5} M. (A) K = 0, (B) K = ∞, (C) C_{ST10} from aqueous solubility in Table 5-1, and (D) model calculations from Equation (2-42). 118

5-12 Total concentration of pyrene in the receptor phase (C_{ST2}) versus time (t) where the surfactant is Brij 35 (0.15 M NaCl); the nominal membrane pore diameter is 300 Å, (#6), $C_{M10'}$ = 4.0 mM, $C_{M20'}$ = 1.0 mM and C_{ST10} = 1.0 x 10^{-4} M. (A) K = 0, (B) K = ∞, (C) C_{ST10} from aqueous solubility in Table 5-1, and (D) model calculations from Equation (2-42). 119

5-13 Total concentration of pyrene in the receptor phase (C_{ST2}) versus time (t) where the surfactant is TBAC (no salt); the nominal membrane pore diameter is 300 Å (#7), $C_{M10'}$ = 2.5 mM, $C_{M20'}$ = 1.5 mM and C_{ST10} = 1.4 x 10^{-4} M. (A) K = 0, (B) K = ∞, (C) C_{ST10} from aqueous solubility in Table 5-1, and (D) model calculations from Equation (2-42). 120

5-14 Total concentration of pyrene in the receptor phase (C_{ST2}) versus time (t) where the surfactant is TBAC, the nominal membrane pore diameter is 300 Å (#7), $C_{M10'}$ = 2.5 mM, $C_{M20'}$ = 1.5 mM and C_{ST10} = 1.4 x 10^{-4} M. This experiment was run with and without NaCl. 123

5-15 Fluorescence emission spectrum of 2 x 10^{-5} M pyrene in n-butanol where the excitation wavelength was 336 nm. 124

5-16 Solubility of pyrene relative to its aqueous solubility versus surfactant concentration for SDS, ●; Brij 35, ■; and TBAC, ▲. All surfactant solutions are below the CMC. 127

5-17 Total concentration of progesterone in the receptor phase (C_{ST2}) versus time (t) where the surfactant is Triton-X 100, the nominal membrane pore diameter is 2000 Å, $C_{M10'}$ = 2.69 mM and $C_{M20'}$ = 0.24 mM. (a) 80% saturation (C_{ST10} = 1.01 x 10^{-4}M), ●; (b) 62% saturation (C_{ST10} = 7.80 x 10^{-5} M), ▲; (c) 31% saturation (C_{ST10} = 3.89 x 10^{-5} M), ■; and (d) the delivery that would be obtained from a saturated aqueous solution (C_{ST10} from Table 5-1). 131

6-1 Schematic of a water-in-oil microemulsion. 135

6-2 Molecular structures of AOT and Arlacel 20. 138

6-3 Maximum water-to-oil volume ratio (χ) and drop volume (V_d) versus weight ratio of AOT and Arlacel 20 in hexadecane. . . . 140

6-4 Maximum water-to-oil volume ratio (χ) versus initial concentration of surfactants in hexadecane (C_S) for various ratios of AOT to Arlacel 20. 143

6-5 Maximum water-to-oil volume ratio (χ) and drop height versus NaCl concentration for AOT and Arlacel 20 (1:1) in hexadecane. The initial concentration of surfactants in oil was 40% w/v. . 144

6-6 Maximum water-to-oil volume ratio (χ) versus initial concentration of surfactants in hexadecane (C_S) for various NaCl concentrations with AOT and Arlacel 20 (1:1). 145

6-7 Maximum water-to-oil volume ratio (χ) versus weight ratio of AOT and Arlacel 20 in hexadecane for various concentrations of NaCl. 148

6-8 Maximum water-to-oil ratio (χ) and drop volume (V_d) versus oil chain length with AOT and Arlacel 20 (1:1) where the initial surfactant concentration was 40% w/v. 149

6-9 Maximum water-to-oil volume ratio (χ) versus initial concentration of surfactants in oil (C_S) for various oil chain lengths with AOT:Arlacel 20 1:1. 150

6-10 Maximum water-to-oil volume ratio (χ) versus weight ratio of AOT and Arlacel 20 for various hydrocarbons. 153

6-11 Hydrodynamic radius of microemulsion droplets in hexadecane (r_M) versus volume fraction of water (ϕ_w) where the initial concentration of AOT and Arlacel 20 (1:1) was 1.0% w/v. . . . 154

LIST OF SYMBOLS

Roman Letters

A	membrane pore area, cm^2
A_m	exposed membrane area between the gaskets in diffusion cell, cm^2
A_d	area of membrane disk, cm^2
C_i	concentration of species i
D_i	diffusion coefficient of species i, cm^2/s
$D_{M\infty}$	diffusion coefficient of micelle in free solution, cm^2/s
D_{Mp}	diffusion coefficient of micelle in pore based on local concentration of micelles, cm^2/s
e	proton charge
f	coefficient of friction
F	Faraday's constant
g	gravitational constant
I	intensity, arbitrary units
J	flux, moles/area-time
k	Boltzmann's constant
K_M	micelle partition coefficient into membrane pore
K^*	partition constant for solute between micelle and water where the micelle concentration is C_M, mM^{-1}
K	partition constant for solute between micelle and water where the micelle concentration is $C_{M'}$, mM^{-1}
L	membrane thickness, cm
n	micelle aggregation number
n_c	number of carbon atoms in the hydrophobic tail of a surfactant
n_p	pore density, pores/cm^2
P	pressure
q	number of counter-ions bound to micelle
r_M	micelle radius, Å
r_p	membrane pore radius, Å
R	gas constant
R_0	total mass transfer resistance, s/cm

R_m membrane mass transfer resistance, s/cm

R_i rate of solute exchange between the micellar and aqueous phases

W weight of membrane disk, g

S dimensionless surface charge density

t time

V_1 volume, Side 1 of diffusion cell, cm^3

V_2 volume, Side 2 of diffusion cell, cm^3

V_d drop volume, µl

V_f flow rate, cm^3/s

V_{HC} volume of a surfactant's hydrocarbon tail, $Å^3$

V_{HG} volume of a surfactant's polar head group, $Å^3$

Y dimensionless streaming potential

z valence

Greek Letters

α degree of dissociation for a charged micelle

β diffusion cell constant, $A/L(1/V_1 + 1/V_2)$

γ interfacial tension

ε permitivity

ζ zeta potential, mV

η viscosity

θ ratio of the distance of the particle's center from the axis of the pore to the radius

κ reciprocal of the Debye length, $Å^{-1}$

κ_b conductivity, µs/cm

λ wavelength, nm

λ_M slope of conductance versus surfactant concentration above the CMC

λ_0 slope of conductance versus surfactant concentration below the CMC

ν slope of streaming potential versus pressure drop plot

ξ ratio of particle to pore radius

ρ membrane density, g/cm^3

σ surface charge density, $\mu C/cm^2$

τ ratio of Debye length to pore radius

φ electrical potential, mV

χ maximum water to oil volume ratio in microemulsions

ψ surface potential, mV

Ψ dimensionless surface potential

Subscripts

SA	free solute
M	micelle
SM	micelle-solubilized compound
ST	total solute, SA + SM
E	supporting electrolyte
F	fluorophore
Q	quencher
S	surfactant
i	species (e.g. SA, M, SM or ST)
1	side 1
2	side 2
0	initially, at t=0

Abstract of Dissertation Presented to the Graduate School
of the University of Florida in Partial Fulfillment of the
Requirements for the Degree of Doctor of Philosophy

TRANSPORT OF MICELLE-SOLUBILIZED COMPOUNDS THROUGH MICROPOROUS MEMBRANES

By

Keith A. Johnson

December 1987

Chairman: Dr. Dinesh O. Shah
Major Department: Chemical Engineering

The effect of solubilization by micelles on the transport of compounds across synthetic microporous membranes has been studied theoretically and experimentally. The theoretical model, which accounts for the flux of free compound as well as the micelle-solubilized compound, required the following parameters: micelle and solute diffusion coefficients in free solution, the distribution coefficient of the solute between the bulk and micellar phases, and micelle and membrane pore radii. The compounds of interest (hydrocortisone, testosterone, progesterone and pyrene) were solubilized in nonionic, anionic and cationic surfactant micelles. Factors influencing the solubilization of water in water-in-oil microemulsions were also investigated.

The effects of micelle/pore interactions (e.g. electrostatic, hydrodynamic and steric) on intrapore micelle diffusion coefficients were studied experimentally and compared with calculations for the hindered

diffusion of neutral and charged spheres in neutral and charged cylindrical pores. Interactions between the micelle and the pore wall were important since micelle diffusion was studied in pores whose radii were as small as three times the micelle radius and in solutions with low ionic strengths where the Debye length was significant when compared to the pore size. In general, data on micelle diffusion were in agreement with theoretical calculations when the experimental conditions were within the constraints for which the models were developed.

In the absence of specific interactions between the solute and the surfactant head group, calculations using the model for the transport of micelle-solubilized compound across microporous membranes were in agreement with experimental data. However, when attractive interactions existed between the solubilizate and the surfactant head group, the solute delivery predicted by the model was lower than the experimental results. It was proposed that when specific solute/surfactant interactions existed, additional diffusion processes (e.g. monomer facilitated or surface diffusion), which were neglected in the model, made significant contributions to the transport of the solute across the membrane. The application of this model to the design of controlled release devices is also discussed.

CHAPTER 1
INTRODUCTION

Surface Active Agents and Solubilization

Surface active agents, or surfactants, are substances that exhibit a marked tendency to adsorb at a surface or interface because they are amphipathic; that is, they are single molecules with both polar and nonpolar functional groups [1]. Surfactants can adsorb at interfaces found between two immiscible liquids, a liquid and a gas or a liquid and a solid. Surfactants adsorbed at interfaces can dramatically reduce the interfacial tension [2,3]. Low interfacial tensions are beneficial in such processes as wetting, foam generation and emulsion stabilization.

Surfactant monomers form aggregates called micelles above a certain surfactant concentration known as the critical micelle concentration or CMC [1,4]. Figure 1-1 is a schematic of a micelle in an aqueous solution where the polar head groups of the surfactant monomers (represented by circles) are oriented toward the surface of the micelle while the nonpolar tails (represented by lines) are oriented toward the micellar core. Monomers in the aqueous phase are in equilibrium with the monomers in the micelle. Physicochemical studies (e.g. light scattering, fluorescence and osmotic pressure) on micellar solutions have shown that micelles may contain 30 to 100 or more monomers and have dimensions ranging from 50 to more than 100 Å in diameter [5-9]. While in most cases micelles are assumed to be spherical, they may be shaped like prolate ellipsoids, oblate ellipsoids or cylinders [6,9,10]. Even

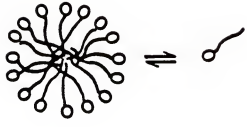

Figure 1-1. Schematic of a surfactant micelle in an aqueous solution.

though Figure 1-1 represents the micelle as a static assembly of molecules, it is important to note that micelles are quite dynamic. Rapid exchange of monomers in the aqueous phase with monomers in the micelle occurs on time scales ranging from microseconds to milliseconds [11,12].

Solubilization is defined as the spontaneous dissolution of a gas, liquid or solid by reversible interactions with surfactant micelles [4,13]. The result of micellar solubilization is a thermodynamically stable, isotropic solution of a compound that is insoluble or only partially soluble in the solvent. The core of the micelle is nonpolar while the region closer to the head group, also known as the palisade layer, is polar. Therefore, a compound with low aqueous solubility can be solubilized at various regions within the micelle and where the locus of solubilization depends on the structure of the solute and of the surfactant [4,13,14]. Hydrocarbons such as decane are solubilized within the micellar core while semipolar molecules like butanol are solubilized in the palisade layer [4,13,14]. The solubilization capacity of the micelle, or the maximum amount of solute that can be incorporated into the micelle, is also a function of the micelle and solute structures.

The ability to enhance the solubility of a poorly soluble compound has many important applications. In the pharmaceutical industry, drugs that are not soluble in water may be solubilized in a formulation that contains surfactant micelles [14]. The removal of soil or detergency is another process that depends on solubilization in surfactant micelles [15,16]. Solubilization in surfactant solutions is also important in enhanced oil recovery [17] and in micelle-enhanced ultrafiltration of organic pollutants from wastewater [18].

Whenever surfactants are used to enhance the solubility of a compound in a particular process, the solubility of the compound is not the only property that changes. For example, the chemical stability of the solute may be altered when solubilized in a micelle [19,20]. Furthermore, the mobility or diffusion coefficient of a solute will be reduced since, in general, micelles are larger than the solutes [21-23]. When the mobility of a micelle-solubilized compound is further reduced by the presence of a barrier (e.g. a porous or nonporous membrane), the interaction of the micelle with this barrier is important as well as the interaction of the solute with the barrier. The micelle-barrier and micelle-solute interactions are the focus of this work.

Surfactants and Synthetic Membranes

Consider the nonporous and the porous synthetic membranes in Figures 1-2 and 1-3, respectively. Each membrane separates a compartment containing a surfactant solution above the CMC from a compartment containing a surfactant solution below the CMC. To reduce this concentration gradient, surface molecules must diffuse from the high concentration (donor) side to the low concentration (receptor) side. Assuming both sides of the membrane are well stirred, the membrane is the only resistance to mass transfer.

Surfactant monomers may pass through the nonporous membrane (Figure 1-2) by partitioning into the membrane material and diffusing through to the other side. Micelles are too large to pass through the nonporous membrane. This was demonstrated by Stroeve et al. [24] and Roy et al. [25] for the diffusion of a nonionic surfactant (Nonoxynol®-9, polyoxyethylene alkyl-phenol) through a nonporous ethylene vinyl acetate membrane. As long as the receptor side of the cell was below the CMC,

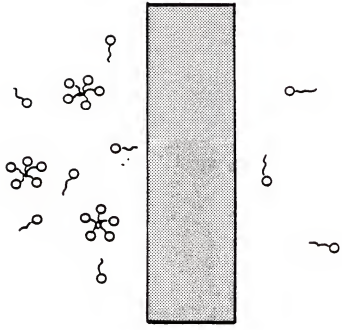

Figure 1-2. Schematic of a surfactant solution above the CMC in contact with a nonporous membrane.

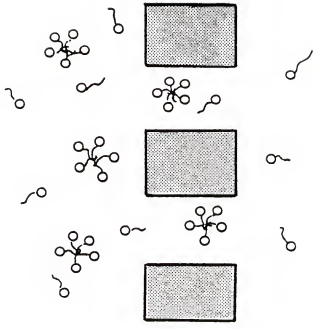

Figure 1-3. Schematic of a surfactant solution above the CMC in contact with a porous membrane. The pores of this membrane are large enough to allow the micelles to enter.

the surfactant diffused across the membrane. However, when the receptor side reached the CMC, the monomer concentrations on both sides of the cell were the same and no further mass transfer occurred.

If the solvent-filled pores of the porous membrane in Figure 1-3 are large enough, then micelles as well as surfactant monomer may pass through the barrier to the other side. This was also demonstrated with Nonoxynol-9 and Triton® X-100 (octylphenoxypolyethoxyethanol) diffusion through Millipore® and Celgard® microporous membranes [24-26]. The pore diameters of these membranes were approximately five times the diameter of the micelles.

There are two regimes of surfactant diffusion during an experiment such as that in Figure 1-3. If the concentration of surfactant in the receptor side is below the CMC, the transport of surfactant will be dominated by the faster moving surfactant monomers. Once the receptor side is above the CMC, there is a decrease in the surfactant flux. However, the surfactant flux does not stop as it does with experiments using nonporous membranes. The lower flux indicates that the surfactant transport is due to the diffusion of micelles since these aggregates are larger than monomers and have a lower mobility. The diffusion coefficients of nonionic micelles measured in microporous membranes were less than the diffusion coefficients of these surfactant aggregates in free solution [24-26]. In other words, the mobility of the micelles was less inside the membrane even though the micelles were five times smaller than the pores. Therefore, the effect of the pore wall on the mobilty of the micelle must be examined.

Particle Diffusion in Microporous Membranes

Figure 1-4 is a schematic of a particle of radius r_M in a microporous membrane pore having a radius r_p. This particle may be a micelle, a globular protein or any spherical colloid. Due to the presence of the pore wall, the diffusion coefficient of the particle in the pore will be less than its diffusion coefficient in free solution unless $r_p \gg r_M$ [27-37]. This phenomenon is known as hindered diffusion. In general, as the ratio of the particle to pore radii increases, the diffusion coefficient of a particle in the pore decreases. Theoretical studies of hindered diffusion, using hard spheres in cylindrical pores as model systems, have yielded analytical expressions for the ratio of the intrapore to free solution diffusion coefficients as a function of the particle to pore size ratio [27-32]. Hindered diffusion experiments have also been performed using polystyrene latex spheres, asphaltenes and globular polymers as particles [33-37].

In addition to the hydrodynamic effect described above, the concentration of micelles in the pore may be different from that in free solution as illustrated in Figure 1-5. If the particle is a hard sphere, the center cannot approach the pore wall any closer than one particle radius. Therefore, the volume one particle radius away from the pore wall is excluded to the center of the particle. Hence, the concentration of particles in the pore will be less than the concentration of particles in solution unless $r_p \gg r_M$. This phenomena is exploited for the separation of macromolecules in size exclusion chromotography [38,39].

If there is a charge on the particle and a charge on the pore, the analysis of a particle partitioning into the pore is more complicated. For example, if the particle and pore have opposite charges, they will

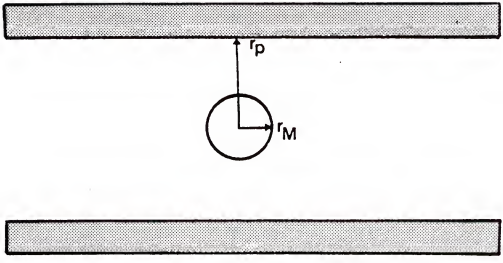

Figure 1-4. Schematic of a spherical particle translating in a solvent-filled pore.

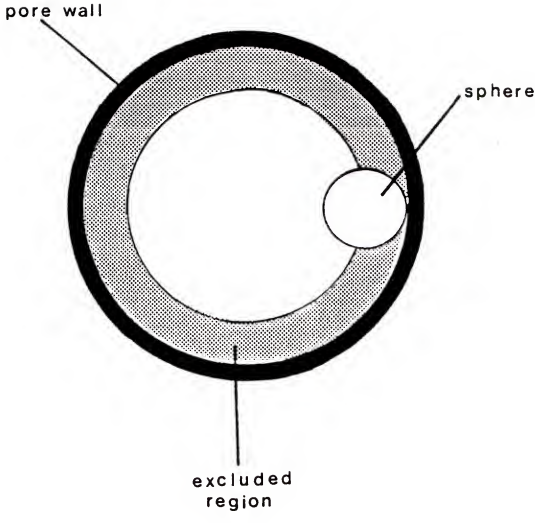

Figure 1-5. Schematic of a spherical particle partitioning into a solvent-filled pore. The shaded region is excluded to the particle since the center can approach the pore wall no closer than one particle radius.

attract each other and the concentration of particles in the pore may be greater than that for an uncharged sphere. However, if the charge on the particle and pore are the same, they will repel each other and the concentration of particles in the pore may be less than that for an uncharged sphere. Electrostatic effects on particles in microporous membranes have been studied by Uzelac and Cussler [40], Anderson and Quinn [41], and Smith and Deen [42,43]. Obviously, the relative sizes and charges of the micelles and the pore wall will greatly influence surfactant transport through the membrane.

Calculations for the diffusion coefficients of nonionic micelles in microporous membranes have been performed where it was assumed that the micelle is an uncharged hard sphere translating through a cylindrical pore or a slit [24-26]. In general, the calculated diffusion coefficients are in agreement (~10-15%) with experimental results even though micelles are not exactly "hard spheres." However, there have been no studies on the diffusion of ionic micelles in charged microporous membranes.

Previous Studies on Transport of Micelle-Solubilized Compounds Through Synthetic Membranes

As mentioned above, the improved solubility of a poorly soluble compound is not the only change in the solute's physical properties when micelles are used to enhance solubility. The mobility of the solute will change drastically since micelles are larger than most solutes. Amidon et al. [21] demonstrated that the mobility of a solute in a nonionic micelle was reduced in their studies of micelle-solubilized progesterone diffusion across the boundary layer of a synthetic, nonporous membrane. The reduced mobility of micelle-solubliized compounds has also been

studied by NMR self-diffusion [22] and Taylor dispersion tube techniques [23].

If the surfactant solution containing a solute is separated from a receptor compartment by a synthetic membrane, the solute transport is influenced by the micelle interaction with the membrane. For example, since micelles cannot pass through nonporous membranes [24,25], any solute in a micelle cannot pass through nonporous membranes. Only free solute in the aqueous phase, which is in equilibrium with solute in the micellar phase, can diffuse through a nonporous membrane. In this case, the solute-loaded micelles serve as a reservoir of the compound that must first partition out of the micelle before it can pass through the nonporous membrane. When free-solute leaves the donor side through the membrane, it is replenished with solute from the micelles [44]. This technique for controlling diffusion across nonporous membranes was demonstrated by Juni et al. [45,46] who studied the transport of micelle-solubilized benzocaine and butamben across ethylene vinyl acetate and silicone membranes. Cellophane membranes, which had pores that were too small to allow micelles to permeate, were used in a study by Withington and Collett [47] on micelle-solubilized salicylic acid diffusion to a receptor phase. Micelle-solubilized cholesterol diffusion across silicone membranes has been studied by Karth et al. [48]. These micelle-solubilized compound/nonporous membrane systems are advantageous in controlled release applications because more solute can be incorporated into the donor solution than possible without micelles. Furthermore, the micelle reservoir provides a more nearly constant rate of solute release through the membrane over a longer period of time.

Solute diffusion through membranes with pores large enough to accommodate the micelles has been studied by Krovvidi and Stroeve [49] who optimized the flux of micelle-solubilized n-heptane through microporous membranes. They found that the solubility of the hydrocarbon was proportional to the micelle size, and although the degree of hydrocarbon solubilization increased with micelle size, the membrane permeability of micelles decreased with micelle size. Hence, there was an optimum micelle size that maximized the n-heptane flux through a membrane. It may be advantageous to use porous membranes to control the release of micelle-solubilized compounds since the solute in the micelle, as well as the solute in the aqueous phase, can permeate the membrane. Therefore, microporous membranes, with pores large enough to accommodate a micelle, were used in the present study of transmembrane micelle and micelle-solubilized compound diffusion.

Scope and Significance

This work reports theoretical and experimental results for the diffusion of micelle-solubilized compounds through microporous membranes. The Nuclepore® membranes used in this study were track-etched polycarbonate films with uniform, cylindrical pores having low tortuosity. Four compounds with a wide range of aqueous solubilities (hydrocortisone, testosterone, progesterone and pyrene) were used in experiments with anionic, cationic and nonionic surfactants. These studies concentrated on solute partitioning between micelles and the aqueous phase, and how this partitioning affects solute transport through a microporous membrane. The importance of electrostatic effects on the diffusion of ionic micelles through charged pores was also examined.

The significance of this work is based on its applicability to technologically relevant problems, such as controlled release, and on the diversity of surfactant/solute systems studied. For example, in the pharmaceutical industry, surfactants are used in many applications: to solubilize drugs, to alter biological membrane permeability, to form emulsions and to reduce decomposition of drugs in solution [14,50-53]. Whenever surfactants are used, it is important to assess the effect of surfactant-drug interactions on the bioavailability of the drug. When the availability of drugs in surfactant solutions is reduced by the presence of a porous membrane, the effects of surfactant-membrane interactions as well as surfactant-drug interactions must be taken into account. The present work addresses some of these problems.

The model for the transport of micelle-solubilized compounds through microporous membranes is presented in Chapter 2. This model accounts for the flux of free solute as well as that solubilized in the micelle. Other transmembrane transport processes such as surface diffusion [54] or monomer-facilitated diffusion [55] were neglected. The theoretical model requires the following parameters: micelle and solute diffusion coefficients in free solution, the distribution coefficient of the solute between the bulk and micellar phases, and micelle and membrane pore radii and surface charges. The details of experimental techniques used to measure micelle and solute transport and to obtain parameters for the model are in Chapter 3.

The diffusion of micelles, ionic and nonionic, in free solution and in microporous membranes is discussed in Chapter 4. Experimental measurements of intrapore micelle diffusion coefficients are compared with theoretical calculations [27-32,43] that account for the steric,

electrostatic and hydrodynamic hindrances experienced by colloidal particles in micropores. The calculations assume that micelles can be treated as neutral or charged hard spheres diffusing in neutral or charged cylindrical pores. Studies on micelle charge and the effect of surfactants on membrane pore wall charge are also presented in this chapter.

Chapter 5 compares the results of experiments on the transport of micelle-solubilized compounds through microporous membranes with calculations using the model that is presented in Chapter 2. It was found that the model developed in Chapter 2 is capable of predicting the transport of micelle-solubilized compounds when there is no specific interaction of the solute with the surfactant head group. However, it is proposed that when specific surfactant/solute interactions exist, other transport paths may make significant contributions to the solute flux (i.e. facilitated or surface diffusion). The model described in Chapter 2 accounts only for free and micelle-bound solute diffusion. Deviations of model predictions from experimental results were correlated with measurments of solute affinity for the surfactant head groups.

While most of the work presented here concerns solubilization and transport of solutes in aqeous solutions, some aspects of solubilization in nonaqueous solvents were also studied in Chapter 6. The effect of oil chain length, surfactant weight ratio and salt on water solubilization in microemulsions using two high molecular weight surfactants was studied. This system is important because it can solubilize almost equal volumes of oil and water without using short-chain alcohols. The major conclusions and recommendations for future work are presented in Chapter 7.

CHAPTER 2
THEORY

In this chapter, the relevant equations describing the diffusion of micelles (nonionic and ionic) and micelle-solubilized compounds through microporous membranes are developed. These equations will be used in later chapters to analyze micelle diffusion data and predict diffusion of micelle-solubilized compounds.

Diffusion of Nonionic Micelles

Consider the diffusion experiment in Figure 2-1 where a porous membrane separates the two compartments of equal volume containing surfactant solutions that are both above the CMC. The concentration of surfactant in Side 1 is greater than that in Side 2. As a result, the surfactant will diffuse from Side 1 to Side 2. It is assumed that the monomer concentrations on each side of the membrane are the same since both sides of the cell are above the CMC and contain the same surfactant. Therefore, the surfactant transport will be due to micelles only. The flux of surfactant from the donor side (Side 1) is given by the following equation:

$$J_S = -nD_M dC_M/dx \qquad (2\text{-}1)$$

where n is the aggregation number or number of surfactant monomers in a micelle, D_M is the diffusion coefficient of the micelle, x is the coordinate parallel to the pore axis and C_M is micelle concentration. The right side of Equation (2-1) contains the factor n since each

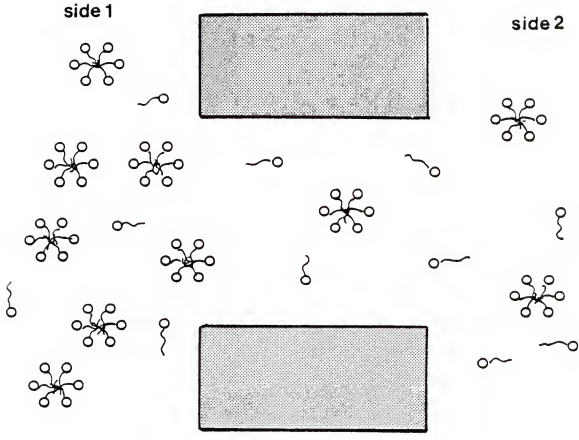

Figure 2-1. Schematic representation of micelle diffusion through a solvent-filled membrane pore. The membrane separated two compartments that are both above the CMC.

micelle contains n surfactant molecules. The micelle concentration is given by the following expression:

$$C_M = (C_S - CMC)/n \tag{2-2}$$

where C_S is the total surfactant concentration. If the membrane is very thin when compared to the volumes of Sides 1 and 2, a pseudo-steady state analysis of the diffusion process may be performed. By substituting (2-2) into (2-1) along with the concentration differences and the membrane thickness L for dC_M/dx, the following is obtained:

$$J_S = -D_M(C_{S2} - C_{S1})/L \tag{2-3}$$

The flux of the surfactant from Side 1 may also be expressed as

$$J_{S1} = -(V_1/A)dC_{S1}/dt \tag{2-4}$$

where V_1 is the volume of Side 1, A is the membrane area and t is time. By substituting (2-4) into (2-3) and rearranging terms, the following equation is obtained:

$$dC_{S1}/dt = AD_M(C_{S2} - C_{S1})/(LV_1) \tag{2-5}$$

A similar expression may be written for the rate of change of surfactant concentration in Side 2:

$$dC_{S2}/dt = -AD_M(C_{S2} - C_{S1})/LV_2) \tag{2-6}$$

If (2-5) is subtracted from (2-6) the difference is

$$d(C_{S2} - C_{S1})/dt = -\beta D_M(C_{S2} - C_{S1}) \tag{2-7}$$

where β is a constant equal to $A(1/V_1 + 1/V_2)$, and in this analysis $V_1 = V_2$. By integrating (2-7) with respect to time,

$$C_{S2}-C_{S1} = (C_{S20}-C_{S10}) \exp(-\beta D_M t) \qquad (2\text{-}8)$$

where C_{S10} and C_{S20} are the initial surfactant concentrations in Sides 1 and 2, respectively.

Diffusion of Ionic Micelles

The same diffusion experiment in Figure 2-1 is considered where the nonionic surfactant is changed to a monovalent, ionic surfactant. There will be no gradient of monomers since both sides to the membrane are above the CMC. However, there will be a concentration gradient of counter-ions as well as a concentration gradient of micelles. Following the treatment of a similar problem by Weinheimer et al. [56], the Nernst-Planck equation is written for the flux, J_i, of each ionic species i:

$$-J_i = D_i dC_i/dx + (F/RT) z_i C_i D_i d\phi/dx \qquad (2\text{-}9)$$

where z_i is the valence of the ionic species, ϕ is the electrical potential, F is Faraday's constant and R is the gas constant. Equations for the flux of micelles and the flux of counter-ions can be obtained from Equation (2-9) and then added together to give the following expression for the total surfactant flux, J_S: $-2J_S = (n+q) D_M dC_M/dx +$

$$(n+q)(F/RT) z_M C_M D_M d\phi/dx + D_C dC_C/dx + (F/RT) z_C C_C D_C d\phi/dx \qquad (2\text{-}10)$$

where the subscript M stands for micelles, the subscript C stands for counter-ions and q is the number of counter-ions bound to the micelle. The factor 2 on the left-hand side of Equation (2-10) accounts for the fact that when a surfactant monomer and a counter-ion cross the membrane, only one surfactant molecule has crossed the membrane. It is important to note that the diffusion coefficient of a counter-ion (D_C) is approximately an order of magnitude larger than the diffusion coefficient of a micelle (D_M).

Several substitutions can be made to simplify Equation (2-10). Using Equation (2-2), dC_M/dx is defined as follows:

$$dC_M/dx = (dC_S/dx)/n \tag{2-11}$$

The total counter-ion concentration may be expressed as

$$C_C = C_E + CMC + \alpha(C_S\text{-}CMC) \tag{2-12}$$

where C_E is the concentration of supporting electrolyte (the same on both sides of the membrane), CMC accounts for the dissociated surfactant monomer (also the same on both sides of the membrane) and α is the degree of dissociation of the micelle (i.e. the number of charges on the micelle divided by the micelle aggregation number). By differentiating Equation (2-12) with respect to x, the following equation is obtained:

$$dC_C/dx = \alpha dC_S/dx \tag{2-13}$$

Substituting (2-11) and (2-13) into (2-10) yields (2-14)

$$-2J_S = [(n+q)D_M/n + \alpha D_C]dC_S/dx + (F/RT)[(n+q)z_M C_M D_M + z_C C_C D_C]d\phi/dx$$

Since there is no net current flowing across the cell, the micellar and counter-ion fluxes must satisfy the following criteria:

$$\Sigma z_i J_i = 0 \tag{2-15}$$

Therefore, (2-16)

$$0 = z_M D_M dC_M/dx + (F/RT)z_M{}^2 C_M D_M d\phi/dx + z_C D_C dC_C/dx + (F/RT)z_C{}^2 C_C D_C d\phi/dx$$

Substituting Equations (2-11) and (2-13) into (2-16) and realizing that $z_C{}^2 = 1$ gives the following equation:

$$0 = [z_M D_M/n + \alpha D_C]dC_S/dx + (F/RT)[z_M{}^2 C_M D_M + C_C D_C]d\phi/dx \tag{2-17}$$

Solving Equation (2-17) for $d\phi/dx$ yields

$$d\phi/dx = -(RT/F)[z_M D_M/n + \alpha z_C D_C](dC_S/dx)/[z_M{}^2 C_M D_M + C_C D_C] \qquad (2\text{-}18)$$

When Equation (2-18) is substituted into Equation (2-14), the following equation is obtained: $-2J_S = [(n+q)D_M/n + \alpha D_C]dC_S/dx -$

$$\frac{[z_M D_M/n + \alpha z_C D_C][(n+q)z_M C_M D_M + z_C C_C D_C]dC_S/dx}{[z_M{}^2 C_M D_M + C_C D_C]} \qquad (2\text{-}19)$$

Equation (2-19) may be expressed as follows:

$$-2J_S = D_{eff} dC_S/dx \qquad (2\text{-}20)$$

where D_{eff} is

$$D_{eff} = (n+q)D_M/n + \alpha D_C - \frac{[z_M D_M/n + \alpha z_C D_C][(n+q)z_M C_M D_M + z_C C_C D_C]}{[z_M{}^2 C_M D_M + C_C D_C]} \qquad (2\text{-}21)$$

Equation (2-21) can be simplified under certain conditions where the concentration of supporting electrolyte is larger than the micelle concentration. If $|z_C C_C D_C| >> (n+q)z_M C_M D_M$ and $C_C D_C >> z_M{}^2 C_M D_M$ then the expression for D_{eff} reduces to

$$D_{eff} = (n+q)D_M/n + \alpha D_C - [z_M D_M/n + \alpha z_C D_C]z_C \qquad (2\text{-}22)$$

But, since $z_M = (n-q)$, D_{eff} reduces to $2D_M$. Therefore, if C_E is sufficiently large when compared to C_M, the flux of ionic surfactant micelles is given by

$$J_S = -D_M dC_S/dx \qquad (2\text{-}23)$$

where Equation (2-23) has the same form as Equation (2-3). Therefore, under the conditions specified above, the flux of an ionic surfactant

across a membrane may be analyzed by the same equation as that used for nonionic micelle diffusion (Equation (2-8)).

Diffusion of a Micelle-Solubilized Compound

The microporous membrane in Figure 2-2 separates two compartments which initially contain solutions having known concentrations of micelles and of solute. The solute is distributed in the micellar and aqueous phases of Side 1. Initially, Side 2 contains only micelles at a lower concentration than the micelle concentration in Side 1. Since the membrane is permeable to the micelles and to the solute, there are fluxes of both micelles and solute across the membrane. The two compartments are well-stirred so that boundary layer resistances to mass transfer are insignificant compared to the membrane resistance. Entrance effects are neglected.

It is assumed that the concentrations of solute in the micellar phase (C_{SM}) and in the aqueous phase (C_{SA}) may be expressed by an equilibrium constant K*:

$$K^* = C_{SM}/(C_{SA}C_M) \tag{2-24}$$

Since micelles diffuse more slowly than free solute, micelle-bound solute molecules do not pass through the membrane as rapidly as free solute, and hence, bound solute must be released from micelles in order to satisfy Equation (2-24). Because the solute transport process consists of simultaneous diffusion and reaction (free solute $\rightleftharpoons$ bound solute), the continuity equations for each species are written as

$$\partial C_i/\partial t = D_i \partial^2 C_i/\partial x^2 \pm R_i \tag{2-25}$$

where i is SA, M or SM, and where R_i is the rate of exchange of solute

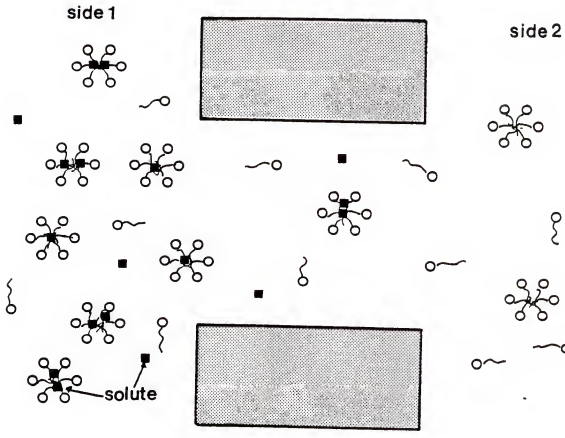

Figure 2-2. Schematic representation of two sides of a diffusion cell separated by a microporous membrane. Initially, side 1 contains micelles plus a solute while side 2 contains only micelles at a lower concentration than side 1.

between the micellar and aqueous phases whose sign depends on whether i is generated or consumed. The intramembrane diffusion coefficient of i is D_i, and D_{SM} and D_M are assumed to be equal; that is, the diffusivity of micelles is unaffected by solubilization of the compound (an experimental result discussed in a later section). Both bulk compartments are above the CMC, so the unmicellized monomer concentrations on both sides of the membrane are the same. Thus, the contribution of unmicellized monomer to transport processes is neglected.

For a micelle-solubilized compound, others have shown that the rate of exchange between free solution and micelles is generally quite fast [57,58]. Therefore, a diffusion-controlled process is assumed to exist, and R_i in Equation (2-25) is neglected. Furthermore, the membrane is thin compared to the dimensions of the diffusion cell, so a pseudo-steady state is assumed; that is, $\partial C_i/\partial t$ in (2-25) is set to zero. With these assumptions, Equation (2-25) is rewritten as

$$D_i d^2C_i/dx^2 = 0 \qquad (2\text{-}26)$$

By integrating Equation (2-26), one obtains

$$J_i = -D_i dC_i/dx \qquad (2\text{-}27)$$

where J_i is the flux of species i in moles/area-time.

Using the pseudo-steady state analysis on page 18, the following equation can be obtained for micelle diffusion across a microporous membrane:

$$C_{M2}-C_{M1} = (C_{M20} - C_{M10})\exp(-\beta D_M t) \qquad (2\text{-}28)$$

where C_{M10} and C_{M20} are the initial concentrations of micelles in Sides 1 and 2, respectively. A material balance on the diffusion cell with

respect to the micellar concentration yields

$$C_{M1} = C_{M10} - (C_{M2} - C_{M20}) \tag{2-29}$$

where the micelles inside the membrane are neglected since the membrane volume is very small compared to the volume of the diffusion cell. With two unknowns in Equations (2-28) and (2-29), C_{M1} and C_{M2} can be calculated at any time t if C_{M10}, C_{M20}, D_M and β are known:

$$C_{M1} = 0.5\{C_{M10} + C_{M20} - (C_{M20} - C_{M10})\exp(-\beta D_M t)\} \tag{2-30}$$

$$C_{M2} = 0.5\{C_{M10} + C_{M20} + (C_{M20} - C_{M10})\exp(-\beta D_M t)\} \tag{2-31}$$

By analogy with Equation (2-5), rates of change in concentration of free and of micelle-solubilized solute in Side 2 are

$$dC_{SA2}/dt = AD_{SA}(C_{SA1} - C_{SA2})/(LV_2) \tag{2-32}$$

$$dC_{SM2}/dt = A\Phi D_M(C_{M1} - C_{M2})/(LV_2) \tag{2-33}$$

where Φ is the molar ratio of micelle-solubilized compound to micelles in the donor phase (C_{SM1}/C_{M1}). It is important to note that C_{SA} and C_{SM} in both sides of the cell are related to the equilibrium distribution coefficient K* and C_M by Equation (2-24). When added, these rates of change yield the rate of change of the total solute concentration C_{ST2} in Side 2:

$$dC_{ST2}/dt = A[\Phi D_M(C_{M1} - C_{M2}) + D_{SA}(C_{SA1} - C_{SA2})]/(LV_2) \tag{2-34}$$

The relationships between the free, micelle-solubilized, and the total solute concentrations found from Equation (2-24) give

$$C_{ST} = C_{SM} + C_{SA} = C_{SA}(1 + K^*C_M) \tag{2-35}$$

Equation (2-35) can be arranged to give for C_{SA}

$$C_{SA} = C_{ST}/(1 + K^*C_M) \tag{2-36}$$

C_{ST} may also be expressed as

$$C_{ST} = C_{SM} + C_{SM}/(K^*C_M) = C_{SM}(1 + 1/(K^*C_M)) \tag{2-37}$$

After some algebraic manipulation, (2-37) becomes

$$C_{SM} = K^*C_MC_{ST}/(1 + K^*C_M) \tag{2-38}$$

When Equations (2-36) and (2-38) are substituted into Equation (2-34),

$$\frac{dC_{ST2}}{dt} = \frac{A}{LV_2}\left[\frac{K^*D_M(C_{M1}-C_{M2})C_{ST1}}{1 + K^*C_{M1}} + D_{SA}\left[\frac{C_{ST1}}{1 + K^*C_{M1}} - \frac{C_{ST2}}{1 + K^*C_{M2}}\right]\right] \tag{2-39}$$

The aggregation number, n, is required to calculate micelle concentrations and K*. The dependence on n can be eliminated by redefining the solute distribution coefficient and making the appropriate substitutions. A new distribution coefficient K is defined as

$$K = C_{SM}/(C_{SA}C_{M'}) \tag{2-40}$$

where $C_{M'}$ is the total surfactant concentration minus the CMC. K and K* are related by the following expressions:

$$K^* = nK \tag{2-41a}$$

$$K^*C_M = KC_{M'} \tag{2-41b}$$

If Equation (2-41a) is substituted into Equation (2-39) and n is factored out of all micelle concentrations, the following is obtained:

$$\frac{dC_{ST2}}{dt} = \frac{A}{LV_2}\left[\frac{KD_M(C_{M1'}-C_{M2'})C_{ST1}}{1 + KC_{M1'}} + D_{SA}\left[\frac{C_{ST1}}{1 + KC_{M1'}} - \frac{C_{ST2}}{1 + KC_{M2'}}\right]\right] \tag{2-42}$$

Now, measurement of n is not required in order to calculate certain parameters in Equation (2-42) as it was in Equation (2-39).

C_{ST1} is eliminated from Equation (2-42) by a material balance on the cell:

$$C_{ST1} = C_{ST10} - (C_{ST2} - C_{ST20}) = C_{ST10} - C_{ST2} \qquad (2\text{-}43)$$

where initially the total solute concentration in Side 2 (C_{ST20}) is zero. After substituting (2-43) for C_{ST1}, Equation (2-42) may be numerically integrated to find the total solute concentration in Side 2 (C_{ST2}) at any time. In the present work, Euler's method was used to integrate (2-42) where the constant required for the numerical solution are A/L, V_1, V_2, C_{M10}', C_{M20}', C_{ST10}, D_M, D_{SA} and K. The methods for experimentally determining these parameters are described in the next chapter. The model for release of a micelle-solubilized solute through a microporous membrane was derived with the following assumptions:

- pseudo-steady state diffusion
- fast exchange of the compound solubilized in micelles with the compound in free solution
- partitioning of the solute between the micellar and aqueous phases was independent of solute concentration
- interactions between micelles and pore walls can be modeled as neutral or charged hard spheres in neutral or charged cylindrical pores
- boundary layer and entrance effects were negligible when compared to the membrane resistance.

The assumptions for the interactions between micelles and pore walls result from the need to find intrapore diffusion coefficient D_M from the experimentally determined bulk solution diffusion coefficient $D_{M\infty}$ and micellar and pore radii, as discussed in Chapter 4. The validity of assuming negligible boundary layer resistance to mass transfer is discussed in the next chapter.

CHAPTER 3
EXPERIMENTS

This chapter describes the materials, instruments and methods used in diffusion experiments. The characterization of the surfactants, solutes and membranes is also discussed.

Materials

Surfactants. Trjton-X 100 (Sigma), cetylpyridinium chloride (CPC, Aldrich), tetradecyltrimethylammonium bromide (TTAB, Aldrich), tetradecyldimethylbenzylammonium chloride (TBAC, Alpha), sodium dodecyl sulfate (SDS, BDH) and sodium dioctyl sulfosuccinate (AOT, American Cyanamid) were used without further purification. All Atlas® surfactants (Brij®, Arlacel®, Tween® and Arlatone®) listed in Table 3-1 were donated by ICI Americas, Inc., and were used without further purification. Sodium dodecyl benzene sulfonate (SDBS) was donated by Alcolac and was purified by the method of Cheng and Gulari [6].

Solutes and fluorescent molecules. Hydrocortisone (Sigma), testosterone (Sigma), progesterone (Sigma), pyrene (Aldrich), 9-methylanthracene (Aldrich) and ruthenium bipyridine (F. G. Smith) were used without further purification.

Salts and reagents. Sodium chloride and alkanols were purchased from Fisher Scientific, and potassium chloride was purchased from Baker Scientific. All reagents were used without further purification.

Membranes. Nuclepore membranes used in this study had nominal pore diameters of 300, 500, 2000 and 4000 Å.

Table 3-1. Chemical Composition* of ICI Surfactants Used in this Study

Product	Chemical Composition
Arlacel C	Sorbitan sesquioleate
Arlacel 20	Sorbitan monolaurate
Arlatone T	Polyoxyethylene 40 sorbitol septaoleate
Brij 30	Polyoxyethylene 4 lauryl ether
Brij 35	Polyoxyethylene 23 lauryl ether
Brij 52	Polyoxyethylene 2 cetyl ether**
Brij 93	Polyoxyethylene 2 oleyl ether**
Tween 61	Polyoxyethylene 4 sorbitan monolaurate
Tween 81	Polyoxyethylene 5 sorbitan monolaurate

*information from ICI Americas, Inc., Wilmington, DE 19897

**contains 0.01% BHA and 0.005% citric acid as preservatives

Diffusion Measurements

Diffusion Cell

In the diagram of the diffusion cell in Figure 3-1, the membrane is held between the two glass half-cells by either Neoprene® or Teflon® gaskets with inside diameters of 1.9 and 2.0 cm, respectively. The volume of each half-cell was 19.5 or 18.5 ml with Neoprene or Teflon gaskets, respectively. A Teflon-coated, magnetic stir-bar extended into each half-cell from a Teflon stopper. When the half-cells were clamped together, the stirrers were rotated by an external magnet. The stirrer speed was kept at 300 ± 10 rpm. The temperature during all diffusion experiments was 25 ± 1°C. To remove dust that could clog pores, all solutions were filtered through membranes (Gelman Sciences) with 0.2 μm pore diameters.

The importance of the gasket material is demonstrated in Figure 3-2 where the total amount of pyrene in the diffusion cell relative to the initial amount is plotted versus time. Approximately 50% of the pyrene was absorbed by the Neoprene gaskets over eight hours while the pyrene loss with Teflon gaskets was negligible. Neoprene gaskets did not absorb the other solutes or any surfactants and provided a tighter seal for the cell than Teflon gaskets. However, Teflon gaskets were used in all experiments involving pyrene diffusion.

Micelle Diffusion Measurements

Micelle diffusion coefficients in microporous membranes were determined by the experiment illustrated in Figure 2-1 where a porous membrane separates the two compartments of equal volume containing surfactant solutions that are both above the CMC. The concentration of

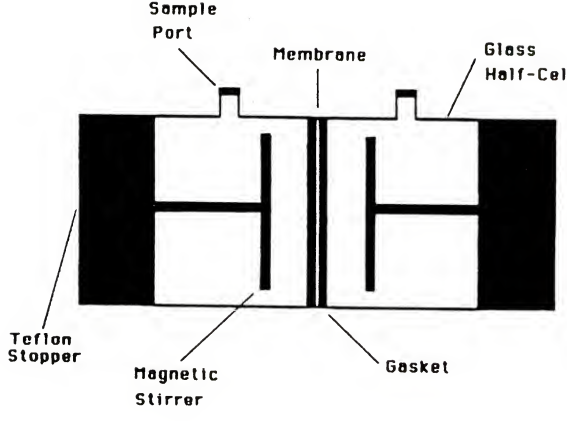

Figure 3-1. Schematic of the glass and Teflon diffusion cell used in experiments. Stirrers were rotated by an external magnet.

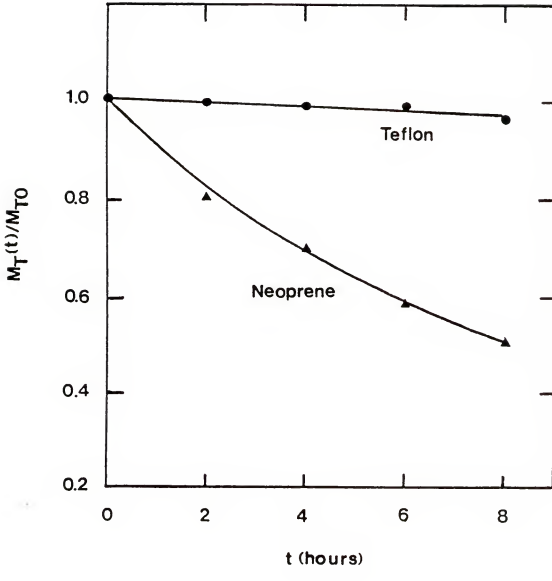

Figure 3-2. Total mass of pyrene in the diffusion cell at time t ($M_T(t)$) relative to the initial mass of pyrene in the cell (M_{TO}) versus time when Neoprene or Teflon gaskets were used to seal the cell. Pyrene was absorbed by the Neoprene gaskets but not by the Teflon gaskets.

surfactant in Side 1 (donor phase) is greater than that in Side 2 (receptor phase). Calculations of intrapore micelle diffusion coefficients were made from measurements of the bulk concentration of surfactant in the donor and receptor phases at various times. The micelle diffusion coefficient was determined from this data by fitting it to a rearranged version of Equation (2-8):

$$\ln[\Delta C_{SO}/\Delta C_S(t)] = \beta D_M t \qquad (3\text{-}1)$$

where ΔC_{SO} and $\Delta C_S(t)$ are surfactant concentration differences across the cell initially (t=0) and at time t, respectively. The slope of a plot of $\ln[\Delta C_{SO}/\Delta C_S(t)]$ versus time is the product of the cell constant β and the intrapore micelle diffusion coefficient D_M.

Before each micelle diffusion coefficient experiment (and every diffusion experiment involving surfactants), the membrane was exposed to a surfactant solution above the CMC for at least 12 hours to allow equilibration. When CMC data were not available, they were obtained by surface tension or conductivity measurements as a function of surfactant concentration [59]. The cell was filled with the filtered micellar solutions where the concentration of micelles on the donor side of the cell was higher than that of the receptor side. Samples ($\sim$1 ml) were withdrawn from each side of the cell at various times; the solutions were analyzed by absorbance spectrophotometry (Perkin-Elmer Model 576 ultraviolet/visible spectrophotometer) and finally placed in the diffusion cell. The sampling process required approximately three minutes. Data for such an experiment are in Figure 3-3 for CPC micelles diffusing across a Nuclepore membrane having pores with nominal diameters of 300 Å. The slope, βD_M, can be obtained by a linear regression of the

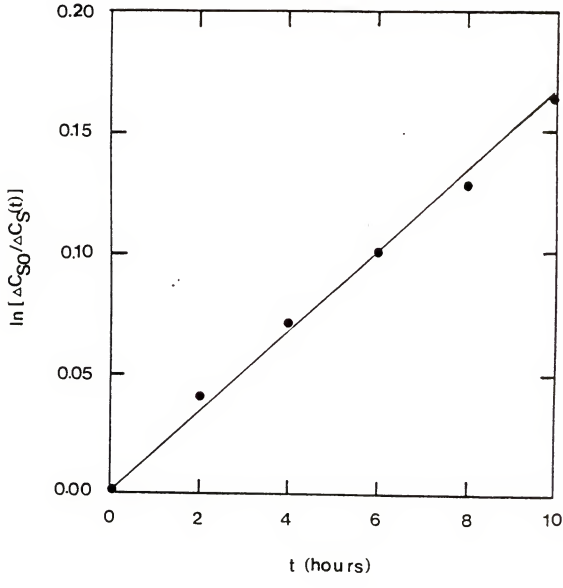

Figure 3-3. The natural logarithm of the initial surfactant concentration difference across the membrane (ΔC_{S0}) relative to the concentration difference at time t ($\Delta C_S(t)$) versus time for CPC micelles diffusing across a Nuclepore membrane with nominal pore diameters of 300 Å. The slope of this plot is βD_M.

data and the determination of β is discussed on page 6. The standard deviations of the micelle diffusion coefficient data were between 5 and 8%.

Solute Diffusion Measurements

Measurements of solute diffusion across microporous membranes were similar to micelle diffusion experiments. The receptor phase was a micellar solution containing no solute while the donor phase had a higher concentration of micelles than the receptor phase plus the solute. At the start of each experiment, the receptor phase was placed in one half-cell; the donor phase was then placed in the other half-cell, and the stirrers were started. The sampling procedure depended on the absorbance of the surfactant and the solute.

If the surfactant and the solute absorbed at different wavelengths or if the surfactant did not absorb at all, a 1 ml sample was withdrawn from the receptor side of the cell, analyzed for solute concentration by absorbance spectrophotometry, then replaced. If both molecules absorbed at the same wavelength, the following procedure was used. At various times, samples (0.4 ml) were withdrawn from the receptor half-cell and immediately replaced with the same amount of fresh receptor phase. The absorbance of samples from the receptor phase was determined in a high-pressure liquid chromatograph (HPLC). This method allowed the determination of solute concentrations without interference from the surfactant. The dilution of the receptor phase was taken into account in all calculations by adding the mass of solute removed at each withdrawal (i.e., 0.4 ml times C_{ST2}) to all subsequent data points.

Membrane Characterization

Membranes with Nominal Pore Diameters > 300 Å

Membrane pore diameters (r_p) and pore densities (n_p) were checked for three membranes from each package using electron microscopy. Carbon-platinum replicas of membranes with nominal pore diameters of 500 Å were examined with transmission electron microscopy (TEM), and membranes with 2000 and 4000 Å nominal pore diameters were examined by scanning electron microscopy (SEM) after being sputter-coated with gold. The results of these examinations of membranes are in Table 3-1. During examination of the carbon-platinum replicas with TEM, it was apparent that many pores were covered over but not penetrated by the coating, leaving vague depressions rather than definite outlines in the replica, and thus complicating the pore density determination. Figure 3-4 is a sample TEM of a carbon-platinum replica of a Nuclepore membrane with nominal pore diameters of 500 Å. Pore diameters from these replicas were determined only from pores that clearly went through the replica. Thus, the pore diameters and densities for the larger pores in Table 3-1 are reliable, and the pore diameter reported for the membranes with nominal pore diameters of 500 Å is reasonable, but because of the difficulties encountered in making carbon-platinum replicas, the pore density reported for the 500 Å pores is unreliable.

The ratio of pore area to pore length (membrane thickness) A/L for a membrane was measured by hydrocortisone diffusion ($D_{SA} = 4.24 \times 10^{-6}$ cm^2/s) through the membrane [60]. The cell constant β was obtained from the slope of a plot of $\ln[\Delta C_{SA0}/\Delta C_{SA}(t)]$ versus time (analogous to micelle diffusion coefficient measurements on page 33). The standard deviations for the hydrocortisone diffusion data were between 3 and 4%.

Table 3-2. Membrane Pore Diameters and Pore Densities from Electron Microscopy

Nominal Membrane Pore Diameter, Å	Pore Diameter Electron Microscopy	Number of Pores/cm^2 x 10^{-8} from Electron Microscopy
500	528 ± 54	3.6 ± 1.2
2000	1730 ± 190	3.2 ± 0.2
4000	3820 ± 306	1.1 ± 0.08

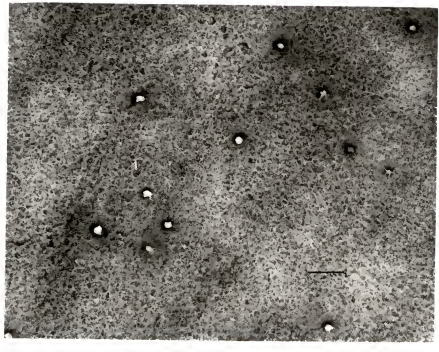

Figure 3-4. Carbon and platinum replica of a Nuclepore membrane with nominal pore diameters of 500 Å viewed by a transmission electron microscope. The bar represents 2600 Å.

Since the volumes of each half-cell were known, A/L was easily calculated (see Equation (2-7)). The results for A/L from hydrocortisone diffusion experiments are in Table 3-2. Using the average pore diameters and densities found with electron microscopy, but taking the pore length to be that stated by the manufacturer, values of A/L were calculated from electron microscopy (see Table 3-2). With the exception of the 500 Å pores, the values of A/L from electron microscopy agreed reasonably well with those from the diffusion experiments. The poor agreement between A/L from electron microscopy and from hydrocortisone diffusion for the 500 Å membranes could be a result of poor replication by the carbon-platinum coating process, as discussed above.

Membranes with Nominal Pore Diameters of 300 Å

Because of the problems encountered in making carbon-platinum replicas, membranes with nominal pore dimeters of 300 Å were characterized by a combination of three independent experiments. The ratio of membrane area to pore length is given by the following expression:

$$A/L = A_m(\pi n_p r_p^2)/L \qquad (3\text{-}2)$$

where A_m is the membrane area exposed between the gaskets and the factor $\pi n_p r_p^2$ is the membrane porosity. The measurement of A/L values was discussed in the previous section. L was determined by measuring the membrane weight (W) and correcting for porosity and pores that are not aligned normal to the surface (0 to 29° from the normal) as follows [61-63]:

$$L = 1.068W/([1 - \pi n_p r_p^2]\rho A_d) \qquad (3\text{-}3)$$

Table 3-3. Comparison of the Ratios of Membrane Pore Area-to-Thickness (A/L) from Hydrocortisone Diffision and Electron Microscopy

Nominal Membrane Pore Diameter, Å	A/L from Hydrocortisone Diffusion, cm	A/L from Electron Microscopy, cm	Agreement, %
500	84.2 ± 4.7	44.7	47.3
2000	242. ± 10.	213.	11.8
4000	390. ± 16.	357.	8.3

where A_d is the area of the membrane disk (3.7 cm diameter), ρ is the density of polycarbonate (1.19 g/cm^3) and the factor 1.068 accounts for pore alignments deviating from the normal. The Poiseuille equation for fluid flow through the membrane pores is [62]

$$V_f/\Delta P = \pi n_p r_p^4 A_m/(8\eta L) \qquad (3\text{-}4)$$

where V_f is the flow rate, ΔP is the pressure drop across the membrane and η is the viscosity of the fluid. Equations (3-2) to (3-4) are a set of three equations with three unknowns (n_p, r_p and L) that can be solved with data from the following experiments: 1) hydrocortisone diffusion to determine A/L,2) weighing the membrane to determine W and 3) measurement of water flow through the membrane under an applied pressure gradient to determine $V_f/\Delta P$.

The results for water flow through a Nuclepore membrane (mounted in the diffusion cell) under a pressure gradient are in Figure 3-5. The flow rate was measured by a calibrated capillary tube while the pressure gradient was provided by an elevated funnel of water. Standard deviations of the data for pressure drop/flow rate experiments were between 2 and 3%. Deen et al. [62] reported that irreversible deformation of Nuclepore membranes occurred when pressure gradients higher than ~40 cm of water were applied. The burst pressure reported by the membrane manufacturers was ~1 atm. or 33.9 ft. of water [61]. In this work the applied pressure was always less than 20 cm of water in all pressure drop/flow rate experiments. The results of these membrane characterization experiments with Nuclepore membranes having nominal pore diameters of 300 Å are presented in Table 3-3. Even though the pore radii deviated significantly from that reported by the manufacturer, they

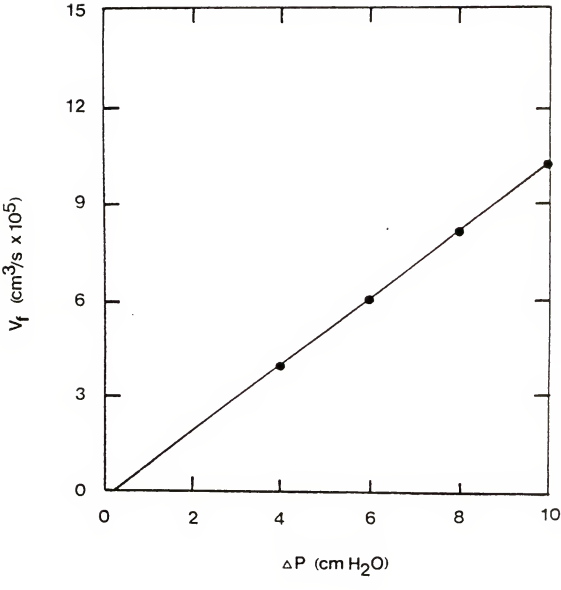

Figure 3-5. Flow rate of water through a Nuclepore membrane with nominal pore diameters of 300 Å (V_f) versus pressure drop across the membrane.

Table 3-4. Pore Size, Pore Density and Pore Length for Membranes with Nominal Pore Diameters of 300 Å

Membrane Number	Pore Radius	Pores/cm^2 x 10^{-8}	Pore Length, μm
1	315	5.72	5.97
2	296	7.13	6.05
3	278	6.79	5.91
4	272	8.80	6.15
5	283	8.75	6.10
6	305	8.34	5.90
7	290	6.10	5.93

were in agreement with the results of other researchers [64-66]. This procedure was repeated for each of the membranes with nominal pore diameters of 300 Å used in this study.

Boundary Layer Resistance

The assumption of negligible boundary layer contribution to mass transfer resistance (R_b) was tested as follows. The overall resistance to mass transfer of the diffusion cell R_0 may be determined from the following relationship [62,63]:

$$\ln(\Delta C_o/\Delta C(t)) = 2A_m t/(VR_0) \qquad (3\text{-}5)$$

where ΔC_o and $\Delta C(t)$ are the concentration differences of the diffusing solute across the membrane initially and at time t, respectively. The membrane resistance to mass transfer R_m is given by [62,63]

$$R_m = L/(\pi n_p r_p^2 D) \qquad (3\text{-}6)$$

For membranes with nominal pore diameters of 2000 and 4000 Å, R_0 was determined by hydrocortisone diffusion experiments in which concentration differences across the cell with time were measured by UV absorbance spectroscopy. Scanning electron microscopy was used to measure r_p and n_p for these membranes, and L was determined from the membrane weight and Equation (3-3). The values of r_p, n_p, L, R_m and R_0 are in Table 3-4. R_m was not calculated for the 500 Å membrane because of the difficulties in obtaining n_p from transmission electron micrographs of carbon-platinum replicas; in addition, the boundary layer resistance should have been even less important for the membranes with pore diameters of 500 Å or less due to the higher values of R_m (see Equation (3-6)).

In Table 3-4, R_m accounts for 92.7 and 89.3% of R_0 for the 2000 and 4000 Å membranes, respectively. Hence, the error in assuming negligible boundary layer resistance (an important assumption in the theoretical treatment) was small. For a Nuclepore membrane with nominal pore diameters of 300 Å, the value of R_m was ~8100 sec/cm and the measured values of R_b (R_0-R_m) were ~220 sec/cm or approximately 2.4% of R_m. It should be kept in mind that boundary layer resistance in practical situations may be significant if there is inadequate stirring. Furthermore, it should be noted that the values of A/L used in some calculations were found from solute diffusion experiments (Table 3-2) and, therefore, already contained small contributions from boundary layer resistances. Hence, while we neglected boundary layer resistances in theoretical derivations, and while the boundary layer contributions were small as shown here, the values of A/L actually used unavoidably contained contributions from boundary layer resistances.

Solubilization of Compounds by Micelles

The total concentration of solute C_{ST} that could be solubilized by a micellar solution was determined by adding a slight excess of solute crystals to an aqueous solution of known micelle concentration $C_{M'}$. After mixing at 25 °C for 96 hours, the suspension was filtered through a membrane with 0.2 μm diameter pores to remove undissolved crystals. The filtrate was diluted with isopropanol and analyzed by ultraviolet or visible absorbance spectroscopy to determine the total solute concentration. For each solute-surfactant pair, plots of C_{ST} versus $C_{M'}$ were linear in the range of surfactant concentrations studied, as in Figure 3-6. The solute distribution coefficient K was obtained by linear regression of such data, where the slope of Figure 3-6 is KC_{SA} and the

Table 3-5. Membrane Parameters and Mass Transfer Coefficients

Nominal Membrane Pore Diameter, Å	r_p,Å	n_p, pores/cm^2 x 10^{-8}	L,μm	R_m,s/cm	R_t,s/cm
2000	895± 54	3.4±0.2	9.80	2690	2900±92.8
4000	1810±101	1.2±0.1	10.1	1920	2150±81.7

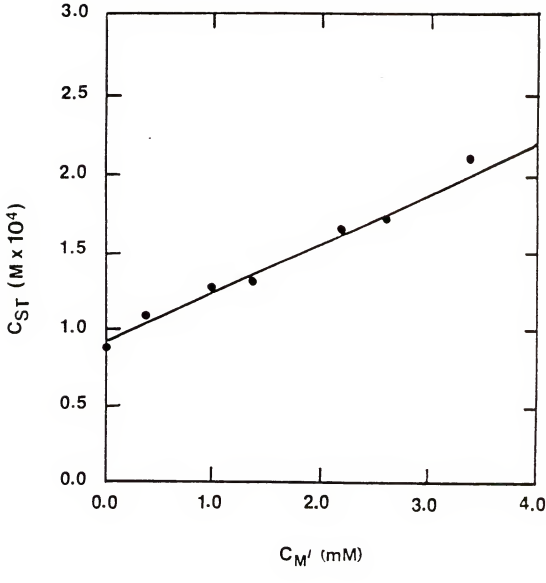

Figure 3-6. Total concentration of testosterone (C_{ST}) versus Triton-X 100 micelle concentration ($C_{M'}$). The slope (KC_{SA}) and intercept (C_{SA}) of the line were obtained by fitting the data to Equation (2-35) where $K^*C_M = KC_{M'}$.

intercept is C_{SA} (see Equations (2-35) and (2-41b)). The standard deviations of data from solubility versus surfactant concentration plots were between 4 and 5%. For diffusion experiments involving micelle-solubilized compounds, the initial concentration of solute in the donor phase (C_{ST1O}) was only 85 to 95% of saturation in order to completely avoid the possibility of precipitation of solute crystals. However, C_{ST1O} in the micellar solution was always greater than the aqueous solubility limit of the solute. Since the overall solubility of solute (C_{ST}) is increased by the presence of micelles, more solute can be added to solutions containing micelles than would be possible in the absence of micelles. This increase in overall solubility is one of the appealing features of micelle-controlled solute release through microporous membranes.

Micelle Characterization

Hydrodynamic Radius and Diffusion Coefficient

The free solution diffusion coefficients $D_{M\infty}$ and hydrodynamic radii r_M of micelles were determined by quasi-elastic light scattering or QELS [67-69]. A 3W Spectra Physics argon-ion laser (514.5 nm line) was used in conjunction with a Brookhaven Instruments Model BI3O 64-channel digital correlator. Sample temperatures were kept at 25 ± 0.1 °C. Data were analyzed using software from the manufacturer. Prior to light scattering experiments, all surfactant solutions were passed through a filter (0.2 μm pore diameter) to remove dust. For spherical micelles, $D_{M\infty}$ is related to the hydrodynamic radius by Stokes-Einstein equation:

$$D_{M\infty} = kT/(6\pi\eta r_M) \tag{3-7}$$

where k is Boltzmann's constant and T is temperature. QELS showed that

in most cases, the micelle size did not change when solutes were added, as expected, since the solute molecules were small compared to the size of the micelles. SDS micelles showed a ~4% increase in size when saturated with hydrocortisone. This was the largest gain for any micelle, and therefore, it was neglected.

Micelle Aggregation Number

The aggregation number, or number of monomers per micelle, was determined using the static quenching technique of Turro and Yetka [7] or micelle volumes calculated from QELS. Both techniques are discussed below.

Consider a solution of unknown micelle concentration C_M containing fluorescent molecules F and quencher molecules Q that are completely associated with the micelles. The Poisson distribution gives the probability that a micelle will contain zero quencher molecules as [70,71]

$$P_0 = \exp{-\langle Q \rangle} \tag{3-8}$$

where $\langle Q \rangle$ is the ratio of quencher molecules to micelles in the solution (C_Q/C_M). This probability is equal to the ratio of the fluorescence intensities of the fluorophore in the presence (I) and absence (I^o) of the quencher, I/I^o [6]. Substituting I/I^o for P_0 and using the definition of C_M from Equation (2-2), Equation (3-8) may be rearranged to the following form:

$$\ln(I^o/I) = (C_Q n)/(C_S - CMC) \tag{3-9}$$

Therefore, if the surfactant concentration and the CMC are known, then n can be determined from the slope of a plot of $\ln(I^o/I)$ versus C_Q.

Equation (3-9) is valid only when the rate of fluorescence quenching in the micelle is faster than the natural decay of the fluorophore [6]. This condition is met for ruthenium bipyridine (RBP) quenching by 9-methylanthrocene (MA) in surfactant solutions [7].

Fluorescence intensities were measured with a Perkin-Elmer Model MPF 44B spectrofluorimeter. The excitation and emission wavelengths for RBP were 450 and 630 nm, respectively. A plot of $\ln(I^o/I)$ versus C_Q for ruthenium bipyridine and 9-methylanthrocene in an SDS solution is in Figure 3-7. The aggregation number determined from this plot was ~50 and agreed with previous results [7,72]. The standard deviation of quenching data was between 5 and 7%.

Ruthenium bipyridine will not bind significantly to cationic or nonionic micelles [73]. Therefore, the results of quasi-elastic light scattering experiments were used to estimate aggregation numbers of cationic micelles. The volume of a spherical micelle can be calculated by the following expression:

$$V_M = 4\pi r_M^3/3 \tag{3-10}$$

where the value of r_M can be determined by QELS (see page 48). The volume of a straight chain hydrocarbon (in $Å^3$) is given by [10]

$$V_{HC} = 27.4 + 26.9n_C \tag{3-11}$$

where n_C is the number of carbon atoms in the tail. The sum of V_{HC} and that of the polar head group (V_{HG}) gives the monomer volume. The aggregation number n can then be determined by dividing micelle volume by the monomer volume. Using TBAC as an example, we find that V_{HC} is 404 $Å^3$ from Equation (3-11), the volume of the $^+N(CH_3)$ group is 170 $Å^3$ from

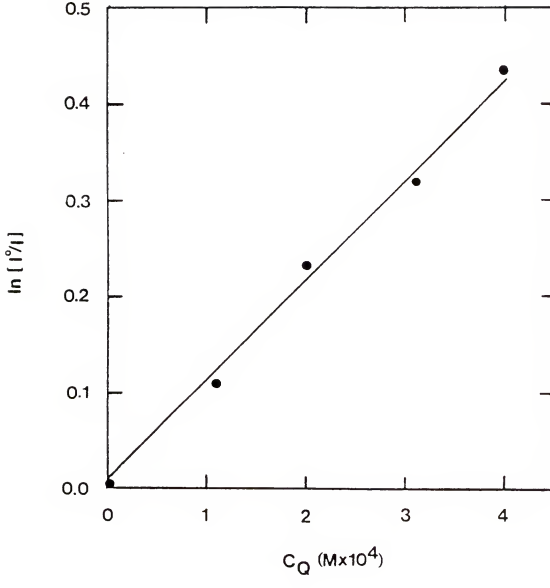

Figure 3-7. The natural logarithm of the fluorescence intensity of 5.2×10^{-5} M RBP in 45 mM SDS solution in the absence of MA(I^o) relative to the fluorescence intensity with MA(I) versus concentration of MA.

Roelants and De Schryver [74] and the volume of the benzene group is 160 $Å^3$ from Reid et al. [75]. The radius of TBAC micelle calculated from QELS experiments was 24 Å (see pages 72, 73). With a micelle volume of 57906 $Å^3$ and a monomer volume of 734 $Å^3$, the aggregation number of the micelle was estimated to be ~79.

Micellar Charge

The charge (number of ionized groups) on a micelle was determined by measuring the aggregation number and the degree of dissociation, α. The methods for determining aggregation numbers were described above. The degree of dissociation was determined from measurements of conductance as a function of surfactant concentration as in Figure 3-8 for TBAC. Zana [76] has shown that α can be calculated from the following expression:

$$\alpha = \lambda_M/\lambda_0 \qquad (3\text{-}12)$$

where λ_M is the slope of the conductance curve above the CMC and λ_0 is the slope below the CMC. The charge on the micelle is the product of the aggregation number and α. The degree of dissociation of a TBAC micelle calculated from Figure 3-8 was 0.31. With the values of n and α, the charge on the TBAC micelle was calculated to be ~24.

Solute Diffusion Coefficients

Diffusion coefficients for testosterone and progesterone were ascertained from diffusion experiments. Using a membrane with a nominal pore diameter of 500 Å, D_{SA} for testosterone and progesterone were determined to be 4.95 ± 0.21 and 5.86 ± 0.23 x 10^{-6} cm^2/s, respectively. After adjusting the results of Amidon et al. [21] at 37°C to 25°C using the Stokes-Einstein equation, their value of D_{SA} agrees well with the

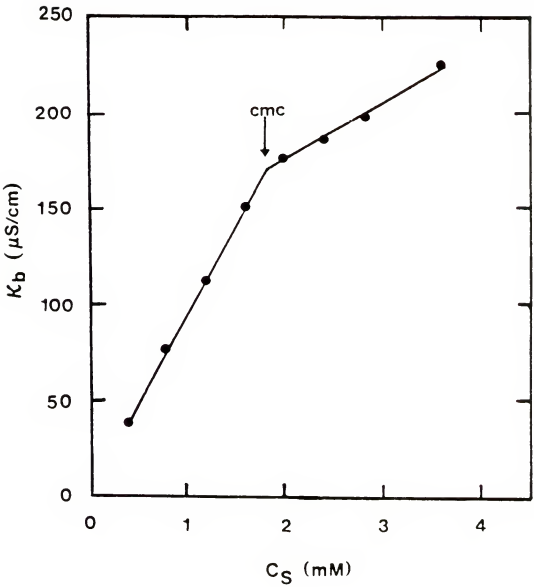

Figure 3-8. Conductance of TBAC solutions versus C_S where the break point of the plot is the CMC.

value of D_{SA} for progesterone obtained in the present study. The diffusion coefficient of pyrene was calculated to be 5.1 x 10^{-6} cm^2/s from the Stokes-Einstein equation after estimating the radius of pyrene to be ~4.6 Å [75].

Membrane Surface Charge

Streaming Potential

Consider a porous membrane that separates two compartments containing electrolyte solutions of equal salt concentration and assume, for example, that the surface of the pore wall has a negative charge. Cations are electrostatically attracted to the pore wall but thermal motion works to randomize the cation distribution. The competition between these forces leads to a potential profile in the pore given by the Poisson-Boltzmann equation [77]:

$$\nabla^2\psi = -(4\pi e/\varepsilon)\Sigma z_i n_{i\infty}\exp(-z_i e\psi/kT) \tag{3-13}$$

where ψ is the electrical potential, ε is the permittivity, e is the proton charge and $n_{i\infty}$ is the number of ions, i, per unit volume far away from the surface. For symmetric electrolyte, one that dissociates into two species with the same magnitude of charge, Equation (3-13) becomes

$$\nabla^2\psi = -(4\pi z e n_\infty/\varepsilon)[\exp(-ze\psi/kT) - \exp(ze\psi/kT)] \tag{3-14}$$

The Poisson-Boltzmann equation for a symmetric electrolyte may be simplified by making the following substitutions:

$$\Psi = ze\psi/kT \tag{3-15}$$

and

$$\kappa^2 = 8\pi z^2 e^2 n_\infty/\varepsilon kT \tag{3-16}$$

into Equation (3-14) to obtain

$$\nabla^2\Psi = \kappa^2 \sinh\Psi \tag{3-17}$$

In Equation (3-16), $1/\kappa$ has the dimensions of distance and is referred to as the Debye length, roughly the thickness of the diffuse part of the electrical double layer. Equation (3-17) is nonlinear unless Ψ is small (<25 mV at 25 °C).

If pressure is applied to one side of the membrane, the solution will be forced through the cylindrical pores into the other side. For low Reynolds numbers [54], the flow through the pore will displace the part of the double layer in the mobile phase from the part in the stationary phase, a displacement that would lead to a current. The potential that develops to oppose the streaming current is known as the streaming potential [78]. Streaming potentials are determined by placing electrodes on each side of the membrane and measuring the potential across the cell (ΔV) as a function of the pressure drop (ΔP). The results of such a measurement are in Figure 3-9 where a solution of 2.5 mM KCl was forced through a Nuclepore membrane. Silver/silver chloride (Ag/AgCl) electrodes were used to measure the potential difference. The remainder of this section describes how the surface charge density at the pore wall, σ_w, can be calculated from streaming potential measurements.

Helmholtz Equation

Determination of surface charge densities from streaming potential data involves simple calculations if the Debye length of the solution filling the pore (Equation 3-16) is much less than the pore radius. If this is true, then the following expression, known as the Helmholtz equation, may be used to calculate the surface potential at the slip

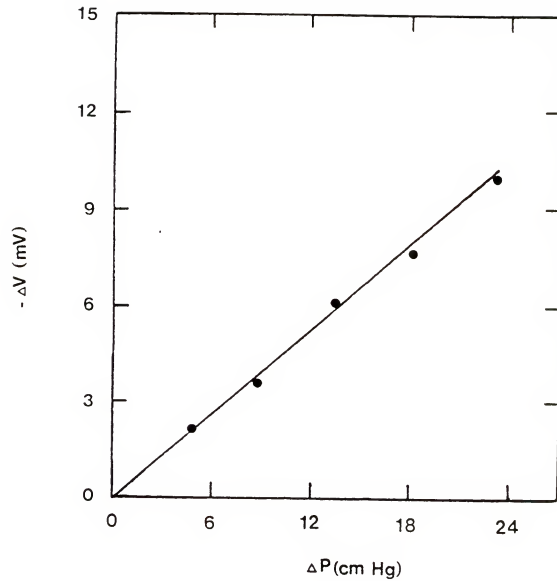

Figure 3-9. Streaming potential (ΔV) across a Nuclepore membrane with nominal pore diameters of 300 Å versus pressure drop across the membrane (ΔP). The electrolyte solution was 2.5 mM KCl.

plane of the fluid-pore wall interface ζ from the slope of a plot such as Figure 3-9 [2]:

$$\nu \equiv \Delta V/\Delta P = \varepsilon\zeta/\kappa_b\eta \tag{3-18}$$

where κ_b is the conductivity of the bulk fluid.

Once ζ is determined, the surface charge density at the pore wall can be calculated from the Gouy-Chapman solution of the Poisson-Boltzmann equation for a planar surface [2]:

$$\sigma_w = \frac{\varepsilon kT\kappa}{2\pi ze} \sinh \frac{ze\zeta}{2kT} \tag{3-19}$$

Equations (3-18) and (3-19) may be used to calculate σ_w from ν assuming 1) the Debye length of the solution is much smaller than the pore radius and 2) the conductivity of the fluid inside the pore is the same as that of the bulk fluid. For small pores at low salt concentrations, assumption 1) may be invalid. Furthermore, the charge on the pore wall must be balanced by counter-ions, and at low salt concentrations it has been shown that the conductivity of the pore fluid may be several orders of magnitude higher than that of the bulk [79,80]. Therefore, the application of the Helmholtz equation is not valid in all situations.

Approximate Solutions of the Poisson-Boltzmann Equation in Cylindrical Coordinates

Even though there are limitations on the Helmholtz equation, it is easy to use for calculating surface charge densities from streaming potential data. In situations where the Helmholtz equation is invalid, approximate solutions of the nonlinear Poisson-Boltzmann equation in cylindrical pores can be used to determine σ_w from ν. The approximations

used in this study are those of Christoforou et al. [81] and are outlined below. First, a dimensionless surface charge density, S, and a dimensionless streaming potential, Y, are defined as follows [81]:

$$S = zer_p\sigma_w/(\varepsilon kT) \tag{3-20}$$

$$Y = ze\eta\kappa_b v/(\varepsilon kT) \tag{3-21}$$

For small potentials ($\Psi<1$), a low potential approximation can be used to solve the Poisson-Boltzmann equation. By making this approximation, the low potential dimensionless streaming potential Y_{LP} is related to the surface charge density by the following expression [81]:

$$Y_{LP}* = \frac{S\, I_0(\tau)}{(\tau)^3 I_1(\tau)} \left[1 - \frac{2\, I_1(\tau)}{\tau I_0(\tau)}\right] \tag{3-22}$$

where $\tau = r_p\kappa$, $Y_{LP} = (\tau)^2 Y_{LP}*$ and I_j are modified Bessel's functions of the first kind and of order j. Equation (3-22) can be solved for S given τ and the dimensionless streaming potential. Equation (3-22) is accurate only when

$$\tau I_1(\tau)/I_0(\tau) \geq S \tag{3-23}$$

If the potential at the wall is large ($\Psi > 1$), a high potential approximation (HP) is used to obtain a solution to the Poisson-Boltzmann equation. Y_{HP} can be calculated from S using the following equations [81]:

$$Y_{HP}* = F(S)/G(S,B) \tag{3-24}$$

$$Y_{HP} = (\tau)^2 Y_{HP}* \tag{3-25}$$

$$F(S) = \frac{4+S}{S} \ln \left[\frac{4+S}{4}\right] - 1 \qquad (3\text{-}26)$$

$$G(S,B) = S\left[1 + B\left[\frac{4}{S} \ln \left[\frac{4}{S+4}\right] + 1\right]\right] \qquad (3\text{-}27)$$

$$B = 4\varepsilon(kT/e)^2/(z\eta(D_+ + D_-)) \qquad (3\text{-}28)$$

where D_+ and D_- are the mobilities of the cation and anion, respectively. S can then be found by solving Equation (3-24) using streaming potential data if the following is true:

$$\tau \leq 2.462[S/(S+4)]^{0.5} \qquad (3\text{-}29)$$

Performing the Streaming Potential Measurement

The diffusion cell in Figure 3-1 was used for electrokinetic measurements where the only modification was a set of plastic supports on both sides of the membrane that protected the membrane against damage by high pressures. Silver/silver chloride electrodes were used because they are reversible to the chloride ion. Electrodes were produced by anodizing 1 cm long silver wires in 0.1 M KCl with 1 mA/wire for 45 min. A piece of copper tubing was connected to the negative pole of the current source. The biases of the electrodes produced were always ≤0.5 mV.

After assembling and filling both sides of the cell with the electrolyte solution, an electrode was inserted in each side through the sample port making a tight seal. The streaming potential was determined by applying pressure to one of the half-cells while the other was open to the atmosphere. Pressure (from compressed nitrogen) was applied through

a bottle of stock solution and measured by a mercury-air mannometer. The potential produced was measured with a Keithley Model 642 electrometer. The same pressure was applied on each side of the membrane, thereby eliminating the effects of the Ag/AgCl electrode biases. Five different pressures were applied on each half cell. Three measurements were made from the lowest to the highest pressure; then two measurements were made between the first three. The last two measurements were made to detect any hysteresis in the $\Delta V/\Delta P$ plot that would be an indication of membrane damage due to pressure. No hysteresis was observed.

Microemulsion Formulation

Microemulsions were prepared by dissolving AOT plus a nonionic surfactant in oil and titrating this solution with distilled water or brine while stirring it with a Teflon-coated magnetic bar. After each addition of water or brine, the solution was checked for clarity and then for birefringence using polarizing plates. The amount of water or brine that made the solution turbid and/or birefringent was the endpoint. The size of microemulsion droplets was measured using the same QELS technique described on page 48 for measuring micelle sizes.

CHAPTER 4
DIFFUSION OF MICELLES IN MICROPOROUS MEMBRANES

When a particle has dimensions comparable with that of the pore through which it diffuses, the diffusion coefficient of the particle can be much smaller than the diffusion coefficient measured in an unbounded solution. The presence of the pore wall restricts the freedom of the particle, thus affecting its distribution between the pore and the bulk phase [38,39]. Furthermore, the viscous interaction between the particle and the solvent is enhanced due to the proximity of the pore wall [27-37]. Therefore, it is necessary to account for the partitioning and hydrodynamic effects when calculations on such systems are performed. This chapter compares calculations for the diffusion coefficients of neutral and charged hard spheres in neutral and charged cylindrical pores with experimental results of nonionic and ionic micelles diffusing through Nuclepore microporous membranes.

Calculations for Hindered Diffusion of Micelles in Microporous Membranes

Partitioning Effects

Neutral hard spheres. As shown in Figure 1-5, the center of a neutral hard sphere can approach an uncharged pore wall no closer than one particle radius. If the "hard sphere" is a nonionic micelle, the ratio of the micelle concentration in the pore (C_{Mp}) to the micelle concentration in the bulk phase (C_M) is equal to the ratio of the volume

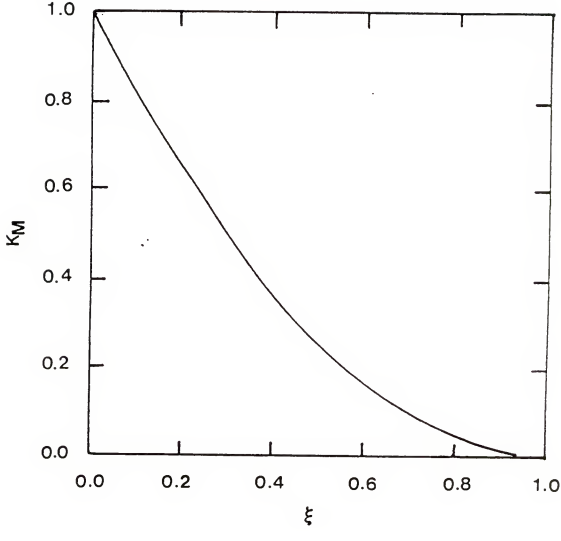

Figure 4-1. The partition coefficient (K_M) of a neutral hard sphere into a cylindrical pore versus the ratio of particle to pore radii (ξ) calculated from Equation (4-2).

of the pore that the micelle can occupy to the total volume of the pore [82,83]:

$$C_{MP}/C_M \equiv K_M = \pi(r_p-r_M)^2L/\pi r_p^2L \qquad (4\text{-}1)$$

where K_M is the partition coefficient of the micelle into the pore. By algebraic manipulation of Equation (4-1), the following expression is obtained:

$$K_M = (1-\xi)^2 \qquad (4\text{-}2)$$

where ξ is the ratio of the particle radius to the pore radius (r_M/r_p). Equation (4-2) is plotted in Figure 4-1 where K_M has a maximum value of one for very small particles in large pores (ξ=0) and a minimum value of zero for a particle and pore with the same radius (ξ=1).

Charged hard spheres. In Figure 4-1, the value of the partition coefficient into the membrane is always less than or equal to one for an uncharged hard sphere in an uncharged cylindrical pore. However, if the particle and pore have opposite charge, they will attract each other and K_M may be greater than one. On the other hand, if the particle and pore have the same charge, K_M may be much less than the value calculated for a neutral hard sphere. In general, the partition coefficient of a micelle into the membrane is given by [43]

$$K_M = 2\int_0^{1-\xi} \exp(-E(\theta)/kT)\theta d\theta \qquad (4\text{-}3)$$

where θ is the ratio of the distance of the particle's center from the centerline of the pore to the pore radius and $E(\theta)$ is the electrical potential experienced by the particle at the dimensionless pore position θ.

The minimum value of θ is zero when the center of the particle is on the pore axis and θ can become as large as $1-\xi$ if the particle's surface touches the pore wall. When $E(\theta) = 0$, (4-3) reduces to (4-2).

The equations developed by Smith and Deen [43] for a hard, charged sphere partitioning into a charged cylindrical pore were used to calculate $E(\theta)$ for a charged micelle in a charged pore. The approach used by Smith and Deen [43] was to obtain general solutions (infinite series) to the linearized Poisson-Boltzmann equation (small Ψ in Equation (3-16)) in both cylindrical and spherical coordinates. The linearized equations were used due to the complexity of the geometry. The boundary conditions on each surface (cylinder and sphere) were used to determine some of the unknown coefficients in the series solutions to the Poisson-Boltzmann equation. Next, one solution was transformed into the coordinate system of the other. This transformation allowed the determination of the remaining coefficients. Once the electrical potential was established, the free energy of the system and the interaction potential could be determined.

While the details of the derivation are beyond the scope of this work, one important point should be made. The surface potential and the surface charge are related to each other by the following equation [84]:

$$\sigma = d\psi/dx\big|_{x=0} \qquad (4-4)$$

Therefore, by fixing either σ or ψ, the other is determined. The calculation of $E(\theta)$ may be performed assuming that the surface charges or the surface potential remain constant during the interaction of the sphere with the cylinder. It has been shown that systems containing charged surfactants are best described by assuming the surface charge

remains constant during the interaction [85,86]. Thus, the calculations in this study will be limited to those equations developed by Smith and Deen [43] using constant surface charge as the boundary condition even though equations for interaction at constant surface potential were also derived.

The result of Smith and Deen's development for the dimensionless interaction potential $V(\theta)$ experienced by a particle (not axisymmetric) in a pore with constant surface charge as a boundary condition is given by the following equation [43]: $V(\theta) =$

$$\frac{\frac{8\pi\tau\xi^4 e^{\tau\xi}}{(1+\tau\xi)^2}\Lambda\sigma_S^2 + \frac{4\pi^2\xi^2 I_0(\tau\theta)\sigma_S\sigma_C}{(1+\tau\xi)I_1(\tau)} + \left[\frac{\pi I_0(\tau\theta)}{\tau I_1(\tau)}\right]^2 \frac{(e^{\tau\xi}-e^{-\tau\xi})\tau\xi L(\tau\xi)\sigma_C^2}{(1+\tau\xi)}}{\pi\tau e^{-\tau\xi} - \frac{2(e^{\tau\xi}-e^{-\tau\xi})\tau\xi L(\tau\xi)\Lambda}{(1+\tau\xi)}} \qquad (4\text{-}5)$$

where ξ is the particle to pore radii ratio, τ is the ratio of the pore radius to the Debye length, $L(\tau\xi)$ is the Langevin function ($L(\tau\xi)=\coth(\tau\xi)-1/\tau\xi$), σ_S and σ_C are the charge densities on the sphere (micelle, σ_M) and cylinder (pore wall, σ_W), respectively, and Λ is given by the following equation:

$$\Lambda = \frac{\pi I_0(\tau\theta)}{2} \sum_{t=0}^{\infty} \frac{\theta^t (2t)!\, I_t(\tau\theta)[\tau K_{t+1}(2\tau)+0.75K_t(2\tau)]}{2^{3t}(t!)^2} \qquad (4\text{-}6)$$

where K_i are modified Bessel's functions of the second kind of order t or t+1.

The dimensionless interaction potential at any dimensionless pore position θ was determined using Equation (4-5). The dimensional interaction potential is given by the following equation:

$$E(\theta) = r_p\varepsilon(RT/F)^2 V(\theta) \qquad (4\text{-}7)$$

The partition coefficient K_M was then calculated using a Simpson's rule numerical integration of Equation (4-3) over 100 θ points. The interval was then halved, and an improved estimate of the partition coefficient was obtained by extrapolation. The computer program used for this calculation is in the Appendix.

Sample calculations for K_M as a function of ξ for various salt concentrations are in Figure 4-2. As the salt concentration increases, the prediction approaches that for an uncharged hard sphere (see Figure 4-1). This is expected since the addition of salt reduces the Debye length. In biological systems, the salt concentration is fixed. Therefore, it is useful to examine the effect of micelle charge on K_M in a solution of 0.1 M of a 1:1 electrolyte for a particular membrane material. Sample calculations of K_M assuming the micelle is inside a polycarbonate membrane (σ_w = 0.2 $\mu C/cm^2$) are in Figure 4-3 where K_M decreases as the surface charge density of the micelle increases. Thus, the surface charge density of a micelle could be used to control the partitioning of the micelle into the membrane by forming mixed micelles of ionic and nonionic surfactants with various surface charge densities.

Hydrodynamic Effects

In Chapter 3, the diffusion coefficient of a micelle (measured by QELS) was used to calculate the hydrodynamic micelle radius using the Stokes-Einstein equation (3-16). The general form of Einstein's equation is

$$D_\infty = kT/f_\infty \qquad (4-8)$$

where f_∞ is the coefficient of friction experienced by the particle. Stokes' law for a spherical particle, $f_\infty = 6\pi\eta r_M$, may be used to

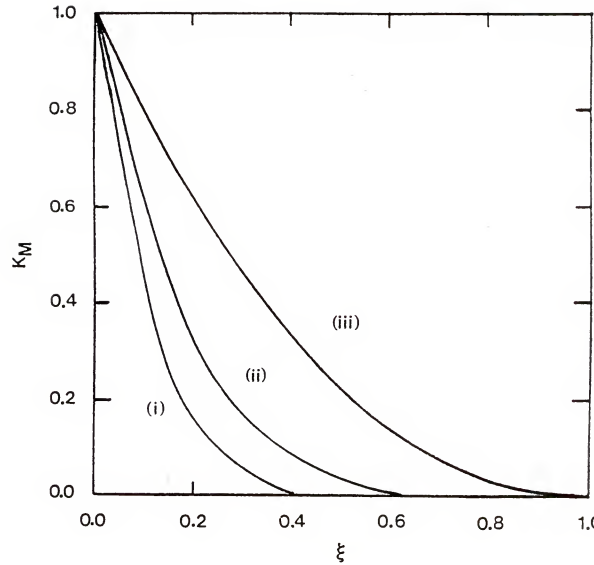

Figure 4-2. The partition coefficient (K_M) of a charged hard sphere into a cylindrical pore with the same charge versus the ratio of particle pore radii (ξ) at various concentrations of a 1:1 supporting electrolyte: (i) 5 mM; (ii) 10 mM and (iii) 100 mM. The sphere radius was 25 Å and the charge densities on the sphere and pore were both 0.2 $\mu C/cm^2$.

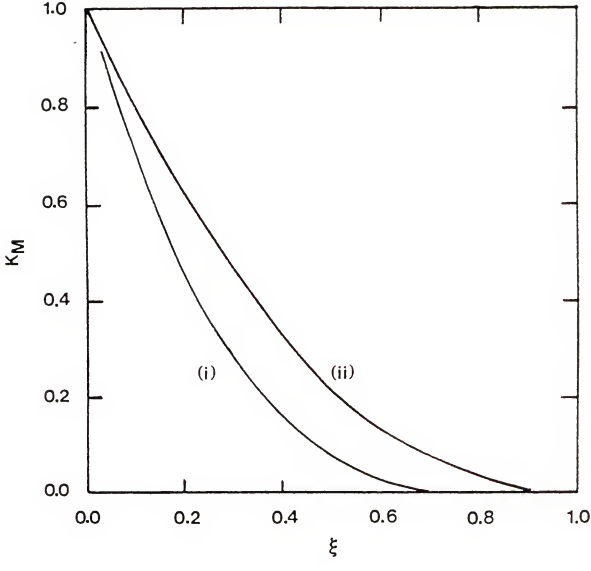

Figure 4-3. The partition coefficient (K_M) of a charged hard sphere into a cylindrical pore with the same charge versus the ratio of particle to pore radii (ξ) where curves (i) and (ii) are for spheres with surface charge densities of 1.0 and 8.0 $\mu C/cm^2$, respectively. The sphere radius was 25 Å, the charge density on the pore was 0.2 $\mu C/cm^2$ and the concentration of the 1:1 electrolyte was 0.1 M.

calculate the friction coefficient under the following conditions:

- the motion of the sphere relative to the fluid is slow
- the fluid is homogeneous
- steady-state motion
- no slip between the fluid and the sphere
- the sphere is rigid
- the fluid is infinite.

The first four conditions are reasonable for any particle or a micelle moving through a fluid-filled pore. Micelles are not exactly hard spheres, but this assumption greatly simplifies hydrodynamic calculations. However, since we are considering micelle diffusion in small pores (0.025-0.2 μm), the last assumption may not always be valid.

The problem of a spherical particle translating through a cylinder has received considerable theoretical and experimental attention through studies of the falling ball viscometer [27-29]. In this experiment, the time required for a spherical ball to fall through the center of a fluid-filled cylindrical container is measured and this result can be used to calculate the fluid's viscosity from Stokes' law if ξ (the ratio of the ball and cylinder radii) is very small. However, experimentalists must work with balls and cylinders of finite sizes and that requires corrections for Stokes' law.

Landenburg proposed that Stokes' law be multiplied by a factor of $(1+2.4\xi)$ to account for wall effects [27]. Therefore, the ratio of the friction coefficient of the sphere translating through the center of a cylinder relative to the friction coefficient of the sphere in an infinite solution, $K^1(\xi)$, is given by [27]

$$K^1(\xi) = 1 + 2.4\xi \qquad (4\text{-}9)$$

where this equation is valid for small ξ values (< 0.08). Brenner and Gaydos derived the following correction for the same problem using the method of reflections [32]:

$$K^1(\xi) = \frac{(1-\xi)^2}{1 - 9/8(\xi)\ln(\xi)^{-1} - 1.54(\xi)} \tag{4-10}$$

Equation (4-10) is valid over the same range as Landenburg's correction. Faxen [27] solved Oseen's equations [87] and arrived at the following correction factor that is valid for ξ values up to 0.4:

$$K^1(\xi) = \frac{1}{1 - 2.104(\xi) + 2.09(\xi)^3 - 0.95(\xi)^5} \tag{4-11}$$

Haberman and Sayre [28] developed a numerical solution of this problem, which is the hydrodynamic analogy to the electrostatic problem solved by Smith and Deen [42], for an axisymmetric sphere. Values of $K^1(\xi)$ are tabulated for various ξ values up to 0.8 and an approximation of those results is

$$K^1(\xi) = \frac{1 - 0.75857(\xi)^5}{1 - 2.1050(\xi) + 2.0865(\xi)^3 - 1.7068(\xi)^5 + 0.72603(\xi)^6} \tag{4-12}$$

Paine and Schere [31] carried out the numerical calculations for $K^1(\xi)$ from Hayberman and Sayre's work [28] for ξ values up to 0.9 and the tabulated results of these calculations were fitted to the following equation by Bohrer [88]:

$$K^1(\xi) = 1.0 + (A + B(\xi) + C(\xi)^2)/(1-\xi)^4 \tag{4-13}$$

where A, B and C are constants whose values are in Table 4-1.

Table 4-1. Parameters for Equation 4-13*

Range	A	B	C
$0.00 \leq \xi < 0.35$	0.0108	1.8950	-2.7800
$0.35 \leq \xi < 0.78$	0.2899	0.4497	-0.8337
$0.78 \leq \xi < 0.90$	3.2404	-6.8920	3.7481

*From reference 88

In the present work, the diffusion coefficient of the micelle in the pore, D_{Mp}, must be calculated given the free solution diffusion coefficient, $D_{M\infty}$ and ξ. The ratio $D_{Mp}/D_{M\infty}$ is the reciprocal of $K^1(\xi)$:

$$D_{Mp}/D_{M\infty} = 1/K^1(\xi) \qquad (4\text{-}14)$$

It is important to note that D_{Mp} in Equation (4-14) is based on the local concentration of micelles in the pore, not the bulk concentration. Calculations of $D_{Mp}/D_{M\infty}$ using (4-9), (4-11) and (4-13) are in Figure 4-4 where Equations (4-9) and (4-11) began to deviate from (4-13) at ξ values of approximately 0.1 and 0.4, respectively. Figure 4-4 also shows that Equations (4-9) and (4-11) agree with (4-13) over their specified ranges.

When intrapore micelle diffusion coefficients were determined experimentally, the bulk concentration of micelles on each side of the membrane was measured. Therefore, D_{Mp} must be multiplied by K_M to account for the difference between the concentration of micelles in the membrane and the concentration of micelles in the bulk solution. The result for micelle diffusion in pores where ξ is less than 0.4 is

$$D_M/D_{M\infty} = K_M[1 - 2.104(\xi) + 2.09(\xi)^3 - 0.95(\xi)^5] \qquad (4\text{-}15)$$

where D_M is the intrapore micelle diffusion coefficient based on the bulk concentration of micelles.

Micelle Diffusion in Free Solution

The diffusion coefficient of a particle or micelle in a pore can be calculated if the following quantities are known: particle radius, pore radius and the diffusion coefficient of the particle in free solution. The free solution diffusion coefficients for micelles were measured by quasielastic light scattering experiments that were described on page 48.

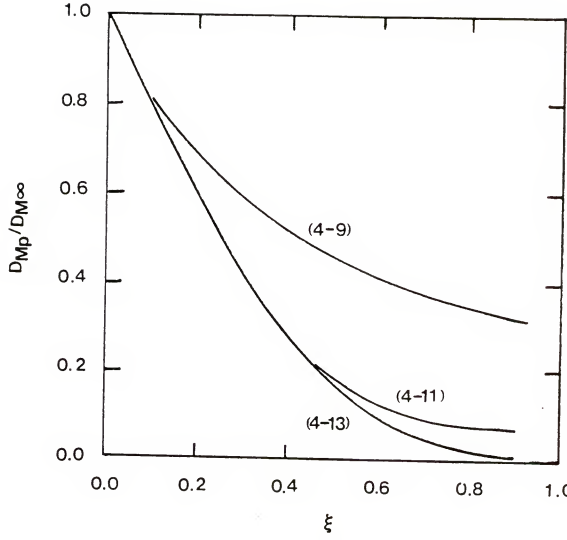

Figure 4-4. Ratio of particle diffusion coefficients in a pore and in free solution ($D_{Mp}/D_{M\infty}$) versus the ratio of particle to pore radii (ξ) calculated using three different corrections for the Stokes law friction factor.

From the measured diffusion coefficient, the hydrodynamic radius of the micelle was calculated from the Stokes-Einstein equation (see Equation (3-7)). This section represents the results of these experiments for nonionic and ionic micelles.

The results of experiments where the diffusion coefficient of nonionic Brij 35 micelles were measured as a function of micelle concentration are in Figure 4-5. Over the range of micelle concentrations studied, the diffusion coefficient remained constant. No interparticle interactions were expected for these nonionic micelles at low concentrations and this assumption is supported by the data. If there was interaction between the micelles, the slope of the plot in Figure 4-5 would be nonzero. In the absence of interparticle interactions, the hydrodynamic radius of the particle can be calculated from Equation (3-7). The diffusion coefficients from QELS experiments and the calculated hydrodynamic radii of Brij 35 and Triton-X 100 micelles are in Table 4-2.

The results of QELS experiments with three ionic micelles are in Figures 4-6 to 4-8. At low concentrations of supporting electrolyte (NaCl), the diffusion coefficients of these micelles increase with surfactant concentration due to electrostatic interactions [6,89]. As the salt concentration is increased, the slopes of these plots decrease and approach negligible slopes as observed for nonionic micelles due to the screening of electrostatic interactions by the electrolyte. Even though interparticle interactions affect the diffusion coefficient at low supporting electrolyte concentrations, the Stokes-Einstein equation may be applied if the values of diffusion coefficients at various micelle concentrations are extrapolated to zero micelle concentration or infinite dilution. The diffusion coefficients at infinite dilution for CPC and

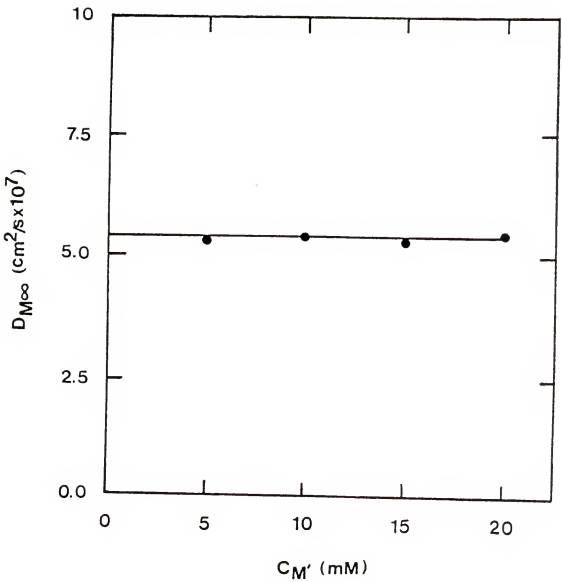

Figure 4-5. Free solution diffusion coefficient of Brij 35 micelles ($D_{M\infty}$) measured by QELS versus the micelle concentration ($C_{M'}$).

Table 4-2. Diffusion Coefficients and Hydrodynamic Radii for Micelles Determined from QELS

Surfactant	D_{M_∞}, $cm^2/s \times 10^{-7}$	Hydrodynamic Radius, Å
Triton-X 100	5.1	48
Brij 35	5.2	45
CPC	9.4	26
TBAC	10.2	24

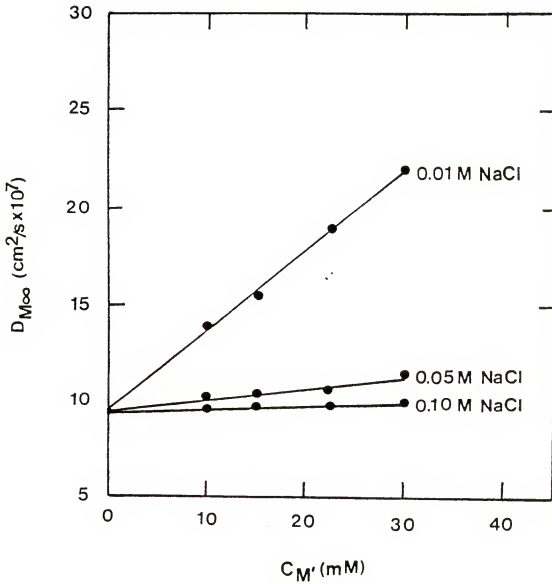

Figure 4-6. Free solution diffusion coefficient of CPC micelles ($D_{M\infty}$) measured by QELS versus the micelle concentration ($C_{M'}$) at various concentrations of a supporting electrolyte.

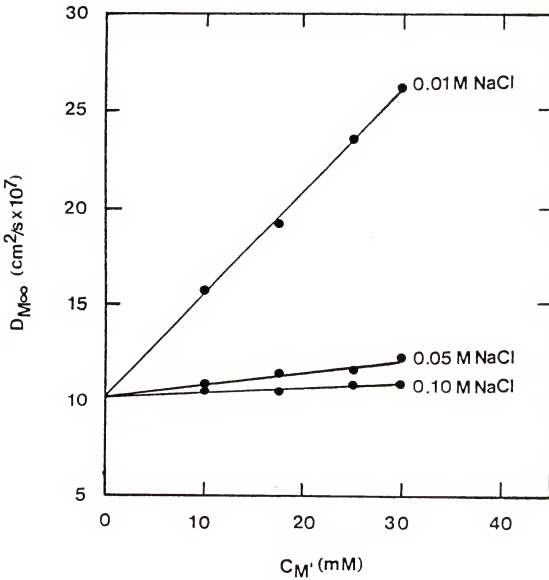

Figure 4-7. Free solution diffusion coefficient of TBAC micelles ($D_{M\infty}$) measured by QELS versus the micelle concentration ($C_{M'}$) at various concentrations of a supporting electrolyte.

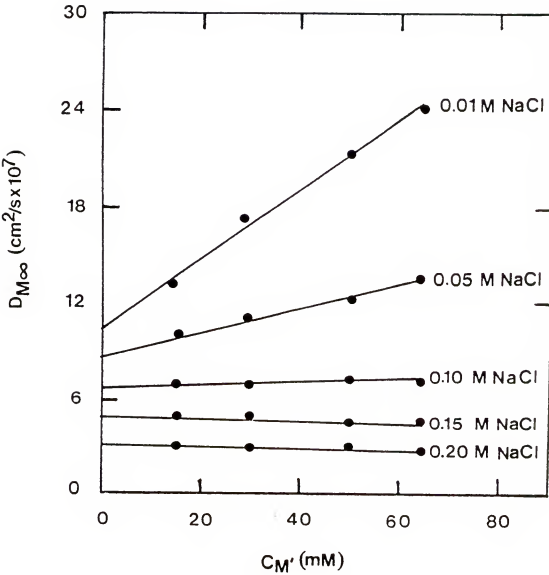

Figure 4-8. Free solution diffusion coefficient of SDBS micelles ($D_{M\infty}$) measured by QELS versus the micelle concentration ($C_{M'}$) at various concentrations of a supporting electrolyte.

TBAC micelles remained constant with increasing salt concentration and are in Table 4-2 with calculated micellar hydrodynamic radii. The value r_M for CPC in Table 4-2 is in agreement with results reported by Anacker [90].

In Figure 4-8, the diffusion coefficients at infinite dilution for SDBS micelles decreased as the salt concentration increased, a result observed by Cheng and Gulari at higher temperatures [6]. The decreases in micelle diffusion coefficients for SDBS indicates that the aggregation numbers of the micelles increased as the salt concentration increased and more ionic monomers were incorporated into the micelle [1,4]. The aggregation numbers of SDBS micelles at various salt concentrations were determined by making static quenching measurements of micelle-bound ruthenium bipyridine with 9-methylanthracene (see page 49) and are in Figure 4-9 with the micelle hydrodynamic radii determined from the light scattering experiments. The free solution diffusion coefficients and hydrodynamic radii reported in this section are used to calculate micelle diffusion coefficients in microporous membranes (see Equation (4-15)).

Nonionic Micelle Diffusion in Microporous Membranes

Effect of Nonionic Surfactant Monomer on Pore Walls

Krovvidi et al. [26] and Bisio et al. [91] found that the pore radii of microporous membranes were reduced by the adsorption of surfactant monomers on the pore walls. Thus, before starting any experiments involving surfactants, a membrane was soaked for at least 12 hours in an aqueous solution of surfactant above its CMC. Using hydrocortisone diffusion, values of A/L were determined for membranes after exposure to Triton-X 100 and Brij 35 (see Table 4-3). After exposure to surfactant, A/L was reduced (compare Tables 3-2 and 4-3) and the reduction of pore

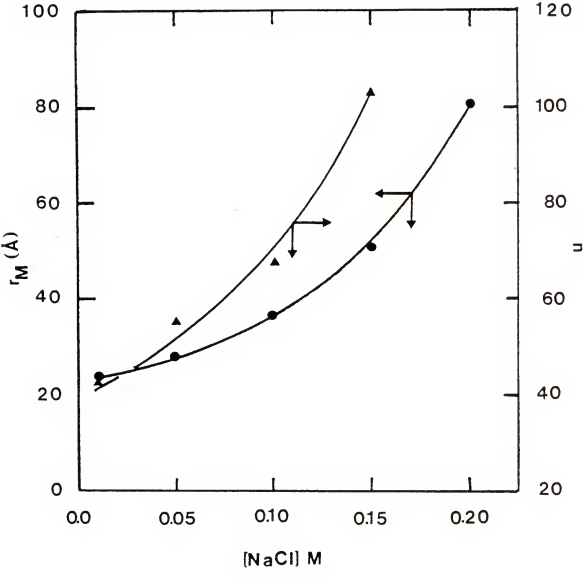

Figure 4-9. Hydrodynamic radius (r_M) and aggregation number (n) of SDBS micelles versus the concentration of a supporting electrolyte (NaCl).

Table 4-3. Ratio of Membrane Pore Area-to Thickness (A/L) After Exposure to Triton-X 100 and Brij 35

Nominal Membrane Pore Diameter, Å	A/L After Exposure to Triton-X 100, cm	A/L After Exposure to Brij 35, cm
500	66.6 ± 3.6	62.0 ± 3.9
2000	226 ± 12	231 ± 10
4000	378 ± 16	368 ± 16

area by either surfactant was approximately the same. Therefore, pore radii in Table 3-1 were reduced by 35 Å, the length of a Triton-X 100 monomer [92], before being used in calculations.

Effect of Pore Radius on Triton-X 100 Micelle Diffusion

Intrapore micelle diffusion coefficients for Triton-X 100 were measured by membrane diffusion experiments, where the receptor phase surfactant concentration was slightly above the CMC and the donor phase surfactant concentration was approximately ten times the CMC. The experimental procedure was detailed on page 33. Briefly, the concentration difference of surfactant across the membrane was measured at various times by absorbance spectrophotometry. Using a pseudo-steady state analysis of the diffusion process, it was possible to calculate the diffusion coefficient of the diffusing species from data on the concentration difference across the membrane with time (see Equation (3-1)).

Diffusion coefficients for Triton-X 100 micelles in three Nuclepore membranes (nominal pore diameters of 500, 2000 and 4000 Å) are in Figure 4-10. As the ratio of the micelle radius to pore radius increased, $D_M/D_{M\infty}$ decreased. The solid line in Figure 4-10 is the calculation of $D_M/D_{M\infty}$ from Equation (4-15) where K_M was determined using Equation (4-2). The agreement between theory and experiment is viewed as good and is comparable to the agreement obtained by other researchers for nonionic micelles diffusing through porous membranes [24-26]. This agreement in Figure 4-10 (~13%) is interesting because, although the equations used were derived for hard spheres, Triton-X 100 micelles are not perfect spheres [9]. Furthermore, micelles are quite dynamic: monomers exchange rapidly with the surrounding aqueous phase, and micellar aggregates undergo

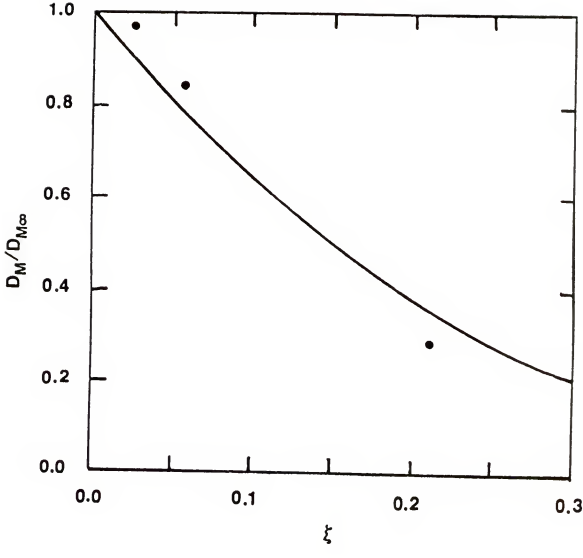

Figure 4-10. The ratio of the intrapore micelle diffusion coefficient to the micelle diffusion coefficient in free solution ($D_M/D_{M\infty}$) for Triton-X 100 micelles versus the ratio of micelle to pore radii (ξ). The curve is Equation (4-15) where K_M was calculated for a neutral hard sphere by Equation (4-2).

breakdown and reformation [11,12]. The lifetime of Triton-X 100 micelles is of order 10 ms [93], or about three orders of magnitude lower than the residence time of the micelles in pores. Moreover, as discussed earlier, the pore wall is at least partially coated with surfactant monomer, and this coating may complicate micelle interactions with the wall. However, comparable agreement between hard sphere calculations and experimental results has been reported for fluid, globular polymer molecules that did not coat the pore wall [37].

Diffusion of Charged Micelles in Microporous Membranes

Effect of Ionic Surfactants on Pore Walls

The Nuclepore membranes used in the present study were made of polycarbonate that dissociates at a pH of 3.9 to give the surface of the pores a negative charge [91]. All diffusion experiments were performed in a pH range of 7 to 8.5. The interaction between the pore wall and the ionic surfactants was studied in more detail than for nonionic surfactants.

Adsorption of ionic surfactants on pore walls. Bisio et al. [91] demonstrated that cationic surfactants absorb on the surface of polycarbonate membranes and reduce the pore radius by approximately the length of two surfactant monomers. Figure 4-11 is the schematic of this process. The first layer adsorbs because of the electrostatic interaction of the positively charged head group with the negatively charged membrane surface and the second layer adsorbs by hydrophobic interactions. The thickness of adsorbed surfactant layers for two cationic surfactants were measured by the techniques described on page 39. The membrane parameters, n_p, r_p and L were measured before the pores were exposed to the surfactant solution. Since the pore density would

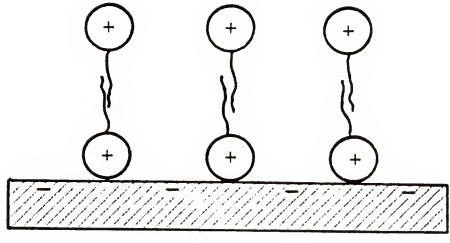

Figure 4-11. Schematic representation of cationic surfactant adsorption on the surface of a negatively charged Nuclepore membrane.

not be affected by the surfactant, only one measurement was required after the membrane was exposed to the surfactant in order to determine the reduced pore radius. After exposure to the surfactant, the pressure drop/flow rate relationship for the solution through the membrane was remeasured and this allowed the calculation of the reduced pore radius. The calculated adsorbed surfactant layer thicknesses for TBAC and CPC agreed with the micelle diameters (~two monomer lengths) measured by QELS and are in Table 4-4.

Anionic surfactants were also found to adsorb to the membrane surface and reduce the pore radius. However, the pore radii were reduced by less than one monomer length. Bisio et al. [91] determined that the amount of co-ion adsorption onto the surface was small. SDS and SDBS adsorption on the pore wall reduced the pore radii by 15 and 18 Å, respectively.

Effect of ionic surfactants on the surface charge of membranes. Figure 4-12 is a plot of the streaming potential measured across a Nuclepore membrane versus the pressure drop before and after the membrane was exposed to a cationic surfactant. Without the surfactant, the slope of the plot is negative indicating a negative surface charge on the membrane (see Equation 3-18). However, the slope becomes positive after the surfactant was added and this change indicates that the membrane pore walls became positively charged after exposure to the cationic surfactant. This is consistent with the bilayer adsorption scheme in Figure 4-11 and agrees with the results of Bisio et al. [91].

From the slopes of plots such as Figure 4-12, the surface charge density for the membrane was determined using the approximate solutions of the Poisson-Botzmann equation developed by Christoforou et al. [81].

Table 4-4. Comparison of Micelle Diameters Determined from QELS and Thickness of Adsorbed Surfactant Layer on Membrane Pore Wall

Surfactant	Micelle Diameter, Å	Thickness of Adsorbed Surfactant Layer, Å
CPC	52	48
TBAC	48	45

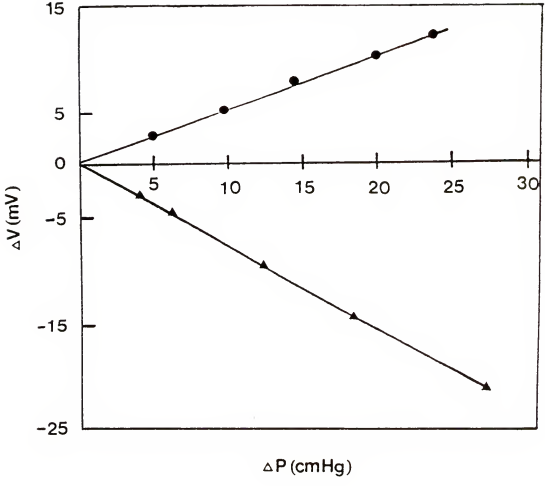

Figure 4-12. Streaming potential (ΔV) across a Nuclepore membrane with a nominal pore diameter of 300 Å versus pressure drop across the membrane (ΔP) before (▲) and after (●) the membrane was exposed to a cationic surfactant (CPC). The electrolyte solution was 1.0 mM KCl.

The dimensionless streaming potential was calculated from Equation (3-21) and then used to find S, the dimensionless surface charge density. The validity of the low potential approximation (Equation (3-22)) and the high potential approximation (Equation (3-24)) were checked by Equations (3-23) and (3-29), respectively. In all calculations, the low potential approximation was valid and the high potential approximation was invalid. Therefore, the surface charge density of the Nuclepore membrane could be calculated unambiguously. The results of these calculations, which are important for determining the partition coefficient of a charged micelle into the membrane, are in Figure 4-13 where σ_w was calculated as a function of KCl ($D_+ = D_- = 2.0 \times 10^{-5}$ cm^2/s) concentration. The values of σ_w for the membrane without surfactant present are in agreement with those found by other researchers [66,91]. The surface charge was also determined when CPC and TBAC were present in the solution below their CMC's (0.2 mM of each surfactant). The value of σ_w with an anionic surfactant present was not required for any calculations in this work and therefore, it was not determined.

Effect of Electrolytes on Charged Micelle Diffusion in Microporous Membranes

The diffusion coefficients of ionic micelles in microporous membranes were measured as a function of supporting electrolyte concentration using the same procedure as that for nonionic micelles discussed earlier in this chapter. However, because of the concentration dependence of the ionic micelle diffusion coefficients (see Figures 4-6 through 4-8), small initial concentration differences across the membrane ($\sim$0.5 mM) were used in all experiments.

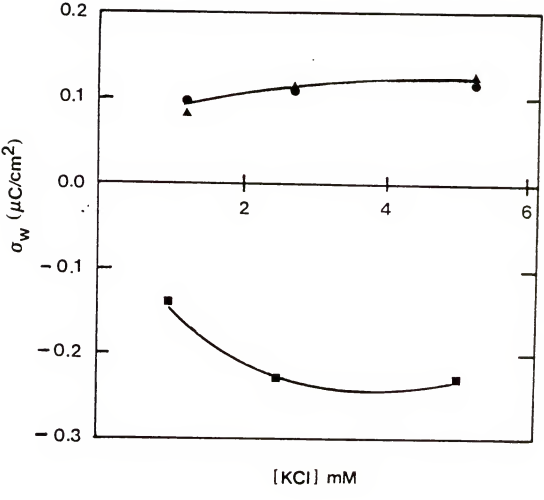

Figure 4-13. Surface charge density (σ_w) of a Nuclepore membrane with a nominal pore diameter of 300 Å as a function of KCl concentration with no surfactant present (■), with CPC present (●) and with TBAC present (▲).

Diffusion coefficients for cationic CPC and TBAC micelles in Nuclepore membranes with nominal pore diameters of 300 Å are in Figures 4-14 and 4-15. The points are data from experiments and the dashed lines are the results one would expect for an uncharged hard sphere diffusing through a cylindrical pore. The predictions for an uncharged hard sphere in Figures 4-14 and 4-15 remained constant over the range of salt concentration studied because the micelle sizes remained constant as the supporting electrolyte concentration was increased (see Figures 4-6 and 4-7). Since the micelle and the pore wall have the same charge (positive), they will repel each other and $D_M/D_{M\infty}$ is below the uncharged hard sphere prediction at low salt concentrations. However, $D_M/D_{M\infty}$ approached the uncharged hard sphere prediction as the salt concentration was increased since the double layer thicknesses in the pore and around the micelle were decreased as the concentration of supporting electrolyte increased. If the electrolyte concentration is high enough, ~0.1 M NaCl in Figures 4-14 and 4-15, the electrostatic interactions between the micelle and the pore are almost completely screened and the micelle diffusion coefficient in the pore is comparable to that of a neutral micelle. The screening of electrostatic forces between micelles was also observed in the QELS measurements of free solution micelle diffusion coefficients $D_{M\infty}$ (compare the slopes of lines in Figures 4-6 to 4-8 at high salt concentrations to the slopes of lines in Figure 4-5).

The solid lines in Figures 4-14 and 4-15 are the results of calculations of $D_M/D_{M\infty}$ from Equation (4-15) where K_M was calculated from the procedure described on page 65, using Equation (4-3). Values for the micelle and pore wall parameters used in these calculations are in Table 4-5. The calculations are in agreement with the experimental results with the exception of the data points when no salt was present

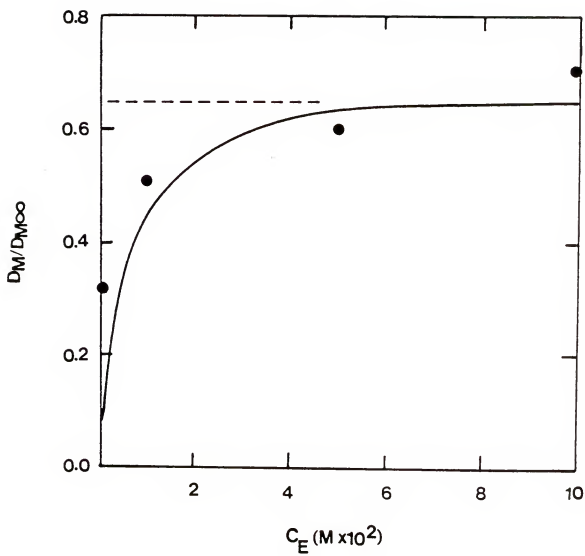

Figure 4-14. The ratio of the intrapore micelle diffusion coefficient to the micelle diffusion coefficient in free solution for CPC micelles in a Nuclepore membrane with a nominal pore diameter of 300 Å (#1) versus the concentration of a supporting electrolyte (NaCl). The solid curve is Equation (4-15) where K_M was calculated for a charged hard sphere by Equation (4-3) using the program in the appendix.

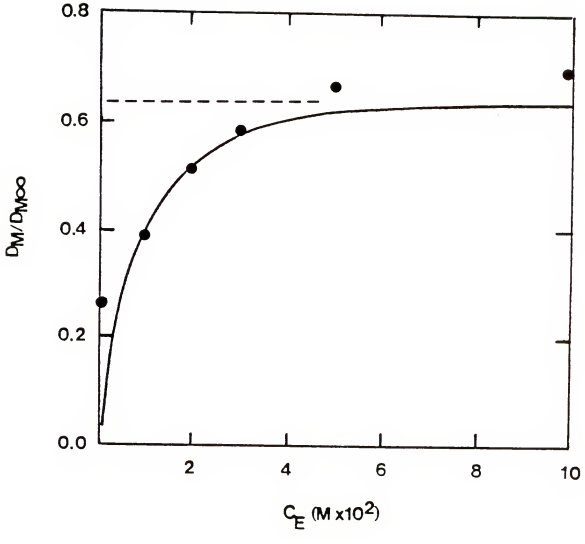

Figure 4-15. The ratio of the intrapore micelle diffusion coefficient to the micelle diffusion coefficient in free solution for TBAC micelles in a Nuclepore membrane with a nominal pore diameter of 300 Å (#2) versus the concentration of a supporting electrolyte (NaCl). The solid curve is Equation (4-15) where K_M was calculated for a charged hard sphere by Equation (4-3) using the program in the appendix.

Table 4-5. Parameters Used for Calculations in Figures 4-14 and 4-15

Surfactant	Micelle Radius, Å	Micelle Surface Charge Density, $\mu C/cm^2$	Pore Radius*, Å	Pore Wall Surface Charge Density, $\mu C/cm^2$
CPC	26	2.8**	267	0.11
TBAC	24	4.8	251	0.12

*Corrected for surfactant adsorption to pore wall

**Calculated from data in reference 90

(i.e. $C_C \approx CMC$). There are two reasons for this large error when compared to the results at higher supporting electrolyte concentrations. First, it was assumed that the only contributions to the ionic strength of the solution came from the supporting electrolyte and surfactant monomers while contributions from the micelles were neglected. The ionic strength, I_s, is given by the following expression:

$$I_s = 0.5\Sigma z_i^2 C_i \qquad (4\text{-}16)$$

Even though the micelle concentration is smaller than the CMC, the valence of a micelle, which is squared in Equation (4-16), is about twenty times that of a surfactant monomer. Micelle contributions to the ionic strength are significant when the surfactant monomers at the CMC are the only supporting electrolyte and insignificant at higher NaCl concentrations. Underestimation of the ionic strength leads to an overestimation of the double layer thickness; hence, $D_M/D_{M\infty}$ would be underestimated as in Figures 4-14 and 4-15 (specifically, for very low values of C_E). A second source of error at low salt concentrations is the assumption that the counter-ion concentration would be high enough to eliminate the diffusion potential, a potential that would make the micelle diffuse faster. The assumption of sufficient supporting electrolyte concentration to eliminate the diffusion potential was made in order to simplify Equation (2-21) and facilitate the calculation of micelle diffusion coefficients from the data. At low supporting electrolyte concentrations, the neglect of the diffusion potential could cause $D_M/D_{M\infty}$ to be underestimated by the calculations developed by Smith and Deen [42,43]. In Figures 4-14 and 4-15, $D_M/D_{M\infty}$ was severely underestimated when the concentration of supporting electrolyte was at its lowest ($C_C \approx CMC$).

Data for SDBS micelle diffusion through a Nuclepore membrane with a nominal pore radius of 300 Å are in Figure 4-16 where the points are data and the solid line is the uncharged hard sphere prediction. This neutral hard sphere prediction decreases as the salt concentration increases since SDBS micelles grow from 22 to 80 Å as the electrolyte concentration increases from 0 to 0.2 M NaCl. Unlike the data on cationic micelles, the diffusion coefficient data for SDBS micelles exceed the hard sphere prediction even when no salt was added. These data are difficult to explain since there is evidence for impurities in the surfactant sample. Even though their surfactant was purified to remove salts (the same procedure was used in the present work), Cheng and Gulari [6] determined that SDBS (obtained from Alcolac) was 80% in the para form and 20% in the ortho form from IR spectroscopic measurements. The manufacturer (Alcolac) also confirmed that the sample was not isomerically pure. It is important to note that an experiment with the unpurified SDBS at low C_E gave the same result as the purified surfactant within experimental error. As the salt concentration increased, the data agreed with the results for uncharged spheres. However, this agreement may be fortuitous because Cheng and Gulari [6] have demonstrated that SDBS micelles form cylinders, not spheres, at high salt concentrations. Hence, it is difficult to make conclusions about the agreement between experiment and calculations for the SDBS system due to the presence of impurities and the non-spherical micelle shape at high salt concentrations.

Conclusions

Measurements of nonionic and ionic micelle diffusion coefficients in microporous membranes were compared with calculations for neutral and charged hard spheres diffusing in neutral and charged cylindrical pores.

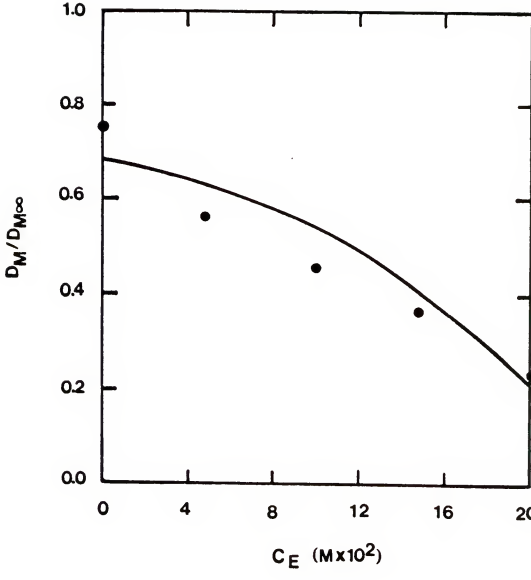

Figure 4-16. The ratio of the intrapore micelle diffusion coefficient to the micelle diffusion coefficient in free solution for SDBS micelles in a Nuclepore membrane with a nominal pore diameter of 300 Å (#3) versus the concentration of a supporting electrolyte (NaCl). The curve is Equation (4-15) where K_M was calculated for a neutral hard sphere by Equation (4-2).

For nonionic micelles in microporous membranes, the diffusion coefficient in the membrane relative to the diffusion coefficient in free solution decreased as the micelle to pore radii ratio increased and was in agreement with calculations for uncharged spheres in uncharged pores. In general, the agreement of data on ionic micelles with calculations was good except for cationic micelle diffusion at low concentrations of supporting electrolyte ($C_C \approx$ CMC). This disagreement can be explained by 1) contributions of the diffusion potential and 2) overestimation of the Debye length since micelle contributions to the ionic strength of the solution were neglected.

The results of membrane diffusion experiments with SDBS micelles were in agreement with predictions for neutral hard spheres in neutral pores over the entire range of supporting electrolyte concentrations studied (0 to 0.2 M NaCl). It is difficult to explain the lack of evidence for electrostatic interactions between the charged micelle and the charged pore since there were at least two isomers of SDBS present in the solution. The agreement of SDBS micelle diffusion data in microporous membranes at high concentrations of supporting electrolyte with calculations for uncharged hard spheres may be fortuitous since these micelles become cylindrical at high salt concentrations [6]. Data and calculations from this chapter are used in the next chapter where the transport of micelle solubilized compounds across microporous membranes is discussed.

CHAPTER 5
TRANSPORT OF MICELLE-SOLUBILIZED COMPOUNDS THROUGH MICROPOROUS MEMBRANES

This chapter presents the results of solubilization and membrane diffusion experiments for the three steroids (hydrocortisone, testosterone and progesterone) and pyrene. Calculations based on the model presented in Chapter 2 are compared with diffusion cell experiments described on page 35. Since some of the surfactants used in micelle-solubilized compound diffusion experiments did not absorb in the UV or visible regions of light, the diffusion coefficients of these micelles could not be measured experimentally. Therefore, the diffusion coefficients of micelles used in solutions of Equation (2-42) were calculated using the measured micelle and pore radii in Equation (4-15) where K_M was determined using Equation (4-2). The only exception was for TBAC micelles where the measured value of D_M was used in the solution of Equation (2-42).

Solubilization of Steroids by Micelles

The distribution coefficients (K in Equation (2-40)) of hydrocortisone, testosterone and progesterone in Brij 35, Triton-X 100 and SDS with 0.15 M NaCl present are in Table 5-1 along with the aqueous solubilities of the three steroids. The surfactant concentrations used to obtain K were from one to twenty times the CMC of the surfactant. It is important to note that all of the plots of compound solubilization versus micelle concentration (e.g., Figure 3-6) were linear in the range

Table 5-1. Distribution Coefficients (K, mM^{-1}) for Steroids in Triton-X 100, Brij 35 and SDS

Steroid	K			Solubility* M x 10^4
	in Triton-X 100	in Brij 35	in SDS	
Hydrocortisone	0.095	0.12	0.25	8.3 ± 0.1
Testosterone	0.35	0.46	1.65	0.79± 0.02
Progesterone	1.86	2.35	6.87	0.21± 0.01

*Solubility in 0.15 M NaCl

of surfactant concentrations studied. In plots such as Figure 3-6, several researchers have reported nonlinearities at high surfactant concentrations, nonlinearities which they attribute to a change in micelle structure known as the second CMC [94-96]. However, since relatively low surfactant concentrations were used, no such nonlinearities were encountered, which allowed the unambiguous determination of K.

In Table 5-1, the K values for Triton-X 100 solutions were lower than those for Brij 35 (perhaps due to the higher amount of polyethylene oxide per mole of Brij 35). As expected, the most water-soluble steroid, hydrocortisone, had the lowest K in all three surfactants. The K values for the steroids in SDS solutions were much larger than those in the nonionic surfactants. Mazer et al. [5] showed that the hydrodynamic radius of SDS micelles in 0.15 M NaCl is approximately 25 Å, smaller than the radii of Triton-X or Brij 35 micelles. Hence, a comparison of K values for SDS with those for the nonionic surfactants shows that it is not always possible to expect a simple relationship between micelle size and solublization. The extent of solubilization depends on the interaction between the solute and various sites within the micelle. Thus, the structures of both the surfactant and the solubilizate would have to be considered in order to predict solubilization phenomena [4,13,14].

The effect of NaCl concentration on the K values for the three steroids in SDS solutions is in Figures 5-1 to 5-3. As the salt concentration increased, the equilibrium, distribution coefficient K, or solubilization capacity of the SDS micelles, decreased. Lundberg et al. [97] reported that the addition of NaCl to tetradecyltrimethylammonium

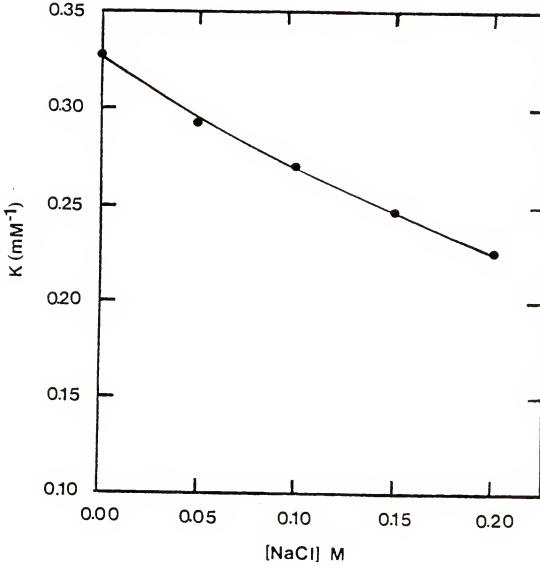

Figure 5-1. K for hydrocortisone in SDS versus concentration of NaCl.

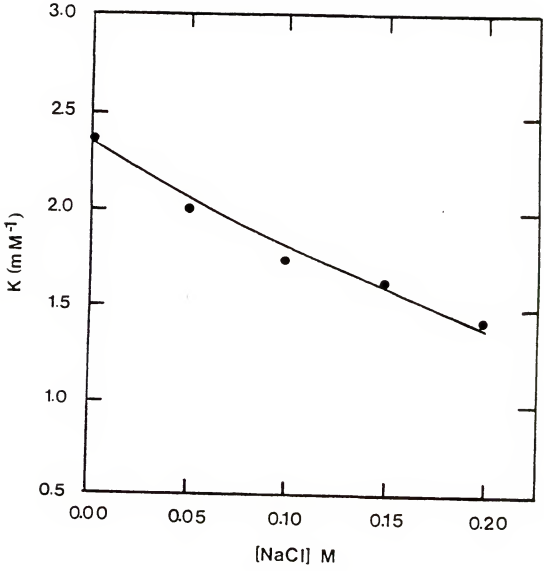

Figure 5-2. K for testosterone in SDS versus concentration of NaCl.

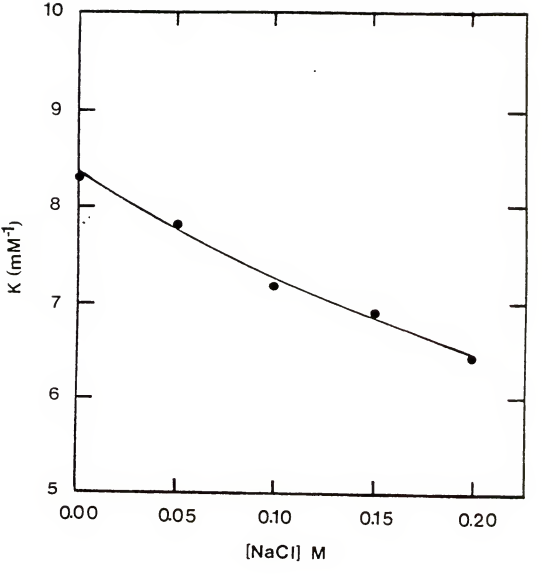

Figure 5-3. K for progesterone in SDS versus concentration of NaCl.

chloride (TTAC) solutions reduced the solubilization capacity of these ionic micelles for testosterone and progesterone. This can be explained by Klevens' [98] solubilization studies with medium- and long-chain alcohols, compounds that can partition strongly into the palisade layer, in ionic surfactant micelles. It was observed that the solubilization capacity of the ionic micelles for the alkanols decreased when salt was added to the surfactant solutions [98]. Since the salt reduces repulsion between the head groups, Klevens [98] proposed that the tighter packing in the head group region reduced the volume available to the solutes and thus, reduced the solubilization capacity. This accounts for the behavior observed in the SDS/steroid/salt systems because the solutes were not very oil- or very water-soluble and were likely to be located in the palisade layer [99,100].

Effect of Steroid Solubilization on Transport Through Micrporous Membranes Nonionic Surfactant Micelles

The solubilization of compounds by micelles can dramatically affect the diffusion of the compounds through microporous membranes, as expected intuitively and as shown by Equation (2-42). Figures 5-4 to 5-6 show the results of membrane diffusion experiments and model calculations for hydrocortisone, testosterone and progesterone in Brij 35 solutions; the nominal membrane pore diameter in these experiments was 2000 Å. The circles in each figure are the data and the four curves are the results of model calculations: curve (A) is the numerical solution to Equation (2-42) assuming that the solute in solution does not associate at all with the micelle (K=0); (B) assumes that the solute is completely solubilized in the micellar phase (K=∞); (C) is the result if the donor phase were an aqueous solution saturated with the solute (no micelles

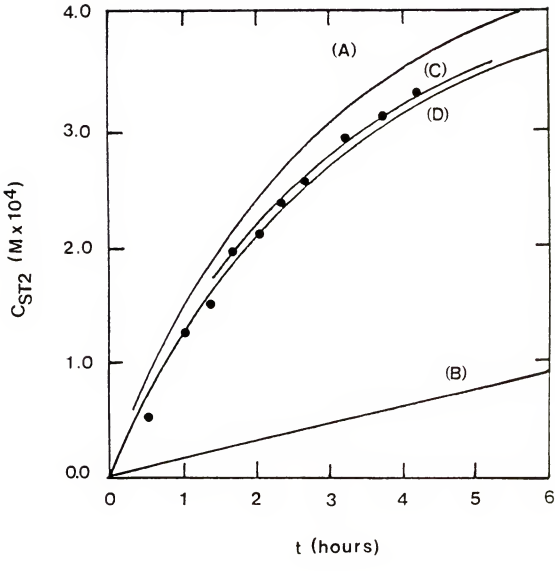

Figure 5-4. Total concentration of hydrocortisone in the receptor phase (C_{ST2}) versus time (t) where the surfactant is Brij 35 (0.15 M NaCl); the nominal membrane pore diameter is 2000 Å, $C_{M1O'}$ = 1.88 mM, $C_{M2O'}$ = 0.13 mM and C_{ST1O} = 9.12 x 10^{-4} M. (A) K = 0, (B) K = ∞, (C) C_{ST1O} from aqueous solubility in Table 5-1, and (D) model calculations from Equation (2-42).

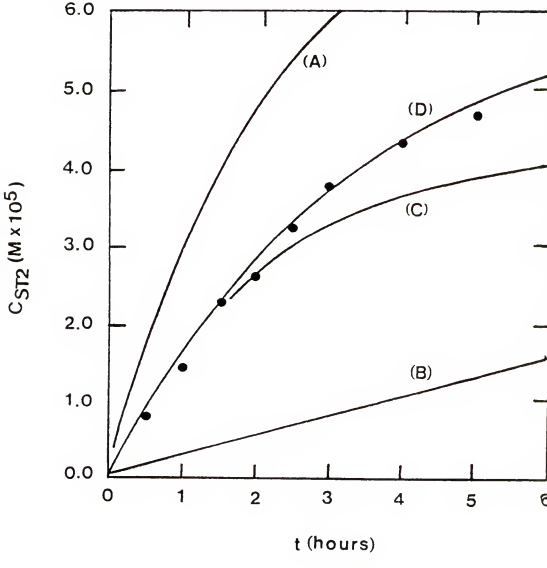

Figure 5-5. Total concentration of testosterone in the receptor phase (C_{ST2}) versus time (t) where the surfactant is Brij 35 (0.15 M NaCl); the nominal membrane pore diameter is 2000 Å, $C_{M10'}$ = 1.87 mM, $C_{M20'}$ = 0.14 mM and C_{ST10} = 1.57 x 10^{-4} M. (A) K = 0, (B) K = ∞, (C) C_{ST10} from aqueous solubility in Table 5-1, and (D) model calculations from Equation (2-42).

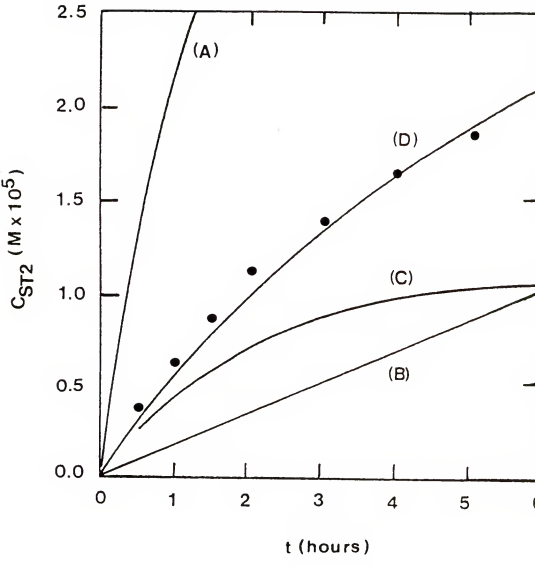

Figure 5-6. Total concentration of progesterone in the receptor phase (C_{ST2}) versus time (t) where the surfactant is Brij 35 (0.15 M NaCl); the nominal membrane pore diameter is 2000 Å, $C_{M10'}$ 1.80 mM, $C_{M20'}$ = 0.14 mM and C_{ST10} = 1.02 x 10^{-4} M. (A) K_{∞} = 0, (B) K_{∞} = ∞, (C) C_{ST10} from aqueous solubility in Table 5-1, and (D) model calculations from Equation (2-42).

present); and (D) accounts for the actual partitioning of the solute between the free solution and micelles using the experimentally-determined values of K from Table 5-1. Curves (A)-(D) are plotted to illustrate that K can have a significant influence on the actual release of steroids into the receptor phase. The average deviations of data from model calculations (curve D) in Figures 5-4, 5-5 and 5-6 are 5.1, 4.3 and 9.4%, respectively.

The significantly lower pore diffusion coefficient of a micelle, when compared to the diffusion coefficient of the solute in free solution, is the basis of the controlled release technique. Since hydrocortisone in Figure 5-4 does not partition strongly into micelles (K values for hydrocortisone in Table 5-1 are the lowest), the rate of release of hydrocortisone into the receptor phase closely follows the release rate that would be expected if hydrocortisone did not partition into micelles (i.e., if K were zero as in curve (A) of Figure 5-4). Thus, hydrocortisone transport is dominated by free solute diffusion, and both the data (circles) and the theoretical predictions (curve D) are relatively close to curve (A). On the other hand, for testosterone and progesterone, where more of the solute partitions into micelles (K is larger), the data and the theoretical predictions (curve D) in Figures 5-5 and 5-6 move away from curve (A) towards curve (B). When micelles significantly influence the solubility of a compound, both the total amount of solute delivered to the receptor phase ($0.5C_{ST10}$) increases and the rate of delivery (compare the slopes of curves (C) and (D) in Figures 5-4 to 5-6) can be increased over those achieved in the absence of micelles. Thus, the affinity of the solute for the micellar phase--as indicated by K, which for hydrocortisone (Figure 5-4) is about twenty

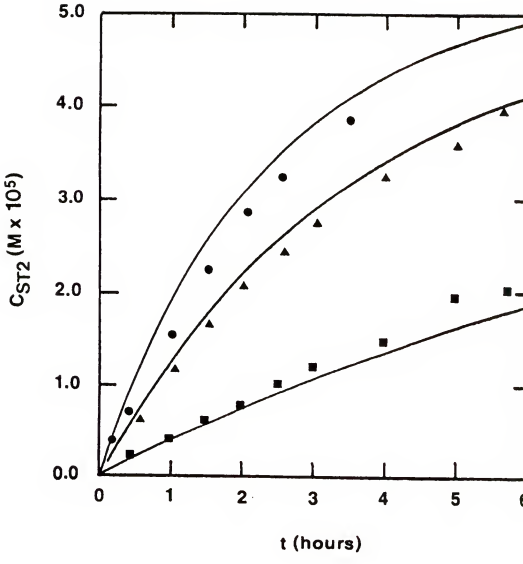

Figure 5-7. Total concentration of testosterone in the receptor phase (C_{ST2}) versus time (t) where the surfactant is Triton-X 100 (0.15 M NaCl): $C_{M10'}$ = 2.7 mM, $C_{M20'}$ = 0.27 mM and C_{ST10} = 1.31 x 10^{-4} M, and the nominal membrane pore diameters are: ●, 4000 Å; ▲, 2000 Å; and ■, 500 Å.

times less than that for progesterone (Figure 5-6)--can dramatically increase the rate and amount of solute transported through the membrane, especially if K is large, as in Figure 5-6. It should be noted that, for the 6-hour experiment in Figure 5-6, the actual rate of solute released (curve D) is not only higher but more nearly constant than if no micelles were present (curve C). This more nearly constant rate over a prolonged period is an appealing feature of a micelle-controlled release system.

Equation (4-15) predicts that D_M/D_∞ decreases as ξ increases. Figure 5-7 shows the results of diffusion experiments using testosterone in Triton-X 100 and membranes with nominal pore diameters of 500, 2000 and 4000 Å. The reduction in the rate of testosterone delivery to the receptor compartment with decreasing pore size reflects 1) a reduction in membrane pore area (A/L in Table 3-2) as well as 2) decreased values of D_M due to hindered diffusion (Figure 4-10). In Figure 5-7, the average deviations of data from model calculations for membranes with nominal pore diameters of 500, 2000 and 4000 Å are 10.3, 4.1, and 8.4%, respectively. Although the two effects mentioned above cannot be separated here, the agreement of the data in Figure 5-7 with the solutions to Equation (2-42) implies that the theoretical model is valid for a variety of membrane pore sizes, even for pores in which micelle size is significant compared to the pore radius.

Ionic Surfactant Systems

The data in Table 5-1 show that anionic SDS micelles have a higher solubilization capacity for the three steroids. It is advantageous to use SDS micelles in steroid diffusion experiments because they extend the range of K values beyond those measured for nonionic micelles. In Chapter 4, however, the electrostatic repulsion between a charged pore and a charged micelle was examined theoretically and experimentally.

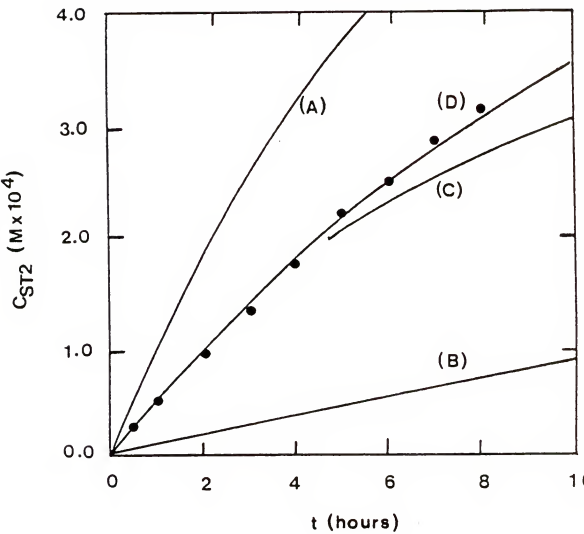

Figure 5-8. Total concentration of hydrocortisone in the receptor phase (C_{ST2}) versus time (t) where the surfactant is SDS (0.15 M NaCl); the nominal membrane pore diameter is 300 Å (#4), $C_{M10'}$ = 4.0 mM, $C_{M20'}$ = 1.0 mM and C_{ST10} = 1.53 x 10^{-3} M. (A) K = 0, (B) K = ∞, (C) C_{ST10} from aqueous solubility in Table 5-1, and (D) model calculations from Equation (2-42).

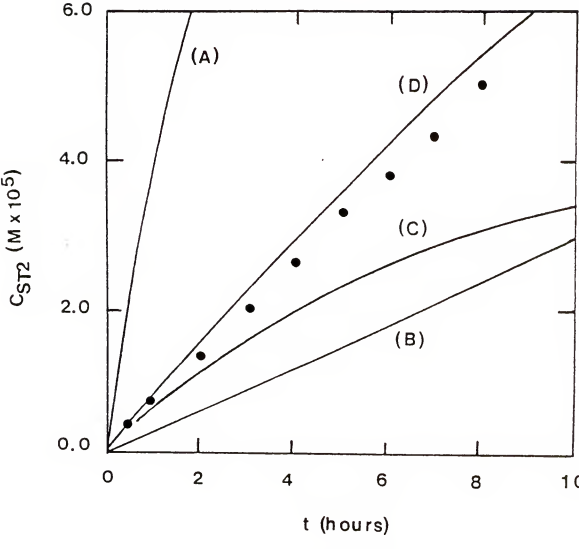

Figure 5-9. Total concentration of testosterone in the receptor phase (C_{ST2}) versus time (t) where the surfactant is SDS (0.15 M NaCl); the nominal membrane pore diameter is 300 Å (#4), C_{M10} = 4.0 mM, C_{M20} = 1.0 mM and C_{ST10} = 5.0 x 10^{-4} M. (A) K = 0, (B) K = ∞, (C) C_{ST10} from aqueous solubility in Table 5-1, and (D) model calculations from Equation (2-42).

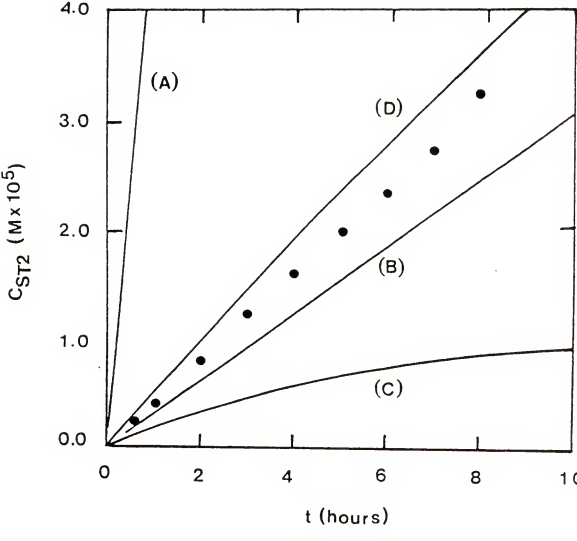

Figure 5-10. Total concentration of progesterone in the receptor phase (C_{ST2}) versus time (t) where the surfactant is SDS (0.15 M NaCl); the nominal membrane pore diameter is 300 Å (#4), C_{M10} = 4.0 mM, C_{M20} = 1.0 mM and C_{ST10} = 5.1 x 10^{-4} M. (A) K = 0, (B) K = ∞, (C) C_{ST10} from aqueous solubility in Table 5-1, and (D) model calculations from Equation (2-42).

This repulsion was significant at low concentrations of a supporting electrolyte but small at higher electrolyte concentrations. To avoid the additional complications of electrostatic interactions, SDS solubilized steroid transport through a Nuclepore membrane with a nominal pore diameter of 300 Å was studied in 0.15 M NaCl. Based on the results of experiments and calculations in Chapter 4, the partition coefficient of the micelle into the membrane, K_M, should not be affected by the charges on the pore wall and micelle. The supporting electrolyte simulated biological conditions, too. Therefore, D_M was calculated using Equation (4-15) where K_M was determined from Equation (4-2). The diffusion coefficient of SDS in a 0.15 M NaCl, measured by QELS, was 9.4×10^{-7} cm^2/sec and the hydrodynamic radius calculated from the Stokes-Einstein equation (Equation (3-7)) was 26 Å. This result agrees with the value reported by Mazer et at. [5].

The results of steroid diffusion experiments with SDS micelles are in Figures 5-8 to 5-10 where curves (A)-(D) are the same as defined in the previous section. Again, as in Figures 5-4 to 5-6, curve (D) and the data move away from curve (A) and towards curve (B) as K increases from hydrocortisone (Figure 5-8) to progesterone (Figure 5-10). Furthermore, curves (C) and (D) become separated as the K value increases. It is also important to note that the data and curve (D) for progesterone and testosterone are more nearly linear over the length of the experiment than for hydrocortisone. The fluxes (proportional to the slope of the data) for progesterone and testosterone were expected to be more constant since these solutes were more strongly bound to the slower moving SDS micelle than was hydrocortisone. The agreement of the data with curve (D) in Figures 5-8, 5-9 and 5-10 (2.1, 7.4 and 12.5%, respectively)

indicates that the model is able to predict experimental results over a wide range of K values.

Transport of Micelle-Solubilized Pyrene Across Microporous Membranes

The diffusion of micelle-solubilized compounds through microporous membranes reported to this point has been for systems with K values ranging from 0.095 to 6.8 mM^{-1}. Progesterone, with an aqueous solubility of 2.2×10^{-5} M, was the most water-insoluble compound used in diffusion cell studies. Pyrene, with an aqueous solubility of 7×10^{-7} M, is an excellent candidate for studies of micelle-solubilized compound diffusion not only for its low solubility but also for its strong absorbance and fluorescence spectra.

Pyrene Solubilization and Diffusion

The K values for pyrene in three surfactants are in Table 5-2. The quaternary ammonium surfactant (TBAC) has the highest solubilization capacity followed by Brij 35 then SDS. The higher solubility of pyrene in TBAC is understandable since pyrene is known to have a weak interaction with quaternary ammonium head groups [8, 101].

The results of diffusion experiments with pyrene through membranes with nominal pore diameters of 300 Å in three different surfactant solutions are in Figures 5-11 to 5-13. In these diffusion experiments, Teflon gaskets were used to seal the diffusion cell instead of the Neoprene gaskets that were used in previous experiments (see page 30). The results using SDS to enhance pyrene solubility (Figure 5-11) are in agreement with the model calculations (curve D). However, the results in Figure 5-12 with Brij 35 deviate from model predictions, and the deviation is worse for TBAC in Figure 5-13. Deviation from calculations

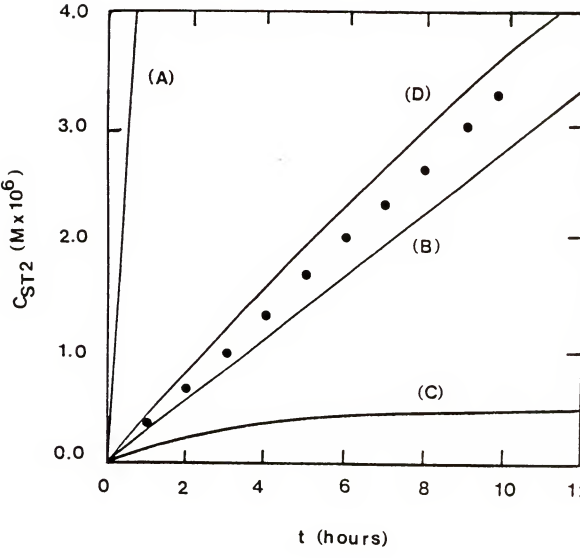

Figure 5-11. Total concentration of pyrene in the receptor phase (C_{ST2}) versus time (t) where the surfactant SDS; the nominal membrane pore diameter is 300 Å (#5), $C_{M10'}$ = 4.0 mM, $C_{M20'}$ = 1.0 mM and C_{ST10} = 4.05 x 10^{-5} M. (A) K = 0, (B) $K = \infty$, (C) C_{ST10} from aqueous solubility in Table 5-1, and (D) model calculations from Equation (2-42).

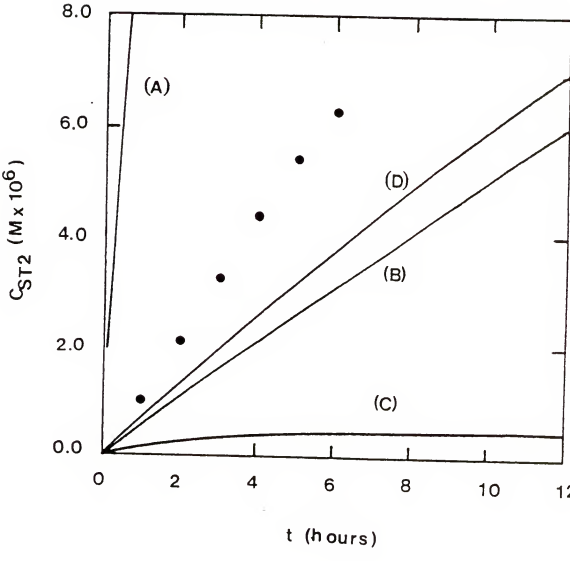

Figure 5-12. Total concentration of pyrene in the receptor phase (C_{ST2}) versus time (t) where the surfactant is Brij 35 (0.15 M NaCl); the nominal membrane pore diameter is 300 Å (#6), $C_{M10'}$ = 4.0 mM, $C_{M20'}$ = 1.0 mM and C_{ST10} = 1.0 x 10^{-4} M. (A) K = 0, (B) K = ∞, (C) C_{ST10} from aqueous solubility in Table 5-1 and (D) model calculations from Equation (2-42).

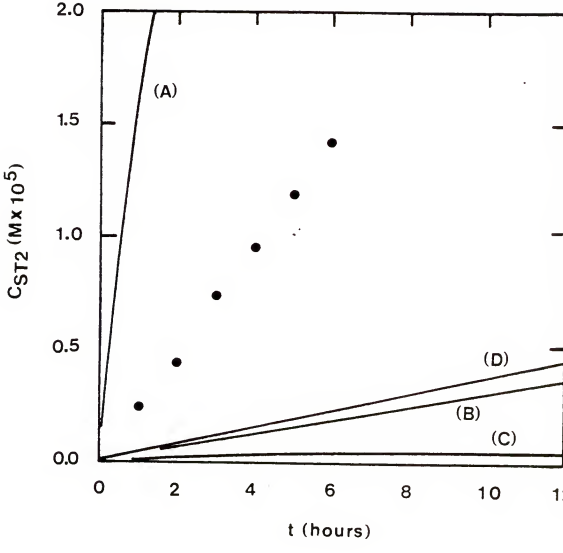

Figure 5-13. Total concentration of pyrene in the receptor phase (C_{ST2}) versus time (t) where the surfactant is TBAC (no salt); the nominal membrane pore diameter is 300 Å (#7), C_{M10}' = 2.5 mM, C_{M20}' = 1.5 mM and C_{ST10} = 1.4 x 10^{-4} M. (A) K = 0, (B) K = ∞, (C) C_{ST10} from aqueous solubility in Table 5-1, and (D) model calculations from Equation (2-42).

Table 5-2. Distribution Coefficients (K, mM^{-1}) for Pyrene in Micellar Solutions

Surfactant	K
SDS	21.5
Brij 35	65.2
TBAC	133.

similar to those in Figure 5-13 were also observed for pyrene in another quaternary ammonium surfactant, TTAB. The experiment with TTAB was performed to determine if the benzene group on TBAC was responsible for the large deviations from calculations. It is important to note that the addition of supporting electrolyte to the solution increases the pyrene flux in TBAC solutions as shown in Figure 5-14 where the lines are drawn through the data. Since the pyrene concentrations in Figures 5-12 and 5-13 were underestimated, diffusion through the membrane occurred at a faster rate than predicted if the solute were so strongly bound to the micelle. The model presented in Chapter 2 accounts for the flux of free and micelle-bound solute and calculations of C_{ST2} made using this model were in agreement with data for all experiments except those where Brij 35 and TBAC were used to solubilize pyrene. Since the data where SDS was used to solubilize pyrene (Figure 5-11) agree with the model, a comparison of the properties of pyrene in SDS with those of pyrene in Brij 35 and TBAC may explain the large deviations from calculations observed in Figures 5-12 and 5-13.

Pyrene Association with Surfactant Head Groups and Monomers

The fluorescence spectrum of pyrene solubilized in n-butanol is in Figure 5-15 where peak I is weak in nonpolar solvents while peak III is strong in all solvents [8]. Therefore, the ratio of the intensities of peaks III to I can be a measure of the polarity of the environment where the pyrene is solubilized. In Figure 5-15, the peaks I and III are almost the same height since n-butanol has both a polar and a nonpolar group. Table 5-3 contains the III/I ratios of 5×10^{-5} M pyrene in solutions of SDS, Brij 35 and TBAC ($C_{M'} = 3$ mM). Pyrene in SDS has the highest III/I ratio indicating the most nonpolar locus of solubilization

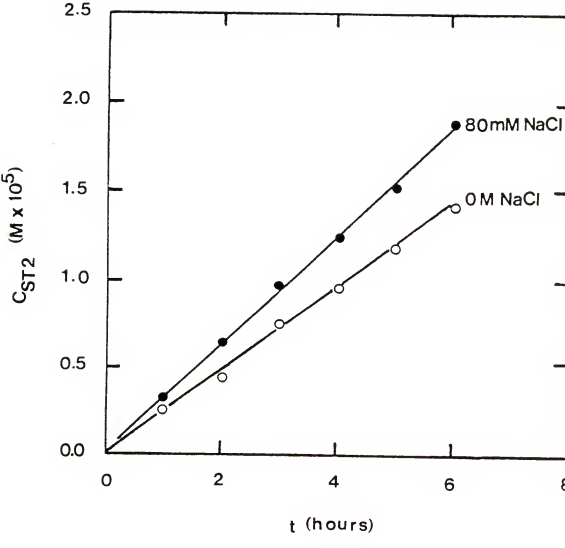

Figure 5-14. Total concentration of pyrene in the receptor phase (C_{ST2}) versus time (t) where the surfactant is TBAC, the nominal membrane pore diameter is 300 Å (#7), $C_{M10'}$ = 2.5 mM, $C_{M20'}$ = 1.5 mM and C_{ST10} = 1.4 x 10^{-4} M. This experiment was run with and without NaCl.

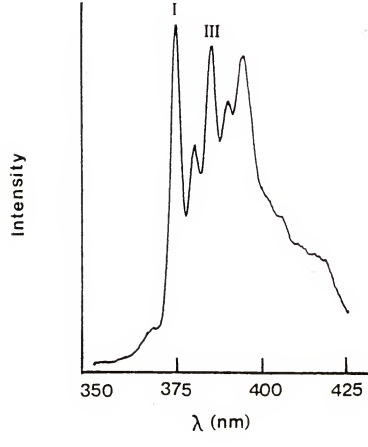

Figure 5-15. Fluorescence emission spectrum of 2 x 10^{-5} M pyrene in n-butanol where the excitation wavelength was 336 nm.

Table 5-3. Ratio of Peak III to Peak I (III/I) from the Fluorescence Spectrum of Pyrene in Micellar Solutions

Surfactant	III/I
SDS	0.89
Brij 35	0.80
TBAC	0.71

while pyrene in TBAC has the lowest III/I ratio indicating the most polar locus of solubilization. This is as expected since pyrene associated with the quaternary ammonium head group of the surfactant [8,101]. The polyethylene oxide head group of Brij 35 would also be a good solvent for pyrene and the III/I ratio for pyrene in this surfactant micelle is higher than SDS but lower than TBAC. Note that the data in Table 5-3 follow the same pattern as the deviations from model calculations in Figures 5-12 and 5-13. Pyrene association with the head group is greatest for TBAC and lowest for SDS with Brij 35 being intermediate.

Evidence for pyrene association with TBAC and Brij 35 monomers is in Figure 5-16. The solubility of pyrene in surfactant solutions below the CMC relative to the aqueous solubility of pyrene is plotted against the surfactant concentration. SDS monomers do not enhance the solubility of pyrene while TBAC and Brij 35 monomers increase pyrene solubility. The enhancement of pyrene solubility by monomers follows the same trend as the deviation of diffusion results from calculations and the degree of head group association as indicated by pyrene's fluorescence spectrum in micelles (i.e. TBAC > Brij 35 > SDS). From the data in Figure 5-16, it is obvious that some K values for pyrene in Table 5-2 should be divided by a factor of $\sim$1.8 since some of the pyrene solubility was due to monomers. However, this would not significantly improve the agreement of the calculations with the data in Figures 5-12 and 5-13.

Additional Mechanisms Proposed to Explain Pyrene Diffusion

The experiments on pyrene fluorescence in micellar solutions and on pyrene solubilization by surfactant monomers established a pattern for deviation from the model derived in Chapter 2. If the compound associates strongly with the head group and is solubilized by the

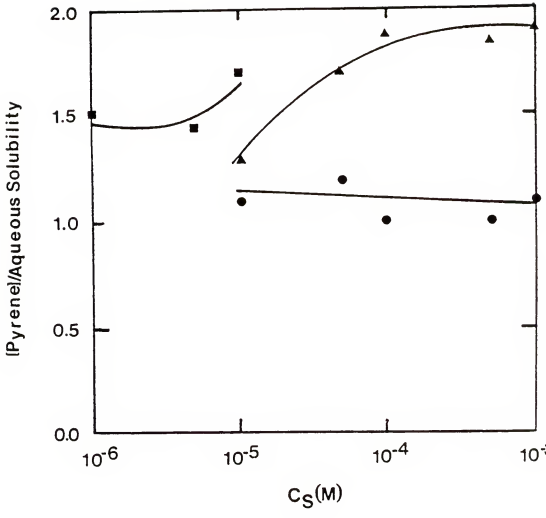

Figure 5-16. Solubility of pyrene relative to its aqueous solubility versus surfactant concentration for SDS, ●; Brij 35, ■; and TBAC, ▲. All surfactant solutions are below the CMC.

surfactant monomers, the model which accounts for micelle-solubilized and free compound diffusion under-predicts the solute flux. Therefore, there must be other processes which contribute to the transfer of solute across the membrane that dominate solute diffusion when there is significant interaction with the surfactant head group. Hence, Equation (2-34), which states the total compound flux is the sum of the free compound flux and the micelle-solubilized compound flux, should be re-written as

$$J_{ST} = J_{SA} + J_{SM} + \Sigma J_i$$

where J_{ST} is the total solute flux, J_{SA} is the flux of free solute, J_{SM} is the flux of the solute via micelles, and J_i are the solute fluxes for other processes. If J_{SA} and J_{SM} dominate the flux, then other contributions would be negligible. However, if other diffusion processes were possible, they could dominate the solute flux if they were faster than J_{SA} and J_{SM}. Two possible additional processes are monomer-facilitated and surface diffusion of pyrene.

The data in Figure 5-16 show that pyrene can be solubilized by TBAC and Brij 35 monomers. Monomers are smaller than micelles and could pass through the pore faster with less hydrodynamic or electrostatic hindrance. Therefore, it would be possible for a monomer/pyrene complex to diffuse across the membrane and release the pyrene to the micelles in the receptor phase. If the complex breaks down, monomers on the receptor side would have to diffuse back to the donor side to reduce this monomer concentration gradient and then repeat the cycle. This process is similar to the facilitated diffusion processes described by Cussler [54]. This process, like the micelle-solubilized compound delivery process, would be diffusion controlled, and monomers diffuse faster than micelles.

SDS monomers cannot solubilize pyrene so they would have little or no effect on pyrene transport.

The pore walls of the membranes are coated (at least partially) with a layer of surfactant molecules. This was proven with measurements of the pore size and charge before and after exposure to a surfactant solution. DellaGuardia and Thomas [102] studied pyrene in dispersions of anionic clay particles with cationic surfactant bilayers on their surface; their data show that pyrene is solubilized in the bilayers surrounding the clay particles near the cationic head group of the outermost surfactant layer. Furthermore, DellaGuardia and Thomas [102] found that pyrene is able to diffuse on the surface of such surfactant-coated particles, a physical situation similar to the surfactant coated pore walls of the microporous membranes of the present study. Hence, it may be possible for pyrene to dissolve in the surfactant layer coating the pore wall and diffuse through the membrane to the other side. This process is known as surface diffusion [55] but it is difficult to assess the magnitude of the surface flux a priori. However, both processes described in this section (monomer facilitated and surface diffusion) would make additional contributions to the transport process and could explain why concentrations of pyrene are higher than predicted by Equation (2-42).

K Values Below Saturation

The K values in Table 5-1 and 5-2 were determined for micellar solutions saturated with solute, and the donor phases in all diffusion experiments initially had solute concentrations between 80-95% of saturation, but still above the aqueous solubility limit of the solute. However, it is important to determine whether the K values calculated by solubilization experiments are still valid at lower solute

concentrations. Figure 5-17 shows the results of experiments using progesterone in Triton-X 100 solutions and a membrane with pore diameter of 2000 Å. In each experiment, the initial surfactant concentrations in the donor and receptor compartments were the same while the degree of solute saturation was changed. Curves (a), (b) and (c) are for 80, 62 and 31% of saturation, respectively, and for each experiment, the data had approximately the same agreement with solutions to Equation (2-42); the average deviations of data from model calculations (curves a-c) in Figure 5-17 for 80, 62, 31% saturation are 5.2, 5.5 and 7.4%, respectively. Since no parameters other than the degree of saturation were changed, we conclude that K remained constant for all three experiments in Figure 5-17.

Curve (d) in Figure 5-17 is the result that would be obtained if the donor phase were an aqueous solution saturated with progesterone. Comparing curve (a) with curve (d), it is clear that more solute can be released at a more constant rate (as indicated by the slopes of the curves) when micelles are present (curve a) than when they are not (curve d). Furthermore, the same amount of solute can be delivered at a more constant rate over a longer period of time. Both of these results are favorable for controlled solute delivery.

It is worth noting that the agreement of data with curves (a)-(c) is not particularly surprising, since even if our Triton-X 100 solutions had been saturated with progesterone, the mole fraction of solute appearing in the micellar phase would have been 0.03, and the mole fraction of progesterone appearing in the aqueous phase would have been very low (3.8×10^{-7}). Thus, both micellar and aqueous phases had dilute concentrations of the solute, and we would not expect K to change since both phases were close to infinite dilution.

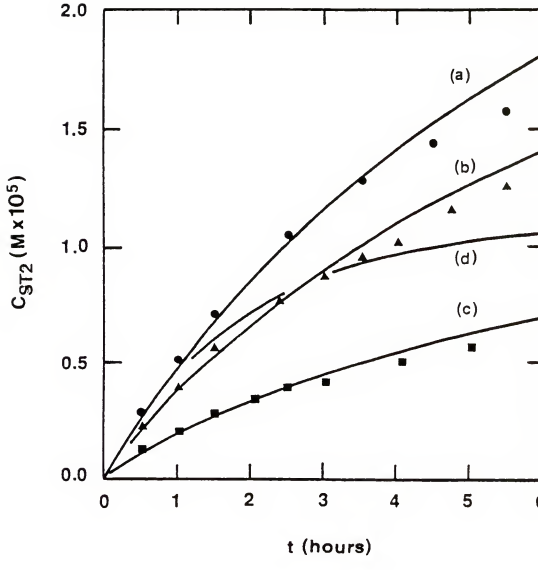

Figure 5-17. Total concentration of progesterone in the receptor phase (C_{ST2}) versus time (t) where the surfactant is Triton-X 100; the nominal membrane pore diameter is 2000 Å, $C_{M10'}$ = 2.69 mM and $C_{M20'}$ = 0.24 mM. (a) 80% saturation (C_{ST10} = 1.01 x 10^{-4}M); ●; (b) 62% saturation (C_{ST10} = 7.80 x 10^{-5} M), ▲; (c) 31% saturation (C_{ST10} = 3.89 x 10^{-5} M), ■; and (d) the delivery that would be obtained from a saturated aqueous solution (C_{ST10} from Table 5-1).

Even though the results in Figure 5-17 indicate that the K value determined at saturation can be used at lower ratios of solute to micelles, no definite conclusion is possible from this data. A better test of the smallest solute/micelle ratios for which the K values determined at saturation are valid would be to start the experiment with the donor phase at 1% or less of satuation. This would better simulate solute/micelle ratios in the receptor phase but would lead to obvious analytical difficulties. Keeping the solute concentration constant and raising the micelle concentration in the donor phase to very high values (the opposite of the experiment in Figure 5-17) would allow the use of larger solute concentrations but could lead to ambiguous results due to structural transitions in micelles at high surfactant concentrations [88,90]. Distribution coefficients of solutes below the saturation point could be measured by NMR self diffusion and by a Taylor dispersion tube as shown by Stilbs [22] and Burkey et al. [23], respectively. These techniques would give accurate measurements of solute distribution between the aqueous and micellar phases over a wide range of solute/micelle ratios.

Conclusions

Solubilization studies showed that the micelle size is not the only parameter to consider when estimating solubilization capacity. SDS micelles, which are smaller than Brij 35 or Triton-X 100 micelles, had the highest solubilization capacity for steroids. Furthermore, pyrene was more soluble in TBAC than in the larger Brij 35 micelle due to specific interactions of pyrene with the quaternary ammonium group of TBAC.

The model presented in Chapter 2 was shown to be capable of predicting the delivery of micelle-solubilized compounds through microporous membranes for steroids in nonionic surfactants and SDS and for pyrene in SDS. However, when specific interactions between the surfactant head group and the solute were present (e.g. pyrene in Brij 35, TTAB or TBAC), the model severely under-predicted the solute concentration in the receptor phase at a given time. Deviations of calculations from data were correlated with solute/head group interactions by fluorescence spectrophotometry and monomer solubilization of the compound. Further experimentation is needed to confirm the validity of solute partition coefficients between the aqueous and micellar phases determined at saturation (K) with those at much lower solute/micelle ratios.

CHAPTER 6
FORMULATION AND PROPERTIES OF AN ALCOHOL-FREE, PHARMACEUTICAL MICROEMULSION

Microemulsions are thermodynamically or kinetically stable, isotropic, low viscosity dispersions consisting of microdomains of oil and/or water stabilized by an interfacial film of surface active molecules [103]. Such microemulsions contain domains with dimensions in the range of 100 to 1000 Å and, hence, appear transparent like a single phase liquid. In general, microemulsions are prepared by mixing oil, water and an appropriate surfactant plus cosurfactant that is usually a short-chain alcohol [104]. Typically, surfactants used in the formulation of a microemulsion have hydrocarbon chain lengths between 12 and 20 carbon atoms. In contrast, the alcohol chain lengths range from four to seven carbon atoms. This difference in chain length is required to produce a disordered and fluid interfacial film [105]. Figure 6-1 is a schematic of a microemulsified water droplet.

Microemulsions have been used extensively in enhanced oil recovery processes [106-110] and recently, Jayakrishnan et al. [111] have shown that microemulsions are useful for solubilizing pharmaceutical or cosmetic agents. Furthermore, Ziegenmeyer [112] demonstrated that a microemulsion can deliver a drug through the skin faster than a cream or a gel. However, the alcohol present in these systems is not always acceptable for human use. Gillberg et al. [113] have formulated alcohol-free microemulsions in hexadecane, but some of the surfactants used were

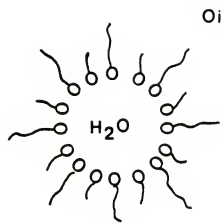

Figure 6-1. Schematic of a water-in-oil microemulsion.

not acceptable in pharmaceutical preparations. Therefore, the formulation of an alcohol-free pharmaceutical microemulsion is desirable. The strategy used to formulate an alcohol-free microemulsion was to combine two high molecular weight surfactants with compatible polar head groups (e.g. no charge repulsion or formulation of complexes between the molecules) and dissimilar lipophilic groups in order to achieve the desired interfacial fluidity. AOT, an anionic surfactant used in some pharmaceutical formulations [114], was blended with various pharmaceutically acceptable nonionic surfactants [115]. Hexadecane was used as the oil in this screening study since it did not have an unpleasant odor.

Screening Experiment

The maximum amount of water solubilized, expressed as the maximum water to oil volume ratio χ, in 10 ml of hexadecane containing 2 g of AOT and 2 g of a nonionic surfactant is in Table 6-1 along with the HLB value of each nonionic surfactant. The HLB, or hydrophilic-lipophilic balance, is a measure of the surfactant's affinity for oil or water and it ranges from 1 for very oil-soluble surfactants to 20 for very water-soluble surfactants [115]. The highest amount of water was solubilized when Arlacel 20 was blended with AOT. From the structures of AOT and Arlacel 20 in Figure 6-2, one can see that the polar head group of Arlacel 20 is sorbitan while AOT has a the sulfonate group, and that Arlacel 20 has a straight lipophilic group while AOT has a branched lipiphilic group. Since the combination of AOT and Arlcel 20 was able to solubilize so much more water than the other surfactant blends, this system was studied in more detail.

Table 6-1. Effect of Cosurfactant on Water Solubilization in Microemulsions with Hexadecane as the Oil and AOT as the Surfactant. Initial Concentrations of Surfactant and Cosurfactant in Hexadecane Were Each 20% (w/v)

Cosurfactant	HLB	Maximum Water to Oil Ratio (w/v)
Brij 35	12.4	0.17
Tween 81	10.0	0.25
Brij 30	9.7	0.32
Tween 61	9.6	0.28
Arlatone T	9.0	0.19
Arlacel 20	8.6	0.88
Brij 52	5.3	0.09
Brij 93	4.9	0.11
Arlacel C	3.7	0.18

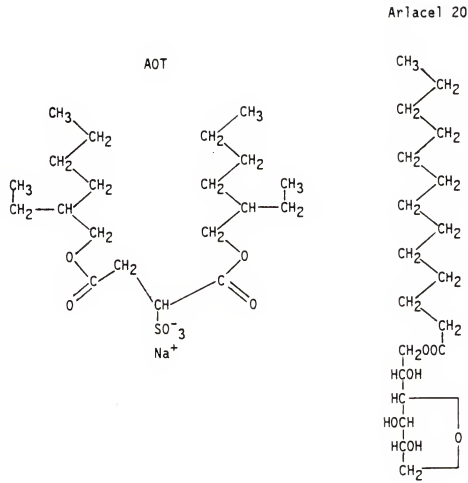

Figure 6-2. Molecular structures of AOT and Arlacel 20.

Weight Ratio Effect

The effect of various weight ratios of AOT and Arlacel 20 (abbreviated as A20) on water solubilization in hexadecane was studied and the results are shown in Figure 6-3 where water solubilization χ peaked when the two surfactants were in a 1:1 weight ratio. Several researchers have reported that maximum solubility of water in oil (or oil in water) occurs when there is ultralow interfacial tension between the oil and water phases [116-118]. Interfacial tensions between the oil and water for the hexadecane/water/AOT/Arlacel 20 system were measured in dilute surfactant solutions by the drop volume method [119]. Wilkinson has shown that the interfacial tension, γ, is related to the drop volume V_d by [120]

$$\gamma = V_d \Delta\rho g / 2rf \qquad (6\text{-}1)$$

where $\Delta\rho$ is the density difference between the two liquids, r is the radius of the syringe, g is the gravitational constant and f is a correction factor for the syringe tip. For these measurements, we assumed $\Delta\rho$ to be constant and the same syringe tip was used for each measurement. With all the other parameters in equation (6-1) constant, γ is proportional to V_d. Drop volume measurements are also in Figure 6-3 where the weight ratio of AOT and Arlacel 20 with the minimum drop volume (minimum γ) corresponds to the weight ratio with the maximum solubilization (i.e. 1:1).

Measurements of water solubility in oil as a function of the total surfactant weight at constant surfactant weight ratio are in Figure 6-4. The slopes (expressed as molar ratios of water to surfactant) and intercepts (horizontal axis) of these plots are in Table 6-2. The slope is highest for the 1:1 weight ratio of AOT to Arlacel 20 or, in other

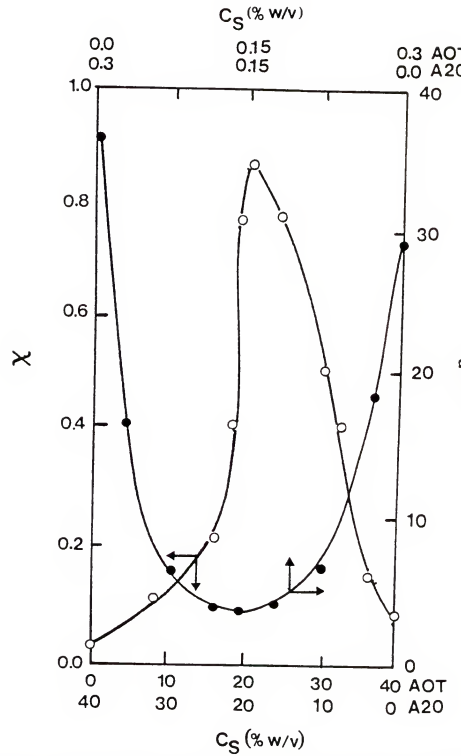

Figure 6-3. Maximum water-to-oil volume ratio (χ) and drop volume (V_d) versus weight ratio of AOT and Arlacel 20 in hexadecane.

Table 6-2. Effect of AOT/Arlacel 20 Weight Ratio on the Slope and Intercept of Plots of Solubilization of Water Versus Initial Concentration of Surfactants in Hexadecane

% AOT of Total Surfactant Weight	Intercept on Abscissa, %(w/v)	Maximum Molar Ratio of Water to Surfactant
0	1.59	2.96
25	0.34	6.32
50	0.19	46.6
75	0.28	22.8
100	1.43	6.96

words, more water is solubilized per surfactant molecule when AOT and Arlacel 20 are blended in a 1:1 weight ratio. For a plot such as Figure 6-4, Bansal et al. [121] have proposed that as the intercept on the horizontal axis moves farther away from the origin, the amount of surfactant at the interface decreases. Intercepts calculated from Figure 6-4 agree with solubilization and drop volume (interfacial tension) measurements because the 1:1 surfactant blend of AOT and Arlacel 20 has the smallest intercept (see Table 6-2) which implies that more surfactant is at the interface (i.e. the interfacial tension is lower).

Salt Effect

The effect of NaCl on the amount of water solubilized is in Figure 6-5 where the amount of brine solubilized decreases as the salinity of the water increases. Since water solubility is related to the interfacial tension [116-118], the interfacial tension for this system must increase as the salinity increases. The sessile drop method was used to test this hypothesis. In Figure 6-5, the height of a 10 μl drop of brine (h) on a Teflon plate submerged in an oil solution of the surfactants (1:1 weight ratio of AOT:Arlacel 20) increases as the NaCl concentration increases. Interfacial tension is related to drop height in the following equation [1]:

$$\gamma = gh^2\Delta\rho/2 \qquad (6\text{-}2)$$

As the salinity increases, the density of the drop and the height increase so, the interfacial tension must increase.

The conclusions made from solubilization and drop height experiments in Figure 6-5 are confirmed by measurements of brine solubilization as a function of total surfactant weight (AOT and Arlacel 20 1:1) in Figure 6-6.

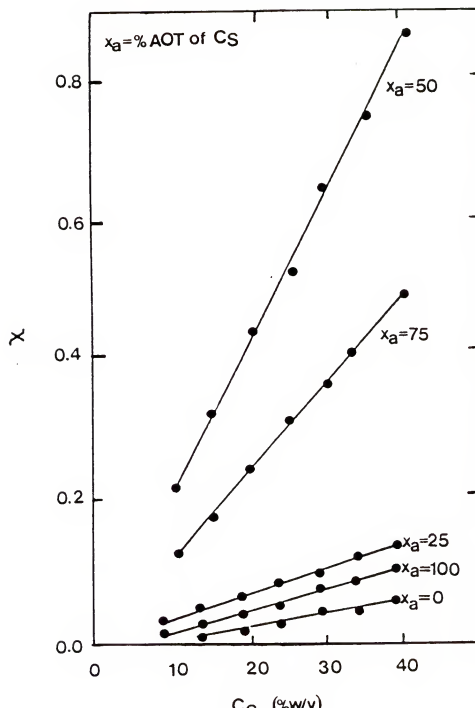

Figure 6-4. Maximum water-to-oil volume ratio (χ) versus initial concentration of surfactants in hexadecane (C_S) for various ratios of AOT to Arlacel 20.

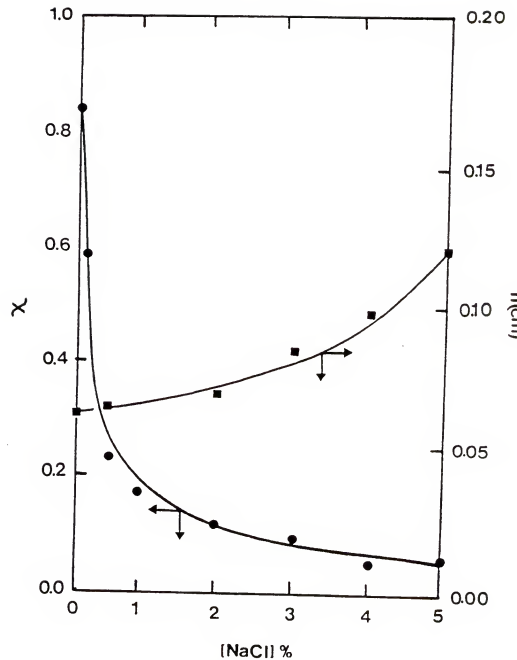

Figure 6-5. Maximum water-to-oil volume ratio (χ) and drop height versus NaCl concentration for AOT and Arlacel 20 (1:1) in hexadecane. The initial concentration of surfactants in oil was 40% w/v.

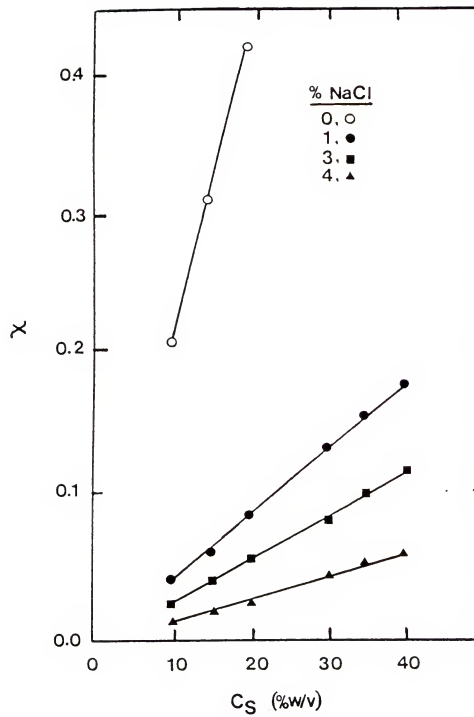

Figure 6-6. Maximum water-to-oil volume ratio (χ) versus initial concentration of surfactants in hexadecane (C_S) for various NaCl concentrations with AOT and Arlacel 20 (1:1).

The abscissa intercepts of these plots are in Table 6-3 and show that as the salinity increases, there is less surfactant at the interface because the intercepts move farther away from the origin. Furthermore, the slopes in Table 6-3 also show that the solubilization capacity of the surfactant blend decreased as the salinity increased. A possible explanation for the effect of NaCl on solubilization is the salting out of AOT by the electrolyte [122]. The effect of the added electrolyte on solubilization in other weight ratios of AOT to Arlacel 20 is in Figure 6-7. As the salinity increases, the maximum solubility of water in oil decreased and the optimal weight ratio shifted to higher percentages of AOT in the blend.

Oil Chain Length Effect

Even though hydrocarbons with low volatility were the best for pharmaceutical applications, different oils were used as the continuous phase because other researchers have found that the oil chain length can alter the solubilization capacity of microemulsions significantly [123,124]. In Figure 6-8, an increase in the oil chain length from seven to sixteen carbon atoms increases the solubilization capacity for the 1:1 AOT and Arlacel 20 blend and decreases the drop volume, which is proportional to the interfacial tension (see Equation 6-1). The plots of solubilization capacity versus total surfactant concentration (AOT and Arlacel 20 1:1) in Figure 6-9, and the slopes and intercepts of these plots are in Table 6-4. As with the weight ratio and salt effects, the oil chain length with the lowest measure of interfacial tension (drop volume or height) and the smallest intercept in plots such as Figure 6-9 had the highest solubilization capacity for water.

Table 6-3. Effect of Salt Concentration on the Slope and Intercept of Plots of Solubilization of Water Versus Initial Concentration of Surfactants (AOT/Arlacel 20 1:1) in Hexadecane

% NaCl in Water	Intercept on Abscissa, %(w/v)	Maximum Molar Ratio of Water to Surfactant
0.0	0.19	46.6
1.0	0.21	9.60
2.0	0.25	6.46
3.0	0.35	3.24

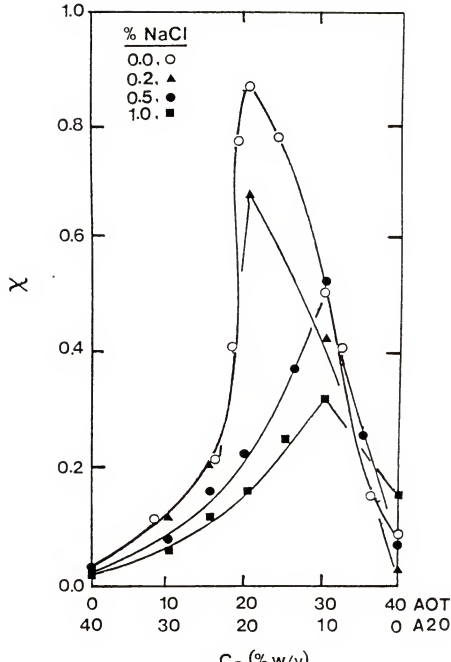

Figure 6-7. Maximum water-to-oil volume ratio (χ) versus weight ratio of AOT and Arlacel 20 in hexadecane for various concentrations of NaCl.

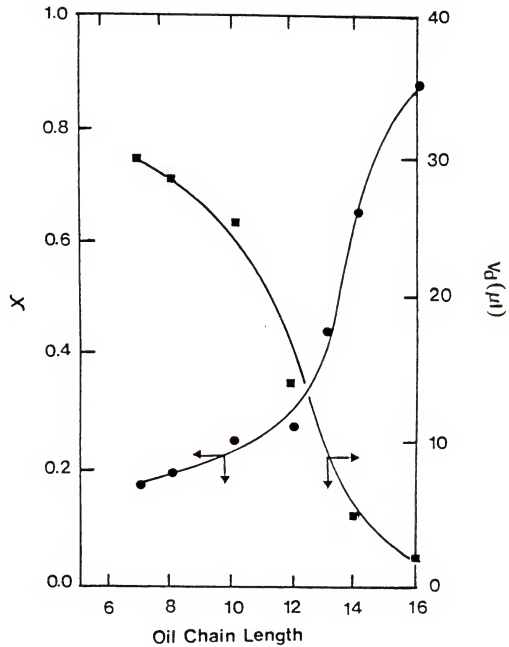

Figure 6-8. Maximum water-to-oil ratio (χ) and drop volume (V_d) versus oil chain length with AOT and Arlacel 20 (1:1) where the initial surfactant concentration was 40% w/v.

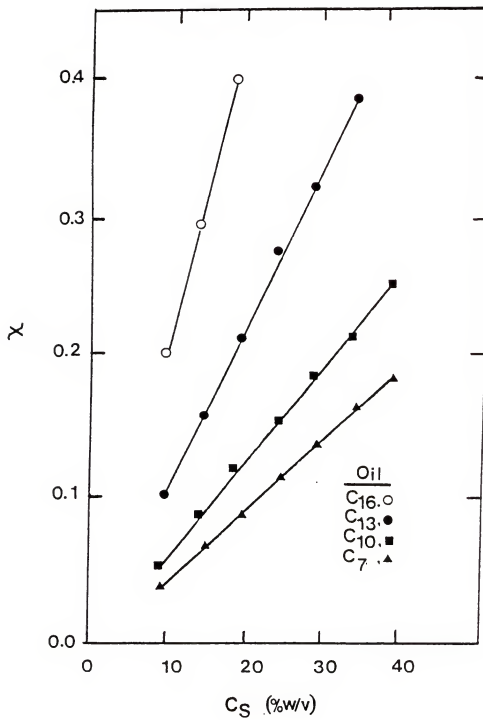

Figure 6-9. Maximum water-to-oil volume ratio (χ) versus initial concentration of surfactants in oil (C_S) for various oil chain lengths with AOT:Arlacel 20 1:1.

Table 6-4. Effect of Oil Chain Length on the Slope and Intercept of Plots of Solubilization of Water Versus Initial Concentration of Surfactants (AOT/Arlacel 20 1:1) in Oil

Oil	Intercept on Abscissa, %(w/v)	Maximum Molar Ratio of Water to Surfactant
Hexadecane	0.19	46.6
Tridecane	0.25	23.6
Decane	0.32	13.4
Heptane	0.55	9.86

The effect of oil chain length on various weight ratios of AOT Surfactant Arlacel 20 is in Figure 6-10. As the oil chain length decreases, the maximum solubilization capacity at the optimum surfactant blend increases slightly and the optimal blend shifts from 1:1 in hexadecane to pure AOT in heptane. The results in Figure 6-10 show that the amount of water solubilized in an oil continuous microemulsion can be optimized by blending the surfactants in various oils. However, for a cosmetic or pharmaceutical formulation, an oil with a longer chain length may be more suitable. Therefore, the 1:1 blend of AOT and Arlacel 20 in hexadecane is the optimal system.

Light Scattering Experiments

The water droplet size in the optimum microemulsion system was measured in dilute solutions of surfactant in oil (~1.0% w/v) by QELS as discussed on page 48. The results of the particle sizing experiments are in Figure 6-11 where the droplet radius (r_M) increased from 50 to approximately 180 Å in radius as the volume fraction of water (ϕ_w) increased from 0.50 to 1.5%. The highest molar ratio of water to surfactant in Figure 6-11 is 41 (~90% saturated). These droplet sizes are within the range of those defined for a microemulsion system [103-105].

Conclusions

A water-in-oil microemulsion can be formulated using two pharmceutically acceptable surfactants without alcohol. The maximum solubilization of water in microemulsions corresponded to measurements of low interfacial tension between the oil and water phases. Salt was shown to reduce water solubility in microemulsions for all blends of AOT and Arlacel 20 while the oil chain length and surfactant weight ratio could

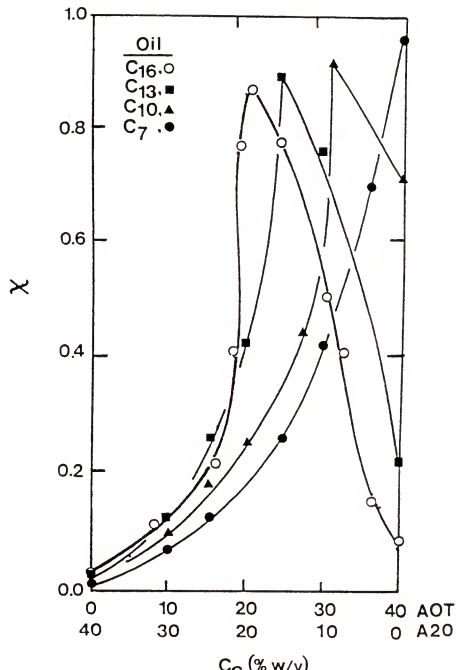

Figure 6-10. Maximum water-to-oil volume ratio (χ) versus weight ratio of AOT and Arlacel 20 for various hydrocarbons.

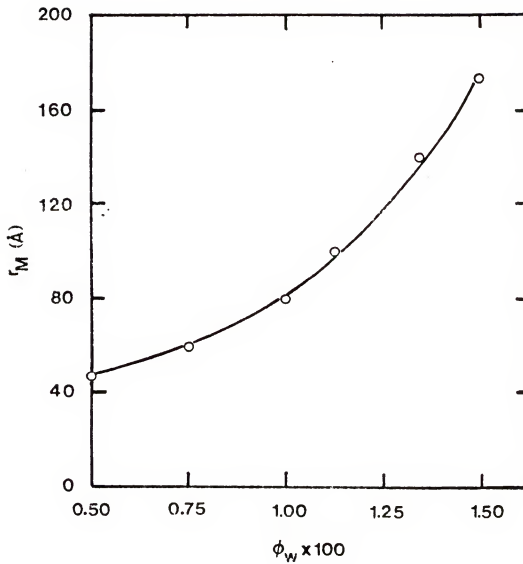

Figure 6-11. Hydrodynamic radius of microemulsion droplets in hexadecane (r_M) versus volume fraction of water (ϕ_w) where the initial concentration of AOT and Arlacel 20 (1:1) was 1.0% w/v.

be varied to increase water solubility in microemulsions. Light scattering experiments confirmed that the sizes of the water droplets were small enough to classify this system as a microemulsion.

CHAPTER 7
SUMMARY AND RECOMMENDATIONS

Summary of Results

A model was developed to describe the diffusion of micelle-solubilized compounds through microporous membranes that accounted for the flux of free solute as well as of solute within the micelles. In the absence of specific solute interactions with the surfactant head group, calculations using the model were in agreement with diffusion cell data. Experiments and calculations showed that it was possible to regulate the release of a solute through a microporous membrane by binding the solute to micelles. If a solute had a significant preference for the micellar phase as compared to the aqueous phase, the solubility of the compound could be significantly increased by the presence of micelles. Furthermore, the rate of solute release could be maintained at higher and more constant levels than in the absence of micelles. These results make the micelle-solubilized compound release technique very appealing. To summarize, some advantages of the micelle-solubilized compound release technique are:

- the release of more solute than would be possible if micelles were absent
- the release of the same amount of solute over a longer interval than if micelles were absent
- the release of solute at a more nearly constant rate

All of these appealing aspects of the micelle-solubilized compound release method are more pronounced if the distribution coefficient for the solute K is high.

Deviations of calculations from data for the diffusion of micelle-solubilized compounds were correlated with measurements of solute affinity for the surfactant head group. Pyrene delivery from TBAC and Brij 35 micellar solutions was underestimated by the model while the results of pyrene delivery from a SDS micellar solution agreed with calculations. The fluorescence spectra of pyrene in the micellar solutions indicated that pyrene associated more with the head groups of TBAC and Brij 35 than with the head group of SDS. Furthermore, it was demonstrated that solubility of pyrene could be almost doubled in TBAC and Brij 35 solutions below the CMC while pyrene solubility was unaffected by SDS solutions below the CMC. Since pyrene delivery from TBAC and Brij 35 solutions was under-predicted by a model that accounts for the flux of free and of micelle-solubilized compound, it was proposed that the surfactant monomers and/or the partially surfactant coated pore wall made significant contributions to the solute transport process when specific interactions between the solute and the surfactant head group existed.

The effects of electrostatic, hydrodynamic and steric interactions of micelles with micropores on the intrapore micelle diffusion coefficients were studied experimentally and compared with calculations for the hindered diffusion of neutral and charged spheres in neutral and charged cylindrical pores. Interactions between the micelle and the pore wall were important since micelle diffusion was studied in pores whose radii were as small as three times the micelle radius and in solutions with low ionic strengths where the Debye length was significant when compared to the pore size. In general, experimental data on micelle diffusion and theoretical calculations were in agreement when the

experimental conditions were within the constraints for which the models [27-32,43] were developed. For example, the contribution of the surfactant micelles to the ionic strength of the solution was neglected when calculating the Debye length inside the pore. At low concentrations of supporting electrolyte, micelles make a significant contribution to the ionic strength and neglecting this contribution resulted in the over estimation of Debye lengths. Therefore, the diffusion coefficients of CPC and TBAC micelles, based on the bulk concentration of micelles were severly under-predicted at low concentrations of supporting electrolyte ($C_C \approx$ CMC). Isomeric impurities present in the solution made comparisons of SDBS data with calculations difficult.

While most of the work presented here concerned solubilization and transport of solutes in aqueous solutions, some aspects of water solubilization in nonaqueous surfactant solutions were also studied. A water-in-oil microemulsion was formulated using two pharmaceutically acceptable surfactants (AOT and Arlacel 20) without alcohol. The maximum solubilization of water in microemulsions corresponded to measurments of low interfacial tension between the oil and water phases. Salt was shown to reduce water solubility in microemulsions for all blends of AOT and Arlacel 20 while the oil chain length and surfactant weight ratio could be varied to increase water solubility in microemulsions. Light scattering experiments confirmed that the sizes of the water droplets, ranging from 80 to 400 Å in diameter, were small enough to classify this system as a microemulsion.

Major Contributions of this Work

Previous studies on the diffusion of micelle-solubilized compounds through microporous membranes by Krovvidi and Stroeve [49] focused on a

single solute (heptane) in several nonionic surfactants. Krovvidi and Stroeve [49] showed that by varying the micelle size and solubilization capacity, one could optimize the flux of heptane through a microporous membrane. In the present work, a model for the diffusion of micelle-solubilized compounds was developed and used to predict the results of membrane diffusion experiments for four solutes in nonionic, cationic and anionic surfactant micelles. It is important to note that the solutes used in the present work (hydrocortisone, testosterone, progesterone and pyrene) had aqueous solubilities that varied from $\sim 10^{-3}$ to $\sim 10^{-7}$ M. By comparing the model, which accounts for the flux of free and micelle-solubilized compound, with data, it was shown that the model under-predicts the solute flux when there are specific interactions between the solute and the surfactant head group. This comparison of calculations with membrane diffusion data (from experiments with a wide variety of surfactant and solute combinations) demonstrated that other solute diffusion processes (e.g. monomer facilitated or surface diffusion on the pore wall) are possible when there are specific interactions between the surfactant head group and the solute. This conclusion could not have been made from the work of Krovvidi and Stroeve [49].

Recently, several studies have been conducted on the hindered diffusion of nonionic micelles in microporous membranes [24-26]. However, the electrostatic effects on the hindered diffusion of ionic micelles in charged microporous membranes were not studied. In the present work, the diffusion coefficients of cationic and anionic surfactant micelles in charged microporous membranes were measured and compared with calculations using the model developed by Smith and Deen [43] that accounted for the electrostatic interaction between a charged

hard sphere and a charged cylindrical pore. The calculations were in agreement with the data when the experiment was performed within the constraints of the model. The importance of electrostatic interactions on ionic micelle diffusion in microporous membranes was not evaluated before the present work.

Potential Applications

The most relevant application of the work is the controlled release of water insoluble compounds from a porous capsule or membrane device containing a surfactant solution plus the compound. By selecting the proper surfactant and pore size, the flux of the compound could be controlled if the diffusion process is dominated by the flux of free and of micelle-solubilized compound. In biolgical applications, the effect of micelle and pore charge on the micelle flux would not be important unless micelles with high degrees of dissociation were used with membranes having very small pore sizes (see Figure 4-3). If the controlled release of a water-insoluble pesticide from a porous polymer pellet in a lake or pond were considered, electrostatic interactions between an ionic surfactant micelle and the pore may be important if the pellets were used in fresh water (i.e. low solution ionic strength). In any application mentioned, biomedical [24] or agricultural [125,126], the effect of boundary layers on the overall mass transfer resistance would have to be evaluated.

Recommendations for Future Work

There are four main areas for future work in the study of micelle-solubilized compound diffusion through microporous membranes. First, the application of solute distribution coefficients between the micelle and

aqueous phases (K) at solute/micelle ratios far below saturation deserves a more critical analysis. In Chapter 5, calculations for the diffusion of micelle-solubilized progesterone using a K value determined at saturation were compared with experiments where the donor phase was at various degrees of saturation. While the data agreed with calculations, some caution must be used because the solute/micelle ratios in the donor phase were still higher than those experienced by the compound when it enters a virtually solute-free receptor phase in the early stages of the experiment. Therefore, it is proposed that solute partitioning studies at low solute/micelle ratios be performed using NMR self-diffusion or Taylor dispersion tube techniques of Stilbs [22] or Burkey et al. [23], respectively. Any deviations of K at low solute/micelle ratios from K determined at saturation could be incorporated into the model in the form of an average K value over a wide range of solute/micelle ratios.

Calculations for the electrostatic effects on ionic micelle diffusion in microporous membrane were in agreement with the data as long as the concentration of supporting electrolyte was sufficient to allow omission of the contributions of the micelles to the ionic strenth of the solution. As a second area for future research, it would be informative to compare calculations based on the model of Smith and Deen [43] with experiments where the Debye length occupied a larger portion of the pore in the range of supporting electrolyte concentrations where micelle contributions to the solution ionic strength could be neglected. This means using membranes having smaller pore radii (<250 Å) and thus, a lower porosity. A low porosity membrane would result in a smaller surfactant flux for any given concentration difference across the membrane. If such experiments were attempted, a more sensitive method of

detection would be required to perform the experiment in a reasonable period of time. It may be necessary to use radioactive-labeled surfactant molecules in these experiments along with a thermostated diffusion cell to control the temperature during longer periods required for the diffusion experiments.

A third area for future research concerns a more direct application of the micelle-controlled solute release technique. In all solute diffusion experiments performed in this work, the receptor phase surfactant concentration was above the CMC which ensured that micelles were present over the entire length of the membrane pore. In most biomedical applications of this controlled release technique, the receptor phase (e.g., gastro-intestinal tract, uterus or rectum) would not be above the CMC. Therefore, at some point in the membrane, there would be no micelles and the possibility of solute precipitation exists. This situation could be avoided by using very high surfactant concentrations in the donor phase such that the portion of the pore below the CMC accounts for less than 1 or 2% of the total pore length. However, experiments that compare data to calculations and subsequent examination of the membrane for the presence of precipitated solute crystals (e.g. thin sectioning of the membrane and electron microscopic examination) after experiments would be a required and interesting research project if the micelle-controlled release technique were to be commercialized.

Finally, further research on the mechanism of pyrene diffusion from TBAC and Brij 35 solutions across microporous membranes is required. The present work has established a correlation between pyrene association with the surfactant head group and deviations from the model presented in

Chapter 2. Contributions from monomer facilitated diffusion and surface diffusion of pyrene have been proposed but not confirmed. Brij 35 and TBAC monomers can solubilize pyrene and nearly double its aqueous solubility below the CMC of either surfactant. These monomers, which are smaller than surfacant micelles, could act as carriers for pyrene across the membrane. DellaGuardia and Thomas [102] demonstrated that pyrene was solubilized in cationic surfactant bilayers surrounding anionic clay particles. While it was demonstrated that pyrene can diffuse in the bilayers [102], the magnitude of its mobility in unknown. Studies on the polarization [127] of pyrene's fluorescence spectra in the cationic surfactant bilayers on clay particles will yield some information about the freedom of motion of pyrene in this environment. While it was shown that electrostatic effects were also important for TBAC-solubilized pyrene diffusion, since the addition of salt increased the pyrene flux (see Figure 5-14), further studies over a wider range of surfactant-solute pairs and studies on the effect of temperature on solute flux may also provide more insight into the exact mechanism of micelle-solubilized compound diffusion across microporous membranes.

APPENDIX

The program in this appendix allows the user to calculate the partition coefficient of a charged spherical particle into a charged cylindrical pore using Equation (4-5). The user must specify the radius of the particle, the surface charge density of the particle, and the surface charge density of the pore (all vlaues in SI units). The program will calculate K_M for values of ξ from 0.05 to 0.8 at salt concentrations of 5, 10, 50 and 100 mM where the temperature is 298 K.

```
1010    F=96485!
1020    R=8.314
1035    TEMP=298
1030    KB=1.38066D-23
1040    P=78.5*8.8541E-12
1050    EV=1.6021E-19
1060    PI=3.1416
1070    DIM K(20)
1080    DIM I(20)
1090    DIM ITTB(20)
1091    DIM S(4)
1092    DIM R(9)
1093    DIM V(205)
1094    DIM B(205)
1095    DIM E(205)
1096    DIM KM(2)
REM *** These are the values for the factorial expression in lambda.
1100    DIM F(16)
1110    F(0)=1
1120    F(1)=2
1130    F(2)=6
1140    F(3)=20
1150    F(4)=70
1160    F(5)=252
1170    F(6)=924
1180    F(7)=3432
1190    F(8)=12870
1200    F(9)=48620!
1210    F(10)=184756!
1261    PRINT "ENTER PORE WALL SURFACE CHARGE DENSITY"
1270    INPUT CC
1271    PRINT "ENTER MICELLE SURFACE CHARGE DENSITY"
1280    INPUT CS
1281    PRINT "ENTER MICELLE RADIUS (M)"
1290    INPUT RM
1291    CLS
1320    S(1)=.005
1321    S(2)=.01
1322    S(3)=.05
1323    S(4)=.1
1330    R(1)=RM/.05
1331    R(2)=RM/.1
1332    R(3)=RM/.2
1333    R(4)=RM/.3
1334    R(5)=RM/.4
1335    R(6)=RM/.5
1336    R(7)=RM/.6
```

```
1337    R(8)=RM/.7
1338    R(9)=RM/.8
1341    FOR M=1 TO 4 STEP 1
1342     PRINT "RM=";RM,"QS=";CS,"QC=";CC
1343    PRINT
1344    PRINT
1345    PRINT "SALT [M]","  XI","    TAU","      KM"
1346    FOR N=1 TO 9 STEP 1
1350    SALT=S(M)
1351    RP=R(N)
1360     KAPPA=(2*SALT/(.001*P*KB*TEMP))^.5*1.24E-07
1370     TAU=RP*KAPPA
1380    XI=A/RP
1400     CDC=F*RP*CC/(R*P*TEMP)
1410     CDS=F*RP*CS/(R*P*TEMP)
1420    TANHX=(EXP(XI*TAU)-EXP(-XI*TAU))/(EXP(XI*TAU)+
         EXP(-XI*TAU))
1430    LTA=1/(TANHX)-1/(XI*TAU)
1440    CALL IONE(TAU,I1T)
1450    NUMA=8*PI*TAU*XI^4*EXP(TAU*XI)*CDS^2/(1+TAU*XI)^2
1460    NUMB=4*PI^2*XI^2*CDS*CDC/((1+TAU*XI)*I1T)
1470    NUMC=PI^2*(EXP(TAU*XI)-EXP(-TAU*XI))*TAU*XI*
         LTA*CDC^2/(TAU^2*I1T^2*(1+XI*TAU))
1480    DEND=PI*TAU*EXP(-TAU*XI)
1490    DENE=2*(EXP(TAU*XI)-EXP(-TAU*XI))*TAU*XI*LTA/(1+TAU*XI)
REM *** This section calculates K1(2*TAU) to K20(2*TAU) for equation (4-6)
1500    X=2*TAU
1510    CALL IZERO(X,I(0))
1520    CALL IONE(X,I(1))
1530    CALL KZERO(X,I(0),K(0))
1540    FOR J=1 TO 10 STEP 1
1550    I(J+1)=I(J-1)-2*I(J)/X
1560    K(J)=(1/(X)-I(J)*K(J-1))/I(J-1)
1570    NEXT J
1580    FOR C=1 TO 2 STEP 1
1590    INC=(1-XI)/(C*100)
1600    B(0)=0
1610     FOR K=1 TO C*100 STEP 1
1620    B(K)=B(K-1)+INC
1630    NEXT K
1640    L=0
1650    FOR THETA=0 TO 1-XI STEP INC
1660    SUMOLD=0
1670    T=0
1680    IF THETA>0 THEN GOTO 1720
1690    LAMBDA=0
1700    I0TB=1
```

```
1710      GOTO 1850
1720      CALL IZERO(TAU*THETA,ITTB(0))
1730      CALL IONE(TAU*THETA,ITTB(1))
1740      FOR J=1 TO 10 STEP 1
1750      ITTB(J+1)=ITTB(J-1)-2*ITTB(J)/(TAU*THETA)
1760      NEXT J
1770      SUMNEW=SUMOLD+THETA^T*F(T)*ITTB(T)*(TAU*K(T+1)
          +.75*K(T))/(2^(3*T))
1780      ER=ABS((SUMNEW-SUMOLD)/SUMNEW)*100
1790      IF ER< .2 THEN GOTO 1830
1800      T=T+1
1810      SUMOLD=SUMNEW
1820      GOTO 1770
1830      CALL IZERO(TAU*THETA,I0TB)
1840      LAMBDA=1.571*I0TB*SUMNEW
1850      V(L)=(NUMA*LAMBDA+NUMB*I0TB+NUMC*I0TB^2)/
           (DEND-DENE*LAMBDA)
1860      E(L)=RP*P*(R*TEMP/F)^2*V(L)
1870      L=L+1
1880      NEXT THETA
REM *** Simpson's Rule integration of E(THETA) over all positions in the pore
1890      SUM2=0
1900      SUM3=0
1910      FOR J=2 TO C*100 STEP 2
1920      SUM2=SUM2+EXP(-E(J-1)/(KB*TEMP))*B(J-1)
1930      IF J=C*100 THEN GOTO 1950
1940      SUM3=SUM3+EXP(-E(J)/(KB*TEMP))*B(J)
1950      NEXT J
1960      KM(C)=2*INC*(EXP(-E(0)/(KB*TEMP))*B(0)+4*SUM2
           +2*SUM3+EXP(-E(100)/(KB*TEMP))*B(100))/3
1970      NEXT C
1980      SLP=(KM(1)-KM(2))/.05
1990      INTC=KM(1)-SLP*.1
2000      PRINT SALT,XI,TAU,INTC
2010      NEXT N
2011      LCOPY
2015      CLS
2020      NEXT M
2040      END
REM *** Bessel functions calculated from formulas available in the "Handbook of
Mathematical Functions" by Abramowitz and Stegun
2050      SUB IZERO(X,I0) STATIC
2060      T=X/3.75
2070      IF X>3.75 THEN GOTO 2100
2080       I0=1+3.5156226#*T^2+3.0899424#*T^4+1.20607492#*T^6+
           .2659732#*T^8+.0360768*T^10+.0045813*T^12
2090      GOTO 2120
```

```
2100    I0A=.39894228#+.01328592#*T^-1+.00225319#*T^-2-
          .00157565#*T^-3+.00916281#*T^-4-.02057706#*T^-5
          +.02635537#*T^-6-.01647633#*T^-7+.00392377#*T^-8
2110    I0=I0A/(X^.5*EXP(-X))
2120    END SUB
2130    SUB IONE(X,I1) STATIC
2140    T=X/3.75
2150    IF X>3.75 THEN GOTO 2190
2160      I1A=.5+.87890594#*T^2+.51498869#*T^4+.15084934#*T^6+
          .02658733#*T^8+.00301532#*T^10+.00032411#*T^12
2170    I1=I1A*X
2180    GOTO 2210
2190      I1A=.39894288#-.03988024#*T^-1-.00362018#*T^-2+
          .00163801#*T^-3-.01031555#*T^-4+.02282967#*T^-5-
          .02895312#*T^-6+.01787654#*T^-7-.00420059#*T^-8
2200    I1=I1A/(X^.5*EXP(-X))
2210    END SUB
2220    SUB KZERO(X,I0,K0) STATIC
2230    IF X>2 THEN GOTO 2260
2240      K0=-LOG(X/2)*I0-.57721566#+.42278842#*(X/2)^2+
          .23069756#*(X/2)^4+.0348859#*(X/2)^6+.00262698#*(X/2)^8+
          .0001075#*(X/2)^10+.0000074#*(X/2)^12
2250    GOTO 2280
2260      K0A=1.24331414#-.07832358#*(2/X)+.02189568#*(2/X)^2-
          .01062446#*(2/X)^3+.00587872#*(2/X)^4-.0025154#*(2/X)^5+
          .00053208#*(2/X)^6
2270    K0=K0A/(X^.5*EXP(X))
2280    END SUB
```

REFERENCES

1. L.I. Osipow, Surface Chemistry, Robert Krieger Publishing Co., New York (1977).

2. A.W. Adamson, Physical Chemistry of Surfaces, J. Wiley & Sons, New York (1982).

3. C.A. Miller and P. Neogi, Interfacial Phenomena, Marcel Dekker, New York (1978).

4. M.J. Rosen, Surfactants and Interfacial Phenomena, J. Wiley & Sons, New York (1978).

5. N.A. Mazer, M.C. Carey and G.B. Benedek, p. 359 in Micellization, Solubilization and Microemulsions, K.L. Mittal (ed.), Plenum Press, New York (1977).

6. D.C.H. Cheng and E. Gulari, J. Colloid Interface Sci., 90, 410 (1982).

7. N.J. Turo and A. Yetka, J. Am. Chem. Soc., 100, 5951 (1978).

8. J.K. Thomas, The Chemistry of Excitation at Interfaces, American Chemical Society, Washington, DC (1984).

9. K.S. Birdi, Progr. Colloid & Polymer Sci., 70, 23 (1985).

10. C. Tanford, The Hydrophobic Effect: Formation of Micelles and Biological Membranes, J. Wiley & Sons, New York (1973).

11. E.A.G. Aniansson, S.N. Wall, M. Almgren, H. Hoffmann, I. Kielmann, W. Ulbricht, R. Zana, J. Lang and C. Tondre, J. Phys. Chem., 80, 905 (1976).

12. R. Leung and D.O. Shah, J. Colloid Interface Sci., 113, 484 (1986).

13. M.E.L. McBain and E. Hutchinson, Solubilization and Related Phenomena, Academic Press, New York (1955).

14. A.T. Florence, in Techniques of Solubilization of Drugs, S.H. Yalkowsky (ed.), Marcel Dekker, New York (1981).

15. B.J. Carroll, J. Colloid Interface Sci., 79, 126 (1981).

16. J.A. Shaeiwitz, A.F. Chan, E.L. Cussler and D.F. Evans, J. Colloid Interface Sci., 84, 47 (1981).

17. M. Bourrel and C. Chambu, SPE J., 71, 408 (1979).

18. R.O. Dunn, J.F. Scamehorn and S.D. Christian, Separation Sci. Tech., 22, 763 (1987).

19. J.H. Fendler and E.J. Fendler, Catalysis in Micellar and Macromolecular Systems, Academic Press, New York (1975).

20. A. Cipiciani, C. Ebert, R. Germani, P. Linda, M. Lovrecich, F. Rubessa and G. Savelli, J. Pharm. Sci., 74, 1184 (1985).

21. G.E. Amidon, W.I. Higuchi and N.F. Ho, J. Pharm. Sci., 71, 77 (1982).

22. P. Stilbs, J. Colloid Interface Sci., 94, 463 (1983).

23. T.J. Burkey, D. Griller, D.A. Lindsay and J.C. Scaiani, J. Am. Chem. Soc., 106, 1983 (1984).

24. P. Stroeve, E. Ruckenstein, S. Roy and J. Lippes, AIChE Sypm. Ser., 79 (227), 11 (1983).

25. S. Roy, E. Ruckenstein and P. Stroeve, J. Colloid Interface Sci., 92, 383 (1983).

26. K.R. Krovviddi, A. Muscat, P. Stroeve and E. Ruckenstein, J. Colloid Interface Sci., 100, 497 (1984).

27. L.R. Bacon, J. Franklin Inst., 221, 251 (1935).

28. W.L. Haberman and R.M. Sayer, "Motion of Rigid and Fluid Spheres in Stationary and Moving Liquids Inside Cylindrical Tubes," David Taylor Model Basin Report, Dept. of Navy (#1143) (1958).

29. P.M. Bungay and H. Brenner, Int. J. Multiphase Flow, 1, 25 (1973).

30. J.L. Anderson and J.A. Quinn, Biophys. J., 14, 130 (1974).

31. P.L. Paine and P. Scherr, Biophys. J., 15, 1087 (1975).

32. H. Brenner and L.J. Gaydos, J. Colloid Interface Sci., 58, 312 (1977).

33. E.M. Renkin, J. Gen. Physiol., 38, 225 (1955).

34. C.P. Bean, p. 1 in Membranes, Vol. 1, G. Eisenman (ed.), Marcel Dekker, New York (1972).

35. D.M. Malone and J.L. Anderson, Chem. Eng. Sci., 33, 1492 (1978).

36. R.E. Baltus and J.L. Anderson, Chem. Eng. Sci., 38, 1959 (1983).

37. M.P. Bohrer, G.D. Patterson and P.J. Carrol, Macromolecules, 17, 1170 (1984).

38. K.H. Altgelt and L. Segal, Gel Permeation Chromoatography, Marcel Dekker, New York (1971).

39. L.R. Synder and J.J. Kirkland, Introduction to Modern Liquid Chromatography, J. Wiley & Sons, New York (1979).

40. B.M. Uzelac and E.L. Cussler, J. Colloid Interface Sci., 32, 487 (1970).

41. J.L. Anderson and J.A. Quinn, J. Colloid Interface Sci., 40, 272 (1972).

42. F.G. Smith and W.M. Deen, J. Colloid Interface Sci., 78, 444 (1980).

43. F.G. Smith and W.M. Deen, J. Colloid Interface Sci., 91, 571 (1983).

44. M. Nakano, J. Mem. Sci., 5, 335 (1979).

45. K. Juni, T. Tomitsuka, M. Nakano and T. Arita, Chem. Pharm. Bull., 25, 2807 (1977).

46. K. Juni, T. Tomitsuka, M. Nakano and T. Arita, Chem. Pharm. Bull., 26, 837 (1978).

47. R. Withington and J.H. Collett, J. Pharm. Pharmac., 25, 273 (1973).

48. M.G. Karth, N.F.H. Ho and W.I. Higuchi, J. Pharm Sci., 74, 618 (1985).

49. K.R. Krovvidi and P. Stroeve, J. Colloid Interface Sci., 110, 437 (1986).

50. J.H. Collett, R. Withington and B. Cox, J. Pharm. Pharmacol., 26, 34 (1974).

51. K.A. Walters, A.T. Florence and P.H. Dugard, Int. J. Pharm., 10, 153 (1982).

52. L.I. Osipow, pp. 295-343 in Surface Chemistry, R.E. Krieger, Huntington, New York (1977).

53. P.B. Sheth and E.L. Parrott, J. Pharm. Sci., 56, 983 (1967).

54. E.L. Cussler in Diffusion: Mass Transfer in Fluid Systems, Cambridge University Press, London (1984).

55. R.E. Cunningham and R.J.J. Williams, p. 9 in Diffusion in Gases and Porous Media, Plenum Press, New York (1980).

56. R.M. Weinheimer, D.F. Evans and E.L. Cussler, J. Colloid Interface Sci., 80, 357 (1981).

57. N.M. Atherton and S.J. Strach, J. Chem. Soc., Faraday Trans. II, 68, 374 (1972).

58. S.C. Wallace and J.K. Thomas, Radiat. Res., 54, 49 (1973).

59. P. Mukerjee and K.J. Mysels, Critical Micelle Concentrations of Aqueous Surfactant Systems, National Bureau of Standards, NSRDS-NBS 36, Washington, DC (1971).

60. P.J.M. Stout, N. Khoury, J. Mauger and S. Howard, J. Pharm. Sci., 75, 65 (1986).

61. Nuclepore Corp., Pleasanton, CA.

62. W.M. Deen, M.P. Bohrer and N.B. Epstein, AIChE J., 27, 952 (1981).

63. D.M. Malone and J.L. Anderson, AIChE J., 23, 177 (1977).

64. A.A. Liabastre and C. Orr, J. Colloid Interface Sci., 64, 1 (1978).

65. D.S. Cannell and F. Rondelez, Macromolecules, 13, 1599 (1980).

66. F.G. Smith, D.Sc. Thesis, MIT (1981).

67. V. Degiorgio, M. Corti and M. Giglio, Light Scattering in Liquids and Macromolecular Solutions, Plenum Press, New York (1980).

68. H.M. Fignaut, J. Chem. Phys., 74, 6857 (1981).

69. B.J. Berne and R. Pecora, Dynamic Light Scattering, J. Wiley, New York (1976).

70. K. Kalyanasundaram, M. Gratzel and J.K. Thomas, J. Am. Chem. Soc., 97, 3915 (1975).

71. S. Atik and J.K. Thomas, J. Am. Chem. Soc., 103, 3543 (1981).

72. H. Coll, J. Phys. Chem., 74, 520 (1970).

73. Personal communication with Prof. J.K. Thomas, University of Notre Dame, Notre Dame, IN.

74. E. Rolants and F.C. De Schryer, Langmuir, 3, 209 (1987).

75. R.C. Reid, J.M. Prausnitz and T.K. Sherwood, The Physical Properties of Gases and Liquids, McGraw-Hill, New York (1977).

76. R. Zana, J. Colloid Interface Sci., 78, 330 (1978).

77. P.C. Hiemenz, p. 688 in Principles of Colloid and Surface Chemistry, Marcel Dekker, New York (1986).

78. A. Kitahara and A. Watanabe, p. 107 in Electrical Phenomena at Interfaces, Marcel Dekker, New York (1984).

79. W.H. Koh and J.L. Anderson, AIChE J., 21, 1176 (1975).

80. G.B. Westermann-Clark and J.L. Anderson, J. Electrochem. Sci., 130, 839 (1985).

81. C.C. Christoforou, G.B. Westerman-Clark and J.L. Anderson, J. Colloid Interface Sci., 106, 1 (1985).

82. E.F. Casassa, p. 119 in Gel Permeation Chromatography, K.H. Altgelt and L. Segal (eds.), Marcel Dekker, New York (1971).

83. C.P. Tally, Anal. Chem., 43, 1512 (1971).

84. S. Usui, p. 223 in Progress in Surface and Membrane Science, J.F. Danielle, M.D. Rosenberg and D.A. Cadenhead (eds.), Academic Press, New York (1972).

85. G. Kar, S. Chander and T.S. Mika, J. Colloid Interface Sci., 44, 347 (1973).

86. H. van Olphen, An Introduction to Clay Colloid Chemistry, Interscience, New York (1963).

87. H. Lamb, Hydrodynamics, Dover, New York (1932).

88. M.P. Bohrer, Ph.D. Dissertation, Stanford University (1980).

89. M. Corti and V. Degiorgio, J. Phys. Chem., 85, 711 (1981).

90. E.W. Anacker, J. Phys. Chem., 62, 41 (1958).

91. P.D. Bisio, J.G. Cartledge, W.H. Keesom and C.J. Radke, J. Colloid Interface Sci., 78, 225 (1980).

92. L.M. Kushner and W.D. Hubbard, J. Phys. Chem., 58, 1163 (1954).

93. C.U. Herrmann and M. Kahlweit, J. Phys. Chem., 84, 1536 (1980).

94. C.J. Chen and S.G. Frank, J. Colloid Interface Sci., 92, 396 (1983).

95. F. Wesoluch, A.T. Florence, F. Puisieux and J.T. Cartensen, Int. J. Pharm., 2, 343 (1979).

96. S. Chou and B.E. Sims, J. Pharm. Sci., 70, 924 (1981).

97. B. Lundberg, T. Lovgren and C. Blomquist, Acta. Pharm. Suec., 16, 144 (1979).

98. H.B. Klevens, J. Am. Chem. Soc., 72, 3780 (1958).

99. T. Lovgren, B. Heikius, B. Lundberg and L. Sjoblom, J. Pharm, Sci., 67, 1419 (1978).

100. B. Lundberg. T. Lovgren and B. Heikius, J. Am. Chem. Soc., 101, 279 (1979).

101. M. Almgren, F. Grieser and J.K. Thomas, J. Am. Chem. Sci., 101, 279 (1979).

102. R.A. DellaGuardia and J.K. Thomas, J. Phys. Chem., 87, 3550 (1983).

103. Y.K. Pithapurwala and D.O. Shah, J. Amer. Oil Chem. Soc., 61, 1399 (1984).

104. D.O. Shah, V.K. Bansal, K.S. Chan and W.C. Hsieh, p. 293 in, Improved Oil Recovery by Surfactant and Polymer Flooding, D.O. Shah and R.S. Schechter (eds.), Academic Press, New York (1977).

105. I.A. Zlochower and J.H. Shulman, J. Colloid Interface Sci., 24, 115 (1967).

106. D.O. Shah, Surface Phenomena in Enhanced Oil Recovery, Plenum Press, New York (1981).

107. W.B. Gogarty, J. Petro. Tech., 28, 93 (1976).

108. R.L. Reed and R.N. Healy, p. 383 in Improved Oil Recovery by Surfactant and Polymer Flooding, D.O. Shah and R.S. Schechter (eds.), Academic Press, New York (1977).

109. M.L. Robbins, Theory of the Phase Behavior of Microemulsions, Paper #SPE 5839, Presented at the Society of Petroleum Engineers Meeting, Tulsa, OK (1976).

110. R.N. Healy and R.L. Reed, Soc. Pet. Eng. J., 14, 491 (1974).

111. A. Jayakrishnan, K. Kalaiarasi and D.O. Shah, J. Soc. Cosmet. Chem., 34, 334 (1983).

112. J. Ziegenmeyer, in Dermal and Transdermal Absorption, R. Brandau and B.H. Lippold (eds.), Wissenschaftliche Verlagsgesellschaft, Stuttgart (1982).

113. G. Gilberg, L. Eriksson and S. Friberg, p. 210 in Emulsions, Lattices and Dispersions, P. Becher (ed.), Marcel Dekker, New York (1978).

114. Merck Index, Merck and Co., Rahway, NJ (1976).

115. Cosmetic Formulary, ICI Americas, Inc., Wilmington, DE 19897.

116. K. Shinoda and H. Saito, J. Colloid Interface Sci., 26, 70 (1969).

117. K. Shinoda and H. Kunieda, in Microemulsions, Theory and Practice, L.M. Prince (ed.), Academic Press, New York (1977).

118. F.I. Iskanderani, Ph.D. Dissertation, University of Florida (1985).

119. M.C. Wilkinson and R.L. Kidwell, J. Colloid Interface Sci., 35, 114 (1971).

120. M.C. Wilkinson, J. Colloid Interface Sci., 40, 14 (1972).

121. V.K. Bansal, K. Chinnaswamy, C. Ramachandran and D.O. Shah, J. Colloid Interface Sci., 72, 524 (1979).

122. E. Ruckenstein and J.A. Beunen, J. Colloid Interface Sci., 98, 55 (1984).

123. S.G. Frank and G. Zografi, J. Colloid Interface Sci., 29, 27 (1969).

124. E. Sjoblom and S. Friberg, J. Colloid Interface Sci., 67, 16 (1978).

125. N. Cardarelli, Controlled Release Pesticide Formulations, CRC Press, Cleveland (1967).

126. H.B. Scher (ed.) Controlled Release Pesticides, ACS Symposium Series #53, ACS, Washington, DC (1977).

127. C.R. Cantor and P.R. Schimmel, Biophysical Chemistry, W.H. Freeman, San Francisco (1980).

BIOGRAPHICAL SKETCH

Keith A. Johnson was born in Pinehurst, North Carolina, on September 10, 1961. After graduating from Cardinal Mooney High School in Sarasota, Florida, in 1979, he attended the University of Notre Dame du Lac where he received his B.S. in chemical engineering in May 1983. He received his M.S. in chemical engineering from the University of Florida in August 1984. During the summer of 1984, he was a visiting researcher at ACO Lakemedel AB in Solna, Sweden. In the fall of 1984, he began working for his Ph.D. in chemical engineering at the University of Florida.

I certify that I have read this study and that in my opinion it conforms to acceptable standards of scholarly presentation and is fully adequate, in scope and quality, as a dissertation for the degree of Doctor of Philosophy.

Dinesh O. Shah

Dinesh Shah, Chairman
Professor of Chemical Engineering

I certify that I have read this study and that in my opinion it conforms to acceptable standards of scholarly presentation and is fully adequate, in scope and quality, as a dissertation for the degree of Doctor of Philosophy.

Brij M. Moudgil

Brij Moudgil
Professor of Materials Science and Engineering

I certify that I have read this study and that in my opinion it conforms to acceptable standards of scholarly presentation and is fully adequate, in scope and quality, as a dissertation for the degree of Doctor of Philosophy.

Gerald Westermann-Clark

Gerald Westermann-Clark
Associate Professor of Chemical Engineering

This dissertation was submitted to the Graduate Faculty of the College of Engineering and to the Graduate School and was accepted as partial fulfillment of the requirements for the degree of Doctor of Philosophy.

December 1987

Herbert G. Berry

Dean, College of Engineering

Dean, Graduate School